The combination of processes influencing fracture in ferritic steels.

Williams, Owen

The Combination of Processes Influencing Fracture in Ferritic Steels

By

Owen Williams

Thesis submitted to the faculty of Engineering
of the University of Wales, Swansea
For the Degree of
DOCTOR OF PHILOSOPHY

Abstract

In order to understand the brittle fracture of ferritic steels, it is necessary to understand all of the processes that have an influence on the brittle fracture. Much work has been done previously on grain boundary geometry and structure, grain boundary segregation, the effects of heat treatments and the fracture process, but little work has been reported on the combined result of these processes and the effects that they have on each other and the process of brittle fracture in ferritic steels. The aim of this project was to investigate the combined influence that the processes of grain boundary structure, segregation, and heat treatment have on the brittle fracture of ferritic steel.

All experiments were carried out on a Fe-0.06wt%P-0.002wt%C and a Fe-0.12wt%P-0.002wt%C alloy, which was subject to a set of specific heat treatments. Investigations were made into the grain boundary structure of the material using Electron Back-Scatter Diffraction (EBSD) and the segregation studied by Auger Electron Microscopy (AES). A number of innovative analysis techniques were developed during the course of the program in order to determine the combined effects of boundary structure and segregation on the fracture process of the material.

Two separate grain growth mechanisms were found to be operating in this material at different temperature ranges. Abnormal grain growth being prolific in this material at annealing temperatures above 900°C, normal grain growth being the dominant grain growth mechanism for annealing temperatures of below 900°C. Both abnormal grain growth and $\Sigma 3$ proportions were found to be dependent on the annealing temperature and both were affected by a transition that occurs at 0.65-0.75 of the melting temperature, given by (T_m). It was also found that 3at% more segregated phosphorus was present on {112} boundary planes than on {110} boundary planes on the fracture surfaces of the material.

Acknowledgements

I would firstly like to express my thanks to the EPSRC for their financial support during this program. also thanks to BNFL Magnox Generation for their financial support and provision of facilities.

I wish to extend my grateful thanks to Professor V. Randle at the University of Wales, Swansea for her support and supervision during this project. I also would like thank Mr. A. Brookes, Mr P. Davies and Mr. D. Jones for their much appreciated technical support and assistance.

I also wish to express my thanks to Dr. R. Corcoran, Dr P. Spellward, Dr J. Cowan, Mr. M. Whittaker and all my colleges at the University of Wales for all their help and support.

Contents

1. Introduction

The boundary between two grains in a metal or alloy is known to have a great deal of influence on the physical properties of materials. Processes such as the segregation of impurities to the boundaries can have a serious effect on the properties of the grain boundaries and can lead to the grain boundary embrittlement of steel specimens.

Grain boundary embrittlement has been shown to be responsible for the lowering of the Charpy impact energy of certain steels and has been known to impair their fracture toughness. The main embrittling element in most steels that are used in industrial applications is phosphorus. Its presence on the grain boundaries of a steel can seriously affect the integrity of the material and the effect that its presence has on the grain boundaries of the material has been extensively studied for many years.

The embrittlement of steels is a subject of much concern to many industries, especially to the nuclear industry, due to the fact that a large number of the components used in the nuclear power stations are manufactured from steels and are subjected to temperatures in the embrittling range.

The crystallography of grain boundaries is thought to alter the potential for intergranular segregation and may be responsible for controlling how much segregation takes place in certain materials. A great deal of work has been undertaken in the past on the following three areas:

- Grain boundary crystallography.
- Grain boundary segregation.
- The mechanisms controlling fracture.

However, little work has been done to date on the effects that these processes have on each other and the combined effects that may be a result of such potentially complex interactions. Until these influencing effects are fully understood, a comprehensive understanding of the physical properties of the steels and the mechanisms leading to brittle fracture will remain unattainable.

The purpose of this study is to perform an exploration of the combined effects of the processes influencing crystallography, segregation and fracture, and the resulting effects that they have on the physical properties of the 0.06wt%P and 0.12wt%P steel alloys. Also included is the development of appropriate experimental methodologies for the acquisition of data from fractured samples. This will provide a valuable insight into the effects of the combined processes that influence grain boundary embrittlement and fracture, an issue that has yet to be comprehensively discussed in the literature. This work will aid in the expansion of the knowledge base relating to the processes governing grain boundary fracture.

2. Literature Review

A great deal of work has been done over many years in order to better understand the grain boundary structure of certain materials and the factors that instigate grain growth, grain boundary segregation and the fracture of ferritic steels. A thorough understanding of these processes will allow better understanding of the properties of the materials, which allows better predictions of the material design life to be made which may lead to reduced industrial costs and increased industrial and domestic safety.

2.1 Grain Boundary Misorientation

The characteristics of a grain boundary can by described by looking at the crystallographic relationship between the two neighbouring grains. The geometry of these two neighbouring grains is represented by five macroscopic degrees of freedom, comprising of the crystallographic orientation relationship between the two crystal lattices; called the 'misorientation' between the two lattices, and the crystallographic orientation of the surface of the grain boundary, which describes the grain boundary 'plane' (Randle, 1996)

Lattice misorientation can be accurately defined by considering the angle by which one crystal lattice is rotated about the other and is represented by θ. The common axis about which this rotation occurs is given by r and results in the definition of the 'angle/axis pair'. The three degrees of freedom that represent the lattice misorientation are usually sufficient for the description of the grain boundary geometry as they accurately describe the degree by which one crystal lattice is rotated about the other in 3 dimensional space. The two remaining degrees of freedom are used to represent the crystallographic orientation of the grain boundary plane in one of the neighbouring lattices.

The misorientation between two grains can be represented by a 3x3 orthonormal misorientation matrix, which is an orthogonal matrix with a determinant of 1. The matrix is orthogonal, since the sum of the squares of each row and each column are unity, and the dot product between each row and column vector are equal to zero. More mathematically, it is a square matrix 'A' equal to the inverse of its transpose $(A^T)^{-1}$.
If two interfacing lattices are denoted as lattice 1 and 2, the columns of the matrix are the direction cosines of the crystal axes of lattice 2 referred to the coordinate system of lattice 1 which is the reference lattice. This allows the angle/axis pair which is obtained from the matrix to be described as:

$$Cos\theta = \frac{(a_{11} + a_{22} + a_{33})}{2} \qquad \textbf{Equation 2.1}$$

$$r = r_1 : r_2 : r_3 = a_{32} - a_{23} : a_{13} - a_{31} : a_{21} - a_{12} \qquad \textbf{Equation 2.2}$$

And when $\theta = 180°$, then r is given by:

$$r = r_1 : r_2 : r_3 = (a_{11} + 1)^{\frac{1}{2}} : (a_{22} + 1)^{\frac{1}{2}} : (a_{33} + 1)^{\frac{1}{2}} \qquad \textbf{Equation 2.3}$$

Where a_{ij} are the elements of the misorientation matrix and r is the axis of misorientation.

The axis of the second lattice with respect to the reference lattice can be chosen in more than one way for the majority of crystal systems. For the cubic system there are 24 different, but equivalent ways in which the orientation matrix can be expressed and hence the cubic system is said to have a multiplicity of 24. These symmetrically equivalent solutions M' are given by

$$M' = T_i M \qquad \textbf{Equation 2.4}$$

Where i = 1, 2....24. The T matrices describe the symmetry of the cubic system and the 24 matrices derived from equ.2.4 give rise to the 24 angle/axis pairs. Due to the fact that

these 24 angle/axis pair solutions are unequivocally identical, it has become common practise to only consider the lowest angle solution when describing a misorientation; this is described as the 'disorientation'. Using the disorientation as a description of the grain boundary geometry allows the simple identification of low angle boundaries, which are boundaries that have a disorientation of less than 15°.

2.2 Models of Grain Boundary Structure

2.2.1 The Coincidence Site Lattice (CSL)

Considering the fact that there are an infinite number of possible orientations that one lattice can have relative to another, it is reasonable to assume that there will be a few special orientations occurring between the two lattices. The best way in which to visualise such an occurrence is in two dimensions. By rotating one lattice on top of another and looking down from above it is possible to see the development of a Moiré pattern. (Moiré patterns are seen wherever a repetitive geometric structure is overlaid with another similar geometric structure.) For certain rotation angles, some of the lattice points of lattice one will be seen to exactly coincide with the lattice point of lattice 2. The resulting structure at these special rotation angles is termed the Coincidence Site Lattice (CSL). The question of whether these special coincidence orientations and the related CSL have any real significance for real grain boundaries has been a subject of much debate over the years (Randle, 2001)

To extend this CSL conjecture to the third dimension it is necessary to consider the relation between the number of lattice points in the unit cell of a CSL and the number of lattice points in a unit cell of the original lattice. This term is denoted $\sum$ (Sigma) and is equivalent to the unit cell volume of the CSL in units of the unit cell volume of the elementary cells of the crystals.

From this definition it can be seen that a $\sum 1$ boundary would represent the case of a perfect crystal with no boundary. However, all boundaries that lie relatively close to the $\sum 1$ orientation are all boundaries with small misorientations, and are thus termed 'low-angle' grain boundaries. Looking at the case of a twin boundary in 2 dimensions it is easy to see that $\sum_{twin}=3$ and it is for this reason that twin boundaries in cubic systems can be termed $\sum 3$ boundaries. The twin boundary is the grain boundary with the most special coincidence orientation, due to the fact that it has the largest number of coinciding lattice points. A similar two-dimensional approach can be used in order to represent rotations that result in higher values of sigma.

If 1 in 5 of the lattice sites from each grain coincide, they will be making a $\sum 5$ boundary. The same principle is true for all higher values of $\sum$, though as the values of $\sum$ increase it would become virtually unrecognisable if drawn schematically. This is representative of the fact that the concept of the CSL is a mathematical condition in which there is either perfect coincidence or none at all. If two points almost coincide, then no CSL will be recognised. The same is true if a lattice is rotated away from a coincidence position by an arbitrarily small angle. In this case, coincidence is totally lost and gives rise to a totally different situation. However, the same physically small changes can be expected to have little changes in the properties of the material.

The concept of the coincidence site lattice provides an understanding of the special orientations between grains that give rise to special grain boundaries. If the concept is extended to encompass grain boundary dislocations, then the CSL can be made applicable to all grain boundaries, because any arbitrary orientation is 'near' a CSL orientation. The maximum deviation form exact coincidence is denoted by v_m and the experimentally measured deviation is denoted by v. Deviations from exact coincidence can therefore be described by a relative deviation, v/v_m.

The variation of v_m with $\sum$ is usually taken to be $\sum^{-1/2}$, which is called the 'Brandon criterion', and corresponds to a relationship, which is based purely on periodicity.

$$v_m = v_0 \sum^{-\frac{1}{2}} \qquad \textbf{Equation 2.5}$$

where v_0 is a proportionality constant based on the angular limit for a low angle boundary, which is 15°. (Randle, 1996)

Despite its obvious of the CSL concept, it is not a powerful enough theory to allow the solution of grain boundaries in all possible cases, due to a number of physical, practical and mathematical reasons.

2.2.2 The Displacement Shift Complete Lattice (DSC)

Certain grain boundaries can contain certain special defects that only exist in grain boundaries. The most important of these defects are grain boundary dislocations. These dislocations are linear defects, similar to lattice dislocations, but with Burgers vectors that can only occur in grain boundaries.

If one grain is displaced with respect to another by a Burgers vector $\underline{b}$ in a way that preserves the structure of the boundary, everywhere except around the dislocation line, such that the structure of the boundary after the shift looks exactly as it did before the shift. If this is done about a CSL boundary, then the set of displacement vectors that preserve the CSL will define a new kind of lattice, which is known as the "Displacement Shift Complete" Lattice (DSC) (Bollman, 1970) It represents a displacement that conserves symmetry.

From this it is possible to determine that dislocations in the DSC lattice preserve the structure of the boundary and leave the coincidence relationship undisturbed. They may

however, introduce steps into the plane of the boundary. Most importantly, a grain boundary that is close to, but not exactly at a low Σ orientation may decrease its energy if grain boundary dislocations with a Burgers vector of the DSC lattice, belonging to the low Σ orientation are introduced so that the dislocation free parts are now in the precise CSL orientation and all of the misalignment is taken up by the grain boundary dislocations.

However, the DSC lattice and its CSL basis are fraught with problems due to the discreteness of the CSL concept. Any theory that allows the thorough description of the special grain boundary structure must be a continuum theory; in that it gives results for a continuous variation of the crystal orientation and grain boundary type.

2.2.3 The O-Lattice Theory (OLT).

The theory of the "O-Lattice was published by Bollmann (1970) and provides a continuum theory of grain boundary structure. The theory is based around two basic principles:

1. Transform lattice 1 by rotation, stretching, or any other means relative to its original position.
2. Determine equivalence point between lattice 1 and the new lattice, lattice 2. These points of equivalence need not be restricted to lattice points, but can be any equivalence points within two overlapping unit cells.

If we designate an arbitrary point within the unit cell of lattice 1 by the vector $\underline{r}(i)$, then it will be transformed to $\underline{r}(ii)$ by the transformation. The point defined by the vector $\underline{r}(ii)$ within the unit cell of lattice 2 is said to be an equivalence point to the point defined by the vector $\underline{r}(i)$ in lattice 1.

It is now necessary to define a mathematical formulation for the conditions at which the coincidence of equivalence points occurs. This can be done by considering the fact that

the point in lattice 2 can be defined by taking the vector $\underline{r}(i)$ from lattice 1 and adding a translation vector to it to define the equivalence point in lattice 2.

There can of course be more than one equivalence point, so we must also define the set of all equivalence points in lattice 1 by C_1 and the set of points in lattice 2 by C_2. The vectors which point to equivalence points of the respective sets can now be defined as $\underline{r}(C_1)$ and $\underline{r}(C_2)$. We can now represent the transformation as:

$$\underline{r}(C_2) = A[\underline{r}(C_1)] \qquad \textbf{Equation 2.6}$$

Where A is the transformation matrix, which describes how lattice 2 originates from lattice 1.

We now assume a coincidence of equivalence points after the transformation has occurred and denote this equivalence point as $\underline{r}_0$. This point can be described by the vector $\underline{r}(C_2)$ or by a translation vector, $\underline{T}(i)$ added to the vector $\underline{r}(C_1)$ as shown below.

$$\underline{r}(C_2) = \underline{r}(C_1) + \underline{T}(i) = \underline{r}_0 \qquad \textbf{Equation 2.7}$$

Now by substituting equation 5 into equation 6 we get $\underline{r}_0 = A^{-1}(\underline{r}_0) + T(i)$. Now rearranging the terms using matrix calculus and introducing the identity matrix gives the fundamental equation of O-Lattice theory:

$$\left(I - A^{-1}\right)\underline{r}_0 = \underline{T}(i) \qquad \textbf{Equation 2.8}$$

This equation implies that for a given orientation relationship between two grains, the solution for $\underline{r}_0$ defines all the coincidence points, now called O-Points of both lattices. The coincidence of lattice points is a subset of the general solution for the coincidence of equivalence points

It is possible to derive the CSL lattice from the O-Lattice, and this is achieved by considering the case where the subset of the O-Lattice where all coinciding equivalence points are also lattice points in both lattices. Implying that the CSL is simply a special case of O-Lattice theory.

2.2.4 CSL / O-Lattice Comparison

Like the CSL, the O-Lattice has no physical reality if not at a grain boundary. Though unlike the CSL, it always exists and is defined in both crystals. The O-lattice also allows the determination of the optimum plane of a grain boundary for any given orientation, unlike the CSL, which can only provide this information for CSL orientations. A boundary between two crystals of a given orientation that intersects as many O-Lattice points as possible will have the best physical fit along the boundary.

2.2.5 Other Models

Other interface models do exist, such as that proposed by Gómez et al (1998) in which the concept of coincidence is generalised in order to formulate a general geometric theory of crystalline interfaces. It is claimed that the theory explains how some boundaries with low values of $\sum$ provide a poor registry between the lattices, whereas for others the agreement is good. They postulate that points of good fit relevant to the construction of a geometric theory of crystalline interfaces are the midpoints of pairs of points from either lattice but where the points are close enough; meaning that they both lie in the intersection of their corresponding cells. Others include the coincident axial direction (CAD) approach to grain boundary structure (Randle and Ralph, 1988), which describes grain boundary geometry in terms of the near parallelism of plane stack normals in neighbouring grains. Boundaries whose axes of rotation are within a certain angular limit of low-index directions are called CAD boundaries. It was demonstrated that the CAD model is a special case of the CSL model and can be applied in an analogous manner.

2.3 Grain Growth

2.3.1 Normal and Abnormal Grain Growth

Grain growth refers to the increase in the average grain size associated with a post recrystallisation anneal (Randle et al, 1986). Grain growth is not a continuation of the primary recrystallisation process but is a separate phenomenon driven by a different force than that driving primary recrystallisation. The driving force behind primary recrystallisation is the stored energy of the cold work, while the driving force for grain growth is the reduction in the energy associated with the grain boundaries accompanied by the decrease in the grain boundary area as the grain grows. The driving forces involved in grain growth are approximately two orders of magnitude less than those for recrystallisation.

Normal grain growth is characterised by an approximately uniform grain size distribution whereas abnormal (or anomalous) grain growth or secondary recrystallisation refers to the case where only a few grains in the structure grow which can give rise to a bimodal grain size distribution. It is possible for this process to continue to the extent that the few growing grains consume all of the fine grain material leaving a structure consisting of a few very large grains, having a uni-modal grain size distribution.

The factors which are believed to restrict normal grain growth are thought to promote anomalous grain growth if the inhibiting influence is distributed in such a way that a few favourable grains exist to act as embryos for the process. These factors are believed to include the segregation of solute species to grain boundaries, the presence of a strong texture in the material and the interaction between grain boundaries and fine particles in the material. (Aust and Rutter, 1959)

Solute inhibition.

It has long been recognised that the presence of solutes at the grain boundary can have a pronounced effect on the grain boundary mobility by a drag effect (Jensen, 1995), resulting in the inhibition of grain growth in the material. It has also been found to be true that the depletion of solutes at a grain boundary can cause an increase in the grain boundary mobility, resulting in more prolific grain growth.

Texture inhibition.

A large amount of texture in a material can cause an inhibition in the grain growth of the material due to the fact that where there is pronounced texture, there will be a corresponding pronounced proportion of low angle boundaries. These low angle boundaries are known to exhibit low mobility; hence the process of grain growth will be inhibited. Any grains which are not of this preferred orientation will then tend to act as embryos for the onset of secondary recrystallisation. Work by Jensen (1995) termed this type of effect 'Orientation Pinning'. It is described as the process whereby the growth of grains with a low probability of being pinned by the immobile low-angle or twin boundaries is the preferred method of grain growth.

2.3.2 Modelling of Grain Growth

The theoretical analysis of grain growth, beginning with the model of Hillert (1965), has been analysed extensively by computer simulations since the early 1980's. These studies have yielded a significant amount of knowledge about the influence of the character and structure of grain boundaries on the properties of polycrystalline material.

The process of normal grain growth is the uniform increase in the average grain size of the material, resulting in the annihilation of small grains by grain boundary migration. The driving force for this migration being the reduction in grain boundary energy, whereby grain boundaries possessing curvature will tend to reduce their area by migrating to the curvature origin. If it is assumed that the migration velocity of a grain boundary is proportional to the curvature then the grain growth behaviour of a polycrystalline material can be represented by

$$r_a^m - r_0^m = Kt \qquad \textbf{Equation 2.9}$$

Where t is the reaction time, r_a is the radius of the grain at time t, r_0 is the initial vale of r_a at t=0, m is the grain growth exponent and K is the kinetic coefficient depending on temperature, mobility and boundary energy. This equation has been verified by a number of different methods and is now a generally accepted equation for the characterisation of normal grain growth behaviour.

Computer simulation models can be broadly divided into to distinct groups, classified as deterministic models and probabilistic models. The most widely used of the probabilistic models is the Monte-Carlo method (Miodownik et al, 1999), which is derived from the principle of atomic jumps across grain boundaries (Anderson et al, 1984). It is an easily implemented simulation both in two and three dimensions, but is limited by the fact that the definitions of lengths and time-scales are not at atomistic scales, the characteristic length scale employed in the Monte-Carlo is more comparable to the length of the

boundary facet than it is to atomic dimensions. Also, there is an unclear relationship between Monte-Carlo time and the physical time. Despite these limitations, the Monte-Carlo method is capable of giving grain size distributions close to those observed experimentally and gives a value of m=2 for Equ.2.9.

For deterministic computer simulation models, the changes in grain boundary energy provide the expression for the velocity of the grain boundary normal to itself, which is proportional to the curvature of the boundary. Deterministic models can be sub-divided into those that use straight-line grain boundaries (Kawasaki et al, 1989), and those which employ curved grain boundaries (Miodownik et al, 2000). In the former models, it must be assumed that the mobility of each grain is much larger than that of the triple point. In the microstructure of straight grain boundaries, a net force is exerted at the triple points by the surface tension of the grain boundaries and the triple points move under the action of this force. The advantage of this modelling method is the provision for a simple description of microstructure.

Monte Carlo (Anderson et al, 1984) simulations of grain growth were performed by Ono et. al. (1999) for two-dimensional poly-crystals with crystallographic orientations being assigned to individual grains in terms of randomly generated Euler angles. Individual grain boundaries were characterized by the orientation relationships of grains across them and grain boundary energies were given with a continuous function of deviation angle from the exact coincidence orientation relationships. Their simulations showed that the energy spectra make the grain size distribution more symmetric, they lessen the average grain growth rate and the fraction of low energy boundaries increases with grain growth.

Work by Kim (2000), recently proposed a model for the grain boundary migration by atomic jumps across grain boundaries, where the moving velocity of the grain boundaries is proportional to $e^{(-1/r)-1}$ not 1/r where r is the grain radius, resulting in a growth rate slower that classical predictions for small grain sizes. In the model, the reduction in grain boundary energy during grain boundary migration was regarded as the driving force for atomic jumps, and an analysis was carried out on the isolated two-dimensional and three

dimensional grains. The results of which, showed there to be a 1/2-power growth law for the average grain size and also that the size and side distributions are time-invariant.
Other models recently developed include a two-dimensional frame-invariant phase field model of grain boundaries (Kobayashi et al, 2000), which allowed one-dimensional solutions for a stable grain boundary in a bi-crystal to be obtained and equilibrium energies to be computed.

2.3.3 Kinetics of Grain Growth

Under isothermal annealing conditions, normal grain growth can be described by the relationship shown in equation 2.9

$$r_a^m - r_0^m = Kt^n$$

The term n in the above relationship is a constant with a theoretical maximum of 0.5 which is only approached for ultra high purity metals at temperatures approaching their melting point (Randle et al, 1986). Much work has been undertaken regarding the determination of the value of n for different materials (Simpson et al, 1971). For other materials n is usually found to be less than 0.4, being as low as 0.06 in some cases. This was thought to be due to the effects of solute inhibition, particle interaction or the effects of texture in the material. Though work by Anderson et al (1984) has suggested that values of $n < 0.5$ are inherent of the growth process and are not a consequence of impurities in the material.

Work by Simpson et al (1971) on dilute cadmium and lead base alloys revealed that there are four stages of grain growth as a function of annealing temperature and solute concentration, with the second stage (occurring at 0.7Tm), resulting in a substantial change in grain size, involving irregular grain growth or secondary recrystallisation. They determined that as a result of the occurrence of four stages of grain growth, the relationship $R - R_0 = k.t^n$ is not valid and there cannot be a single value for activation energy. It was also determined that the latter stages of grain growth may not be a true effect, but merely a change in the grain growth rate due to surface effects occurring as the average grain diameter becomes comparable to the sample dimensions.

2.3.4 Abnormal Grain Growth

Secondary recrystallisation may be initiated by an incomplete restriction on normal grain growth or by an inhomogeneous initial grain size distribution in which there exist grains with an initial size advantage and hence these grains will become a driving force for continued growth. Work by Hillert (1965), predicted that grains with an initial radius that is 1.8 times greater than the average grain size would be unstable with respect to grain growth. However, computer simulations seem to indicate that the presence of abnormally large grains in the microstructure is, in itself, an insufficient factor in the nucleation of secondary recrystallisation but that retained strain energy from primary recrystallisation may be an important factor in anomalous grain growth.

The presence of texture in the material can have a pronounced effect on the extent of grain growth. Grain growth can be inhibited by the texture in the material due to the fact that boundaries between the grains of a preferred orientation tend to be low angle boundaries that exhibit low mobility. Grains that are not of a preferred orientation or are larger than the average grain size may then act as a catalyst for the process of secondary recrystallisation.

Grain growth is achieved by the migration of grain boundaries through the material, the driving force for grain growth being the reduction of the grain boundary area. Grain boundary mobility depends on the grain boundary energy, grain boundary structure, solute interaction and a number of other factors including the misorientation between the adjoining grains. During the process of grain growth, the different rates of grain growth are responsible for the texture and final grain size distribution in the material.

Grain boundary migration models are usually based on the assumption that the atoms are continually detached from a grain and that they move into the disordered region between the two grains. The atoms that are detached from their parent grain can then either be reattached to the same grain or can become attached to another neighbouring grain. As the detachment and reattachment of atoms from grains can occur simultaneously, the rate

of grain boundary migration is dependant on the rate at which the process takes place (Humphreys and Hatherly, 1995) The energy required for this process comes from the thermal activation and thus the grain boundary mobility depends on temperature according to an Arrhenius type equation.

Work by Aust and Rutter (1959) confirmed that the differences in grain boundary mobility arise from an orientation dependence of solute segregation to the boundary in high purity metals, rather than an intrinsic relation between the grain boundary mobility. Aust and Rutter also showed that the coincidence site lattice (CSL) boundaries are more mobile than random boundaries up to an impurity level of 0.006 wt% Sn in Pb. At higher impurity levels the differences between the CSL boundaries and the random boundaries become trivial (Humphreys and Hatherly, 1995).

For some time, work has been carried out in order to determine the types of boundaries that are responsible for abnormal grain growth. Work by Harase et al (1991), led to the idea that certain CSL boundaries have certain high mobility's which give rise to the onset of abnormal grain growth, they argued that among various CSL boundaries, $\sum 9$ played an important role in the development of {110}<001> texture in Fe-3% Si electrical steel, although the influence of other CSL boundaries was not ruled out. Much work has been published on the possible role of $\sum 9$ and other CSL boundaries on abnormal grain growth, yet this role has not been adequately confirmed.

Experimental observation by Lin et al (1997) determined that there was a 13% probability of formation of $\sum 3$-$\sum 9$ CSL boundaries in the primary recrystallised matrix and that they can be assumed particularly mobile. They also concluded that there is no structural or energetic basis for an enhanced stability of the $\sum 3$ boundary in bcc materials.

Other groups (Hayakawa et al, 1996) have debated the role of high-energy grain boundaries in the middle misorientation range ($20\text{-}45^0$) have on abnormal grain growth. Work by Hayakawa and Szpunar (1997) successfully explained the Goss texture development in Fe-3% Si steel using EBSD measurements and Monte-Carlo simulations

under the assumption that high-energy grain boundaries have a high mobility. They emphasised the importance of the systematic pinning of precipitates on the high-energy grain boundaries that are responsible for the abnormal growth of Goss orientation. A computer technique developed by Rajmohan et al (1999). to study the mobility conditions for abnormal grain growth in a matrix of primary recrystallised Fe-Si steel showed that Goss grains grow abnormally in both conventional and high permeability steels by assigning a high mobility to grain boundaries in the interval of 20-45^0. This simulation reproduces the experimentally observed grain boundary character distribution (GBCD) around the Goss grain during grain growth.

Other work by Hayakawa et al (1998) implied that the role of CSL boundaries in the process of secondary recrystallisation is negligible, due to the fact that there are too few of them, and the frequency that they occur does not change during grain growth. The only exceptions they found to this were in the proportions of $\sum 1$ and $\sum 3$ boundaries, which displayed an increase in proportion after annealing which they attributed to the fact that both $\sum 1$ and $\sum 3$ boundaries are less mobile than other boundaries, hence will be more abundant in the latter stages of grain growth.

2.3.4 Strain and Anomalous Grain Growth.

The development of anomalous grain growth can be enhanced in austenitic stainless steel, by the application of a post-recrystallisation strain of less than 2%. This increase is attributed to a reduction of two orders of magnitude in the grain growth incubation period and an increase in both the rate of grain growth and the number of anomalous grains (Randle and Brown, 1988). It was found that the proportions of CSL boundaries increased during post-strain anneals and that most of the CSL's tended to occur in clusters, the clustering being most prolific towards the end of the grain growth incubation period. From this information it was proposed that 'special' boundary clustering is an instrumental factor in the initiation of anomalous grain growth (Special boundaries being those with $d/a>0.15$, where d is the interplanar spacing in the boundary plane relative to the lattice parameter a). Further work by Randle (1993) on pure nickel suggested that the grain growth incubation period is in fact a grain boundary recovery stage involving thermally induced structural rearrangements of the grain boundaries, with or without migration, which leads to an increase in the development, and degree of anomalous grain growth.

2.4 Segregation

2.4.1 Introduction

The segregation of impurities to grain boundaries in a material during high temperature heat treatment has a great number of effects that have been extensively studied over the years. In the case of low alloy steels, this interest is due to the fact that the segregation of elements such a phosphorus and sulphur can cause the grain boundaries to become very weak and brittle.

The grain boundaries in a material can often be found to have chemical compositions that are very different from the surrounding matrix. It is primarily the enrichment of impurity elements at the grain boundaries which gives rise to these compositional differences and this is responsible for the significant effects on the properties of the material. These segregated impurities can have many effects, such as intergranular brittle fracture and intergranular environmental failures and it is these problems that has led to the vast amount of research that has been undertaken in the area of segregation and the understanding of how segregation occurs.

2.4.2 Segregation Processes

The process of grain boundary segregation occurs due to the diffusion of atoms from the matrix to the grain boundaries. The impurity atoms are often a different size to the atoms making up the matrix and hence prefer to make chemical bonds in sites other than those imposed by the lattice. The energy of the system may be lowered if the impurity resides in the grain boundary, where an array of sites are available to it. Thus, if a diffusing atom moves into a grain boundary site, it may be become trapped. It is this process that gives rise to the increase in the concentrations of some impurity elements at grain boundaries (Briant, 1999)

Another parameter than can affect grain boundary segregation is grain boundary structure. High angle grain boundaries absorb more segregant than twin or low angle grain boundaries, but among high angle grain boundaries there can be variation in the amount of segregant (Ogura et al, 1978).

2.4.3 Segregation Analysis

For Auger analysis, the specimens are fractured by impact at low temperatures, where the fracture is generally brittle for ferritic materials. However, the appearance of the fracture surface may be very different, since either intergranular fracture or transgranular cleavage can be observed. Intergranular fracture indicates a weakening of intergranular cohesion, and it can be clearly shown that the degree of intergranular fracture increases with the grain boundary concentration, e.g., of phosphorus (Cowan, 1997) When the specimens also contain some carbon, the degree of intergranular fracture decreases with increasing bulk and grain boundary concentration of carbon. This is caused not only by the competition for sites and the displacement of phosphorus by carbon but also by an increase in grain boundary cohesion caused by carbon. The latter conclusion was drawn from the observation that Fe-P specimens show more intergranular fracture than Fe-P-C specimens, also in cases of equal grain boundary concentrations of phosphorus. This difference in the effect of phosphorus and Y) carbon was suspected by earlier authors (Briant, 1999).

A more quantitative characterization of this effect is possible by the use of notch impact tests, in which the impact temperature is measured as a function of specimen temperature. Curves are obtained from a lower range of brittle fracture at a low impact energy, which increases in a higher temperature range to the upper energy corresponding to ductile fracture. The temperature at which the impact energy is one-half of the upper energy, i.e., the ductile to brittle transition temperature (DBTT), can be taken as a measure of brittleness. The higher the DBTT, the more brittle the material. It is also possible to use

the fracture appearance transition temperature (FATT), at which the fracture is 50% brittle and 50% ductile.

It has been demonstrated for several steels that the DBTT or FATT increases proportionally to the grain boundary concentration of phosphorus. Thus, this measure of embrittlement is clearly correlated to the presence of an embrittling element at the grain boundaries. Suzuki et al (1983) measured the DBTT for several binary and ternary Fe alloys. They clearly showed for a Fe-0.52% P-8ppmC alloy that as a result of an increase of C grain boundary concentration at constant P grain boundary concentration the DBTT decreases, i.e., the material becomes less brittle. The DBTT decreases with increasing C bulk concentration, which is explained by site competition and the displacement of P by C and also by the increase in grain boundary cohesion. The increase in DBTT by the addition of >100 ppm C is due to the formation of pearlite nodules along the grain boundaries. The same authors measured grain boundary segregation and DBTT for Fe-Mo-P, Fe-Cr-P, Fe-Ni-P, and Fe-Si-P alloys. They confirmed that the addition of Mo has no effect on the grain boundary segregation of P, in agreement with earlier studies, whereas the DBTT and yield stress decrease with increasing Mo bulk concentration. The DBTT decrease is attributed to the relatively low grain boundary segregation of Mo.

The effects of Cr are very similar. It has no effect on P segregation, and it decreases the DBTT and reduces intergranular fracture. For Fe-Ni-P alloys the addition of Ni had no effect on the segregation of P but reduced the DBTT. However, the reduction of the DBTT was explained to be a result of the solution softening of Ni. The addition of up to 1.0% Si to an Fe-0.2% P alloy reduces intergranular fracture and increases the DBTT; the addition of more Si enhances transgranular fracture and increases the DBTT. The reduction of intergranular fracture is partly attributed to the decrease of P segregation and increase of C segregation caused by the Si addition. The segregation of Si itself increases the grain boundary cohesion, to explain fully the reduction of intergranular fracture.

There has been much controversy about the role of manganese. It has been clearly proven that increasing the concentration of Mn in Fe-Mn-P alloys free of carbon does not affect

the grain boundary segregation of P. Only if carbon is present is there an increase of P segregation with Mn content (Grabke et al, 1987), due to the reduction of carbon concentration in the solid solution and at the grain boundaries.

However, Mn itself segregates to the grain boundaries. The manganese segregation may cause a certain embrittlement and induce intergranular fracture (Yu-Qing and McMahon, 1987). In fact, the DBTT was found to increase for Fe-Mn alloys up to about 8 wt% Mn (Lee and Morris, 1983). For higher Mn contents it decreases continuously, and the fracture is intergranular at high Mn concentrations. This peculiar behaviour, however, is microstructurally determined. Thus, the main effect of Mn is to reduce the carbon solubility and grain boundary segregation, thereby allowing enhanced P grain boundary segregation. Secondly, its own segregation may cause some embrittlement.

These fundamental results are partially reflected in empirical equations meant to describe the embrittlement of steels by some alloying and impurity elements. Two of the embrittlement parameters are widely used: the Bruscato factor X and the J factor proposed by Watanabe and Murakami (1981)

$$X=[10P+5Sb+4Sn+As]\times 10^{2}\ \text{wt\%}$$

$$J = [Si + Mn]\,[P + Sn] \times 10^{4}\ \text{wt\%}$$

The lower these factors, the less embrittlement is to be expected for low alloy ferritic steels. In the Bruscato factor, only the embrittling elements themselves are considered, in the J factor, Si and Mn are also important, where the role of Si is not yet clear and Mn mainly accelerates embrittlement by enhancing the diffusivity of P (Grabke, 1987).

An attempt was made to measure directly the effect of non-metal atoms on the adhesion of two iron surfaces brought into contact with each other in a UHV system in which surface concentrations on the specimens are measured before contact (Hartweck and Grabke, 1981). The results showed that in the monolayer region adsorbed non-metal atoms C, N, S, and P all increase the adhesion. This result appears reasonable, since all

these non-metal elements have attractive interactions with iron and form compounds with it. If all non-metal elements are able to enhance grain boundary cohesion, then the question remains as to why S and P embrittle grain boundaries. As a possible explanation, an effect on the grain boundary structure has been put forward (Grabke, 1987) that is based on the observation that faceting has been observed on grain boundary fracture faces of embrittled iron or nickel, caused by grain boundary segregation of S, Se, Te, or Sb. Most probably, the segregation of these strongly embrittling elements leads to a reconstruction of the grain boundary faces and formation of two more or less faceted surfaces, which are easily separated. In the case of Te, this separation occurs spontaneously without any load being applied. For the other elements the reconstruction is less severe but still causes separations, whereas in the case of P in iron only a certain loss of coincidence is caused by the segregation and the formation of high-angle boundaries with less cohesion. In contrast, carbon, nitrogen, and boron will fit very well in low-angle boundaries and may stabilise and strengthen such strong grain boundaries by additional covalent bonding with the iron atoms. More studies are necessary on the structures of grain boundaries affected by segregation to answer the question of the cause of embrittlement.

2.5 Fracture

2.5.1 Introduction

The fracture of materials is a critical factor in the design and application of any material, especially for a material where its performance has a direct result on public safety. The understanding of the fracture process allows us to better protect ourselves from the catastrophic failures that have caused disaster in the past.

Fracture is defined as the separation of an object into two or more separate pieces as a response to active stresses applied below the melting point of the material and may occur in either a ductile of brittle manner. The mode of fracture is dependent on the properties that control the amount of plastic deformation in the material; these include the modulus of elasticity, the crystal structure of the material and the temperature at which fracture occurs.

Ductile fracture differs from brittle fracture in that 'necking' occurs to the sample, i.e. the sample stretches and becomes narrower at its middle due to plastic deformation and energy absorption before failure. This mode of fracture can usually be recognised due to the presence of a 'cup and cone' structure on the fracture surfaces.

Brittle fracture occurs in metals with virtually no plasticity and low energy absorption before failure. It can be recognised by the following features:

1. Little or no macroscopic plastic strain to failure is observed.
2. There is little evidence of local micro structural-scale plastic strain accompanying failure.
3. Crack propagation is spontaneous and rapid, occurring perpendicular to the applied stress forming an almost flat fracture surface.

4. Unstable or catastrophic failure occurs at applied stresses less than the general yield strength of the un-cracked specimen at the start of instability.

The commonly identified fracture mechanisms in metals are transgranular cleavage and intergranular fracture, both of which are of great significance to the world of technology.

Transgranular cleavage is the process of fracture where the fracture path travels through the grains of the material. The fracture path will change its direction of propagation from grain to grain due to the different lattice orientations of the atoms within each grain. Cracks will naturally choose the path of least resistance and will choose a new path or plane of atoms along which to travel should a path of lower resistance become available.

Intergranular fracture is the process whereby the crack follows along the grain boundaries of the material and does not travel through the grains themselves. It is usually the preferred method in materials where the cohesive energy of the grain boundary is lower than the cohesive energies within the crystal lattice of the grain. The proportion of intergranular fracture can be greatly increased by factors such as the segregation of embrittling elements to the grain boundaries of the material.

2.5.2 Fracture Mechanics.

Much work has been done in an attempt to understand the nature of brittle fracture, and it is generally agreed that brittle fracture can be thought of as a simple elastic extension of atomic bonds to the point of final separation and that the key to its understanding lies with the nature of the atomic bond. The process of brittle fracture can thus be though of as the sequential breaking of atomic bonds. The exact nature of the bond rupture process in fast fracture has yet to be identified and it is not clear what sequence of events occurs during the fracture process (West et al, 1999)

2.5.3 Griffith Theory of Brittle Fracture.

Work by Griffith (1920) proposed a theory by realising that a crack will propagate when the decrease in elastic strain energy is at least equal to the energy required to create new crack surfaces. He was able to conclude that the critical propagation in a brittle material is given by:

$$\sigma_f = \left(\frac{2E\gamma_s}{\pi c}\right)^{1/2}$$

Equation 2.10

Although this equation gives a physical relation for the critical fracture stress, it has limited application due to the fact that it is specific to the case of uniform stress and infinite relative dimensions.

Irwin (1948) used the Griffith approach as the basis for his subsequent work, he used the term G to represent the strain energy release rate and crack driving force; where $G=2\gamma_s$. This results in the Griffith equation for fracture stress becoming:

$$\sigma_f = \sqrt{\frac{GE}{\pi c}}$$

Equation 2.11

Irwin was also responsible for defining the stress intensity factor, K, which could be used to uniquely define the stress state at the crack tip, without the need to determine the actual stress. This eliminated the problems of equations tending to infinity.

$$K = \sigma\sqrt{\pi a}$$

Equation 2.12

This stress intensity factor can be used like stress in order to predict the critical condition at fracture. Fracture will occur in a material if;

$$\frac{K_c}{K} \geq 1$$

Equation 2.13

Where K_c is a material property known as the fracture toughness and K is the stress intensity factor for a particular combination of crack length and stress in the component. It should be noted that the stress intensity factor is defined for the special case of an idealised crack in an infinite plate. Real cracks are affected by the geometry of the component, the applied stress field and a number of other factors.

Plane Strain Fracture Toughness

The parameter K_c is dependant on the thickness of plate up to a certain point above which it becomes a constant. This constant value is known as the plane strain fracture toughness, and is denoted by:

$$K_{Ic} = Y\sigma\sqrt{\pi a}$$

Equation 2.14

With the I subscript denoting a "Mode I" crack displacement. There are three modes designated by Roman numerals as; I (Opening), II (Sliding), III (Tearing), the most critical being Mode I due to the fact that the crack tip carries all the stress. In modes II and III some of the stress is carried by the interaction of opposing crack faces. Brittle materials tend to have low K_{Ic} values that lead to catastrophic failures, whereas ductile materials tend to have much higher K_{Ic} values. The value of K_{Ic} increases as the grain size of the material increases and decreases both with increasing strain rate and decreasing temperature.

2.5.4 Causes of Brittle Fracture.

The most important factor that causes a material to fracture in a brittle matter as oppose to a ductile manner is temperature. At higher temperatures the yield strength of the material is lowered and the fracture becomes more ductile in nature. At lower temperatures, the yield strength is greater while the fracture of the material becomes more brittle in nature. This is due to the fact that at higher temperatures, the atoms in the material vibrate with a greater frequency and amplitude. This increased vibration allows the atoms under stress to slip to new places in the material and this slippage of atoms is seen on the outside of the material as plastic deformation. At lower temperatures the atoms in the material are less inclined to slip to new locations, so when the stress on the material becomes high enough the atoms simply break their bonds and do not form new ones. This results in very little plastic deformation and thus a brittle fracture. At moderate temperatures, with respect to the material, the material exhibits characteristics of both fracture types.

Another factor that induces brittle fracture is the dislocation density of the material. The higher the dislocation density, the more brittle the fracture will be, for as the dislocation density increases due to the applied stress above the yield point, it becomes increasingly difficult for the dislocations to move due to the fact that their strain fields interact with each other (Chen et al, 1993). Materials that already have a high dislocation density are only able to deform a certain amount before it fractures in a brittle manner.

The third factor that induces brittle fracture is the grain size of the material. As the grains get smaller, the fracture process tends to be more brittle. This is due to the fact that in smaller grains, the dislocations have less space to move before they make contact with a grain boundary. As the dislocations cannot move very far, there is very little plastic deformation. Thus, the fracture mode of the material is more brittle.

2.5.5 Atomic Simulation of Brittle Fracture

The fracture of any material is ultimately determined by the behaviour of the atoms of which the material is composed. This is never more evident than for the process of brittle fracture, due to the requirement that the crack in a perfectly brittle material must be atomically sharp at its tip. The crack then propagates in such a way as to break individual bonds in the material. However, most brittle fracture analysis is done in a way that does not consider the complexities that occur on the atomic scale, such as the work by Griffith. (1920).

Continuing improvements in computational power over the last decade have however allowed the analysis of atomic-scale fracture simulations to take place and have allowed more sophisticated models of atomic interactions to be developed. These have then gone on to update some of the classical models that have been unable to accurately predict material properties. Hauch et al (1999) noticed that many commonly studied interatomic potentials predict that silicon is ductile at low temperatures, where it is actually brittle.

Work by Gumbsch and Cannon (2000), also addressed the fact that continuum fracture mechanics is insufficient in its explanation of many common experimental observations. They dealt with the phenomenon of "lattice trapping', first identified by Thomson et al (1971), and showed that it gives rise to directional anisotropy and cleavage along surfaces that are not low in energy. They also performed a detailed analysis of the cases where lattice trapping can contribute significantly to the difference between the observed energy release rate for crack propagation and the work required to create two new surfaces.

Other work on atomic simulation theory by Selinger and Farkas (2000) revealed how the structure of low angle symmetrical tilt boundaries can give rise to directional anisotropy in fracture resistance, another feature that cannot be predicted by Griffith theory. All the work that has taken place in this field has shown that atomic-scale processes that occur at the crack tip produce macroscopic effects, that cannot be explained by continuum theories alone.

2.5.6 Fracture Modelling

In α-iron and ferritic steels, the preferred cleavage planes are {001} and the fracture path will choose to travel along these planes. When this is not possible, due to the orientations of the grains, the fracture path will be forced to travel intergranularly, in order for the crack to propagate. Localised intergranular fracture will then be seen on the fracture surface of the material, as well as cleaved {001} facets. Crocker et al (1996) used three-dimensional theoretical models in order to show that grain boundary fracture may occur by one of four distinct mechanisms. Their models yield an estimate of 30% for the proportion of intergranular failure, though their experimental data gives a figure of 20% for α-iron and as low as 2% for ferritic steel. They were able to account for this by the fact that grains in polycrystals are multi-connected, allowing alternative routes for the fracture path. They also outlined the importance of the grain boundary surface energy and the orientation of the applied stress and the necessity for these factors to be taken into consideration more comprehensively by the model if a better correlation with the experimental data is to be obtained.

It is clear to see from this that the modelling of the fracture process in α-iron and ferritic steels is not a trivial matter. However, the work by Crocker et al (1996) showed that geometrical factors have a major influence on crack propagation in polycrystalline materials in the cleavage regime.

Work by Wolf (1991) used a Random Grain Boundary model in order to determine the work of adhesion of symmetrical high angle twist grain boundaries. From this work, he was able to conclude that there are two types of grain boundary planes with different properties; Firstly, there are the most widely spaced planes, termed 'special', whose energies and grain boundary ideal cleavage fracture energy are governed by the interplanar lattice spacing. On the vicinal planes, the grain boundary and cleavage energies are determined by the Read-Shockley model; i.e. by the shapes of the related energy cusps. Wolf was also able to determine that the twist boundaries on the 'special'

planes have the highest cleavage energies. This he attributed to the dramatically different elastic energies associated with grain boundary dislocations and surface steps. During the fracture process, long range dislocation strain fields are converted into short range elastic strain fields associated with the surface steps. Wolf also outlines the similar distinctions between this work and the case of flat and vicinal free surfaces.

2.5.7 Segregation and Fracture

Intergranular fracture indicates a weakening of intergranular cohesion, and a large contributing factor to this reduction in cohesion is the segregation of solute elements to the grain boundaries in the material. It has long been known that the segregation of phosphorus to grain boundaries can cause a reduction in the grain boundary cohesion Erhart and Grabke (1981) of the material and the presence of carbon in the material has the effect of reducing the proportion of intergranular fracture. This can be partially attributed to site competition, where phosphorus is displaced from the boundary by carbon, but is also due to the fact that carbon actually increases the extent of grain boundary cohesion. This conclusion was made by Erhart and Grabke (1981), based on the observation that Fe-P specimens show more intergranular fracture than Fe-P-C specimens.

It has been of much debate as to why some elements such as phosphorus and sulphur are able to embrittle grain boundaries and elements such as carbon, are able to strengthen them. Quantum mechanical calculations have shown (Briant, 1999) that P and S will be negatively charged when they are surrounded by iron atoms, and hence they draw an electronic charge away from the metal atoms. From this it was concluded that the metal-metal bonds in the vicinity of the P atoms are weakened and thus an easy path for fracture is created in the lattice planes that are in the vicinity of a grain boundary that has P segregation present on it. Carbon is thought to be positively charged and hence has the opposite effect.

2.5.8 Methods of Fracture Surface Analysis

A number of authors have described experimental methodologies for the purposes of data acquisition by fracture surface analysis, many of which are described later on. Numerous practical methods have been used in an attempt to accurately determine the crystallographic morphology of a fracture surface and most of these techniques are fraught with challenges. A thorough understanding of the fracture surface when combined with other crystallographic and compositional information would provide much about the fracture process and may help to provide a better understanding of the causes of fracture and the prevention thereof.

Direct Fracture Surface Analysis.

The direct analysis of a fracture surface by EBSD is a non-destructive technique by which crystallographic information is acquired directly from the fracture surface (Randle and Davies, 1999). This information can then be used together with the topographical information from the surface in order to produce an accurate correlation between the crystallographic and macroscopic orientation of the fracture facets. One of the first experiments of this type was performed by Slavik et al (1996) using quantitative tilt fractography in order to determine the fracture facet crystallography of an Al-Li-Cu alloy. The orientation of the grains was determined by EBSD taken from a polished surface perpendicular to the fracture surface. SEM images of the fracture surface were then acquired at a number of different tilt angles and a series of measurements of the projected lengths between features on the fracture surface were made, which was combined with the EBSD data in order to determine the fracture surface crystallography.

In recent years, photogrammetry and stereo photogrammetry has been surpassed by the introduction of computer assisted stereo photogrammetry, whereby two images are acquired from the fracture surface with a small tilt angle between them (usually +2° and -

2° with respect to the primary beam direction). These images are then used by the computer, which calculates the parallax shift for each pixel using a digital image correlation analysis routine provided by the software. This data in then used by the computer in order to construct a three dimensional representation of the topography of the fracture surface, sometimes called a '3D elevation map'.

Other software has been developed for the purposes of representing and reconstructing fracture surfaces and cracks. One such package is termed 'FRASTA', or Fracture Surface Topography Analysis and was developed by SRI International (Kobayashi and Shockey, 1991). FRASTA can be applied to a fracture surface in order to create a series of fractured-area-projection plots, which are similar to the 3D elevation maps created by computer aided stereo photogrammetry. However, FRASTA can also produce cross sectional plots (XSPs), equivalent to an X-ray radiograph taken perpendicular to the fracture surface. The XSP displays a section perpendicular to the fracture surface displaying the microcracks in profile. It also shows how the two surfaces mach each other, the amount of overlap necessary before fracture (inelastic deformation) and the crack-face-opening displacement, which can be correlated to the stress intensity factor in order to determine the fracture toughness of the material and/or loading conditions.

Only a few experiments have attempted to combine such topographical information with crystallographic information acquired by EBSD (Semprimosching et al, 1997). This has mainly been due to the complexities involved, such as the constraints on the EBSD geometry and the laborious nature of the investigations.

Indirect Fracture Surface Analysis.

It is possible to determine the crystallographic orientation of facets on a fracture surface without taking measurements from the fracture surface itself. These indirect methods are achieved by taking EBSD measurements from a polished surface perpendicular to the average plane of fracture and combining this with fracture surface profile information

from at least two serial sections taken through the plane perpendicular to the fracture plane (Randle and Hoile, 1998).

A variation of this technique is to obtain data from a single polished section. Recently this has been achieved by the use of a 'matched fracture' specimen, where the specimen is mounted in such a way that the two halves be arranged as they were prior to fracture. The specimen can then be prepared for EBSD as if it was an un-fractured specimen. This technique allows transgranular and intergranular fracture facets to be immediately obvious, being identified by 'colour matching' across the fracture surface by overlaying the EBSD crystal orientation map over the secondary electron image. Proportions of intergranular and transgranular fracture can then be easily quantified (Williams et al, 2000).

2.5.9 Crystallography and Fracture

The influence of texture on the brittle fracture of polycrystalline materials has been a subject of much interest in recent years though little work has actually been done in the area. Motivated by the desire to better understand the processes that effect brittle fracture, many groups have applied the technique of electron back-scatter diffraction (EBSD) to failed specimens in the hope of determining whether there are specific crystallographic properties that are able to preclude or instigate fracture in a material.

A propagating inter-granular crack will continue along a grain boundary until it reaches a triple point in the crystal structure, upon where it has the option to either continue along one of the two available grain boundaries or to travel through the grain at which it has arrived. The choice is always along the path of least resistance as the crack weaves it way through the weaker, less cohesive route. If the cohesive strength of the matrix is greater than the cohesive strength of the boundaries, then the type of fracture will be primarily intergranular. If the opposite is true, the fracture will be transgranular. A number of different factors are known to influence the cohesive strength of a boundary, such as grain boundary segregation and irradiation. The crystallographic orientation of the grains can also have an effect on the path that the fracture decides to take through the material and much work has been done in order to better understand these effects.

Work by Field (1997) outlined the possibility of using EBSD on fracture surfaces in order to glean more information about the crystallographic properties that influence fracture. He described a technique where orientation measurements are taken directly from the fracture surface of the material, in order to determine the orientation of the grain boundary plane of the fractured grains. His work also outlined the numerous errors and inaccuracies that are manifest with this technique.

For the successful application of EBSD to fracture surfaces, a number of special parameters are required as well as normal crystallographic information to determine the

crystallographic orientation of a fracture plane. Much work on the application of EBSD to the determination of grain boundary plane has been achieved by a number of different techniques by (Randle, 1999., Randle and Davies, 2002), such as twin surface trace analysis and parallel sectioning. These techniques, though accurate, are very laborious and time consuming and thus cannot yield significant quantities of data (Williams, 1999).

The direct analysis of fracture surfaces by EBSD however, returns a significant quantity of data for very short analysis times, as it is possible to map the entire fracture surface. This allows data from all fractures facets that are orientated favourably with respect to the EBSD geometry to be acquired. This usually results in approximately 30% of all facets being indexed (Williams et al, 2000), with the possibility of up to 50% being suggested (Field, 1997). The accuracy of this data is a matter of much dispute as there are a number of assumptions being made, such as the notion that all facets from which data is being acquired are aligned at 70° to the incident electron beam and parallel to the phosphor screen. Estimates of this error are in the order of 5-10° from being normal to the mount (Field, 1997), though the effect of this error on the data has not precisely determined. This technique has however been used to some success previously by the author, in the determination of the cleavage plane of fractured Fe-P-C alloy (Williams et al, 2000), whereby it was accurately shown that cleavage is favoured along {001} planes. This is consistent with other work on similar materials and the fact that the {001} plane is the plane of lowest atomic density in bcc materials.

Wright and Field (1998) utilised a similar EBSD technique for this purpose and was able to acquire diffraction patterns from the fracture surface of a nickel based alloy, which showed a slight tendency for the fracture facet to correlate with the {200} plane in the crystal lattice. Fracture facets for a titanium alloy were also analysed and were found to closely align with the basal planes of the primary alpha grains.

EBSD techniques were also employed by Kim and Marrow (1999) to study cleavage fracture and crystal texture in age-hardened duplex stainless steel. They showed that the EBSD technique could be used in conjunction with trace analysis to determine the

orientation of cleavage planes in bulk samples. Their work showed that cleavage of ferrite in duplex stainless steels could occur along {001} planes and {112} twin habit planes.

Other work by Wright and Field (1998) confirmed the fracture resilience of annealing twins in fcc material, by determining there to be a deficiency of 60° boundaries present at the fracture surface of a stainless steel sample, even though they are prolific throughout the microstructure. It was also determined that 40° boundaries showed a propensity for cracking as there were a great number more in the fracture data than there were in the microstructure data.

The effects of grain boundary properties on the failure of materials were also investigated by Lehockey and Palumbo (1997) who determined there to be significant reductions in creep rate of nickel with increasing proportions of low-$\sum$ CSL grain boundaries. Other work by Lopes et al (1997) showed that the grain boundary character distribution of FeAl is a key factor in the propensity of intergranular fracture in the material. This led to the conclusion that there exists a potential correlation between grain boundary structure and the occurrence of intergranular fracture.

3. Experimental Procedures.

This chapter outlines the experimental procedures that were used in the investigations of the two Fe-P-C alloys. It also outlines the techniques that have been previously developed, to best determine the physical properties of the material under investigation. The principal technique for the majority of the analyses was electron back-scatter diffraction (EBSD), used in order to determine the crystallography properties of the specimens. Other established techniques used for this project include Scanning Electron Microscopy (Section 3.2), Auger microanalysis (Section 3.6), for the measurement of grain boundary segregation and computer-aided stereo-photogrammetry for the analysis and three-dimensional reconstruction of fracture surface topography (Section 3.5).

Other techniques had to be developed during the course of the project in order to be able to acquire the desired data. These included:

- Fracture Surface Analysis (FSA), used for the crystallographic analysis of fracture surfaces and combining fracture surface topographical measurements.
- Polished Fracture Surface Analysis (PFSA), enabling the combined acquisition of fracture surface crystallography, fracture surface topography and microstructure information near to the fracture path such as deformation twinning.
- Fracture Surface Serial Sectioning (FSS), used in order to acquire grain boundary populations using both halves of a fractured sample in order to determine the boundary types most resilient to grain boundary fracture.
- Finally, the development of the innovative A-FSA technique, a method for the combined acquisition of grain boundary segregation data, grain boundary facet crystallography and topographical information from individual facets on the surface of a fractured sample. Thus allowing data for the combined effects of all the fracture influencing processes to be acquired from the same facet, a technique seldom described in the literature and for which no experimental data has been reported.

3.1 Specimens.

All of the specimens used throughout the course of this investigation were made from two Iron-Phosphorus-Carbon (Fe-P-C) alloys that were originally supplied by British Steel Technical, Swinden Laboratories, Rotherham. The approximate compositions of the two alloys are detailed below.

Alloy 1 – Fe – 0.06wt%P – 0.002wt%C
Alloy 2 – Fe – 0.12wt%P – 0.002wt%C

These alloys were chosen due to the fact that they were test alloys that were produced specifically for the analysis of phosphorus segregation. Much work had been previously done on the 0.06wt%P alloy (Williams, 1999), hence a great deal of information was already known about its material properties. This knowledge was used as a basis for subsequent investigations.

Initial heat treatment trials were carried out on the samples in order to determine the range of heat treatments that would give rise to the most suitable set of samples for the experimental techniques involved.

A lower limit for the heat treatment temperatures had been determined from work done previously (Williams, 1999). It was necessary to determine an upper temperature limit for the samples to be used for fracture surface analysis as too high a degree of abnormal grain growth would cause too many very large grains during analysis, giving rise to very small data sets. An analysis of a sample that had been aged during this project at a temperature of 1000°C for 1hour showed (figures 3.1a,b) that at this temperature, the degree of abnormal grain growth was too severe for the sample to be used for fracture surface analysis, as it would be highly probably that samples would be single crystals at the point of fracture.

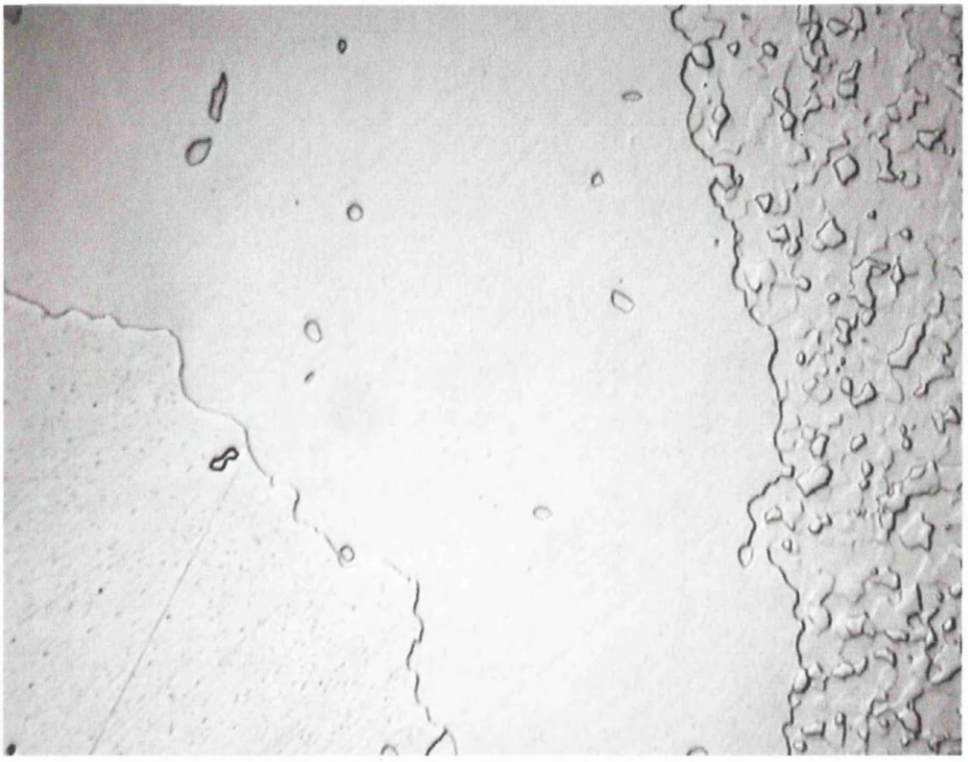

Figure 3.1a,b Optical micrographs showing the high degree of abnormal Grain growth that is prolific in the material at annealing temperatures of 1000°C

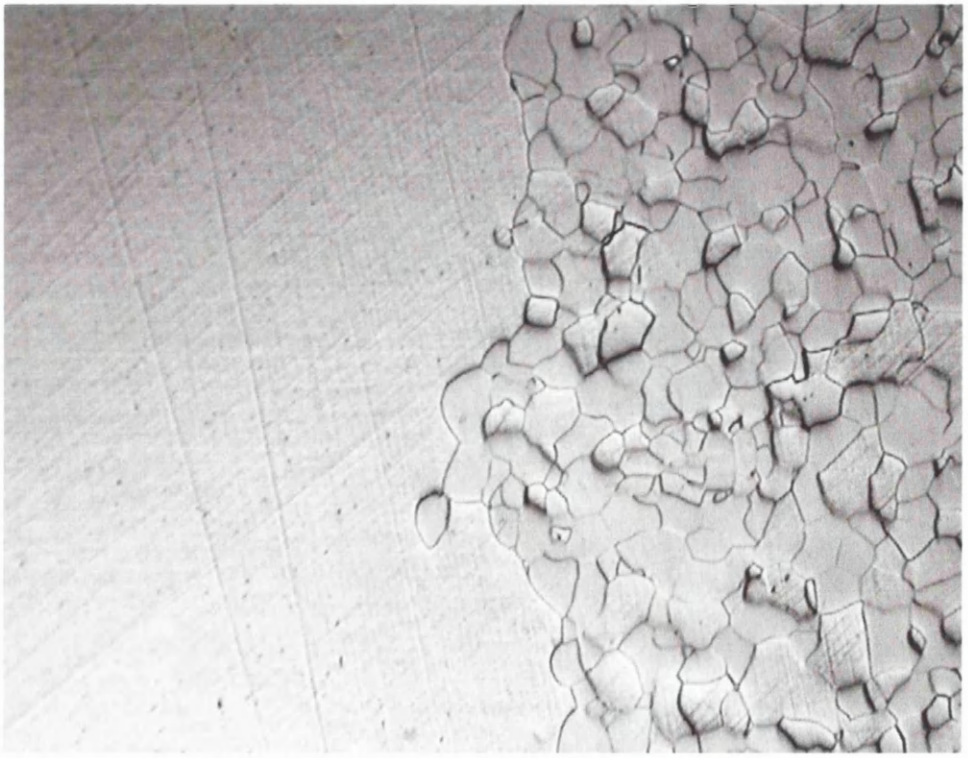

3.2 Scanning Electron Microscopy - Imaging.

The Scanning Electron Microscope (SEM) is a microscope that uses electrons instead light to form an image of the sample under investigation. The SEM is far superior to a light microscope, due to its combination of higher magnification, larger depth of field, greater resolution, and ease of sample observation. It is these factors that make the SEM one of the most heavily used instruments in research areas today.

The SEM has the advantage of a large depth of field, which allows a large amount of the sample to be in focus at one time, allowing samples with a high degree of surface topography, such as fracture surfaces, to be examined. The SEM also produces images of high resolution, which means that closely spaced features can be examined at a high magnification. Preparation of the samples is relatively easy since the only requirement of the SEM is that the sample is conductive, or is made conductive by means of coating in a conductive medium.

The beam of electrons that is required for the operation of the SEM is produced at the top of the microscope by the heating of a filament. The electron beam follows a vertical path through the column of the microscope. It makes its way through electromagnetic lenses, which focus and direct the beam down towards the sample. Once it hits the sample, other electrons, which can be backscattered electrons or secondary electrons, are ejected from the sample. Detectors collect the secondary or backscattered electrons, and convert them to a signal that is sent to a viewing screen similar to the one in an ordinary television, producing an image of the sample. These images can then be used in order to determine information about the sample under investigation in much the same way as images acquired from a normal light microscope.

3.3 Electron Back-Scatter Diffraction

Rapid developments in both hardware and software in the past 10 years has made Electron Back-Scatter Diffraction (EBSD) an ideal technique for the rapid analysis of microstructures and crystallography in a range of crystalline materials (Randle and Engler, 2000)

To successfully acquire Electron Back-Scatter Diffraction Patterns (EBSPs), a polished sample must be tilted to a relatively high angle (typically 70°) inside the SEM. The electron beam is then directed at the point of interest on the sample surface. The initial elastic scattering of the incident beam causes the electrons to diverge from a point just below the sample surface and to impinge upon crystal planes in all directions (Goodhew and Humphreys, 1992). Wherever the Bragg condition for diffraction is satisfied by a family of atomic lattice planes in the crystal, two cones of diffracted electrons are produced (Figure 3.2). These cones are produced for each family of lattice planes. These cones of electrons can be imaged using a phosphor screen attached to a sensitive camera (Figure 3.3). The camera is usually positioned horizontally, so that the phosphor screen is close to the sample in order to capture a wide angle of the diffraction patterns. Where the cones of electrons intersect with the phosphor screen, they appear as thin bands. These are called "Kikuchi bands", and each one corresponds to a family of crystal lattice planes (Randle and Engler, 2000). The resulting Kikuchi Pattern (Figure 3.4) is made up of the many Kikuchi bands and can be thought of as a map of the angular relationships between the directions and planes in the crystal. Linear distances measured on the diffraction pattern represent angles and interplaner angles can also be obtained from the Kikuchi pattern, but are not of much relevance to orientation measurements.

The acquired Kikuchi pattern can be enhanced, by removing a background image with no diffraction pattern from the original pattern. This has the effect of improving the contrast of the Kikuchi lines from the acquired image, allowing easier identification of the Kikuchi lines by both manual and automated methods. The Oxford EBSD software uses this difference in contrast to automatically detect the positions of the individual Kikuchi

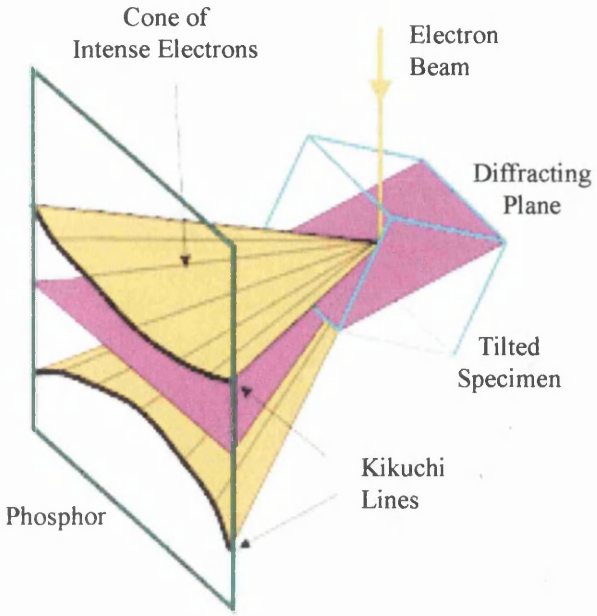

Figure 3.2 Diagram showing the production of two cones of diffracted electrons from the lattice planes

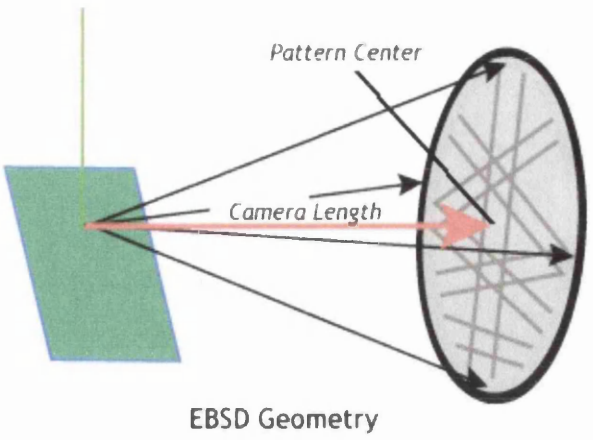

Figure 3.3 Diagram showing imaging of the electron diffraction pattern on a phosphor screen

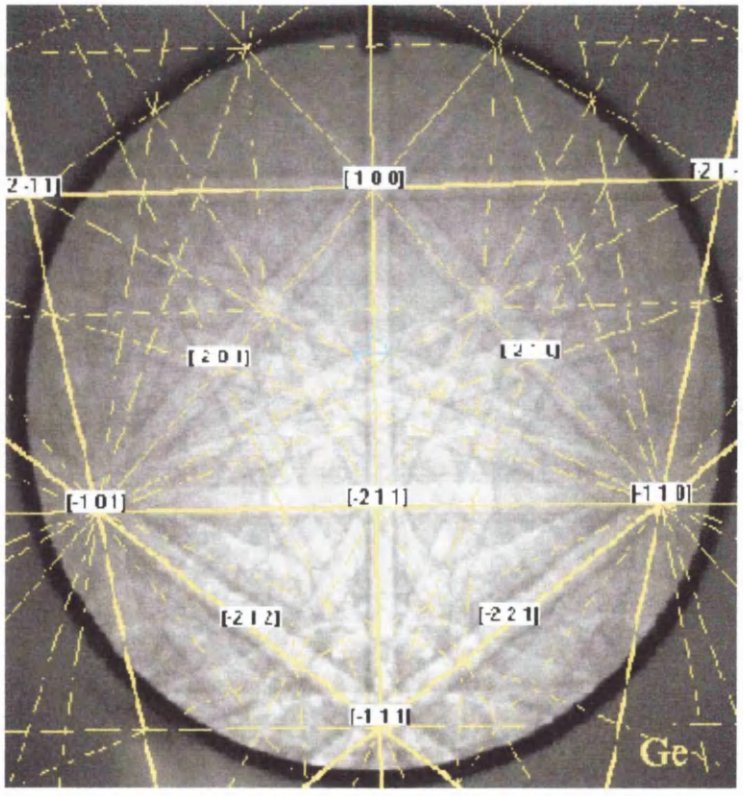

Figure 3.4 An image of a typical kikuchi diffraction pattern, showing the automated pattern recognition software being utilised to identify and solve the kikuchi pattern

bands. Using this information, along with information regarding the sample geometry and the material and crystal structure specified by the user, the software is able to compare the geometry and structure of the pattern with a software database in order to quickly identify the crystallographic orientation of the grain being analysed.

From this, it is possible to produce a stereographic representation of the crystallographic orientations of the grains in the material, which can then be used to determine the misorientations between neighbouring grains.

3.4 Crystal Orientation Mapping (COM)

Crystal orientation mapping is the most common approach to sample analysis using EBSD. The electron beam is stepped across the surface of the sample at regularly predefined steps. At each point, an EBSP is collected and automatically indexed by the EBSD software.

The crystal orientation information is stored by the software and can then be used to reconstruct the microstructure in the form of an orientation map. This map can then be manipulated in order to provide the complete microstructural characteristics of the sample. Orientation mapping has become a very fast and comprehensive approach to characterisation of microstructures.

Electron Back-Scatter Diffraction (EBSD) was performed on both alloys using two different EBSD software packages. The first system utilised Oxford Instruments EBSD software 'OPAL' fitted to a JEOL 6100 Scanning electron microscope (SEM) and was used for the majority of the investigations and technique developments. The other EBSD system used was the 'Channel 5' software developed by HKL Technologies that was fitted to the Philips XL30 digital SEM.

From previous work (Williams, 2000), it was decided that taking crystal orientation maps (COM) from the polished surface of the material would be the best form of EBSD

analysis for the acquisition of grain boundary proportions. This was to ensure that as much data as possible was available from each sample and ensured that samples would not need to be re-analysed in order to acquire different data at a later date should it have been required.

The magnification and step size were adjusted for each analysis in order to achieve the optimum maps from each sample. For example, samples of large grain size were analysed at lower magnifications, after confirmation by higher magnification analyses that vital features such as deformation twins would not be overlooked. Step sizes for all analysis were made in the region between 3μm and 10μm except where quoted as otherwise.

Taking COMs from fracture surfaces would prove to be a more complicated procedure, as the topography of the fracture surface introduces large errors into the data and can dramatically reduce the number of solvable Kikuchi patterns that can be acquired from the surface of the sample. A great deal of technique development was needed during this project, in order to acquire reliable and accurate data from sample fracture surfaces and the errors involved in the techniques had to be analysed and quantified. This is reported fully in section 4.1.

3.5 Stereo Facet

In order to better understand the data acquired from the fracture surface, it was decided that the Oxford Instruments' computer assisted stereo-photogrammetry software 'Stereo Facet' would be employed in an attempt to reduce the errors present in the fracture surface EBSD technique. Two stereo images were acquired separately, tilted at +2° and –2° with respect to the primary beam direction. Assuming the image acquisition system of the SEM is similar to that of a parallel projection with negligible image distortion, the co-ordinates of each pixel is related to the measured displacement through the following equations. (Themelis et al., 1990)

$$X = (x_1 \sin\theta_2 - x_2 \sin\theta_1) / \sin(\theta_2-\theta_1) \quad \textbf{Equation 3.1}$$

$$Y = y_1 = y_2 = (y_1+y_2) / 2 \quad \textbf{Equation 3.2}$$

$$Z = (x_2\cos\theta_1-x_1\cos\theta_2) / \sin(\theta_2-\theta_1) \quad \textbf{Equation 3.3}$$

Where the true co-ordinates XYZ of each pixel in space are determined from the projected co-ordinates (x,y), relative to the reference axes, at the two tilt angles 1 and 2. The parallax shift data for each pixel can then be calculated using a digital-image correlation analysis routine provided by the software, which is then used to construct a '3D-elevation map' of the area being analysed (Figure 3.5).

This technique can easily be performed when the sample is mounted with the fracture surface perpendicular to the incident electron beam, though for the technique to be integrated with the EBSD analysis the sample must be mounted at 70° to the incident beam. The effects of this sample geometry set-up had to be analysed in order to ensure that the results from the stereo facet program are still valid for a sample mounted at 70° using digitally tilt corrected images.

3.6 Auger Electron Spectroscopy

Auger Electron Spectroscopy (AES) is a commonly used surface analysis technique. It was developed in the late 1960's and became popular in the early 1970's with the development of commercial spectrometers. The AES process involves the irradiation of a surface with a beam of energetic electrons, which results in the ionisation of the surface due to the impact of the electrons. After the emission of the initial electron, reconstruction of the electron structure takes place and the excess energy from the process is released in the form of a photon (X-ray) or by the ejection of a secondary electron. This secondary electron is referred to as an Auger electron.

The grain boundaries of an alloy material can be chemically quite distinct from the alloy bulk, such as in the case of temper embrittlement of alloys due to the segregation of elements such as phosphorus to the grain boundaries of the material. An Auger electron

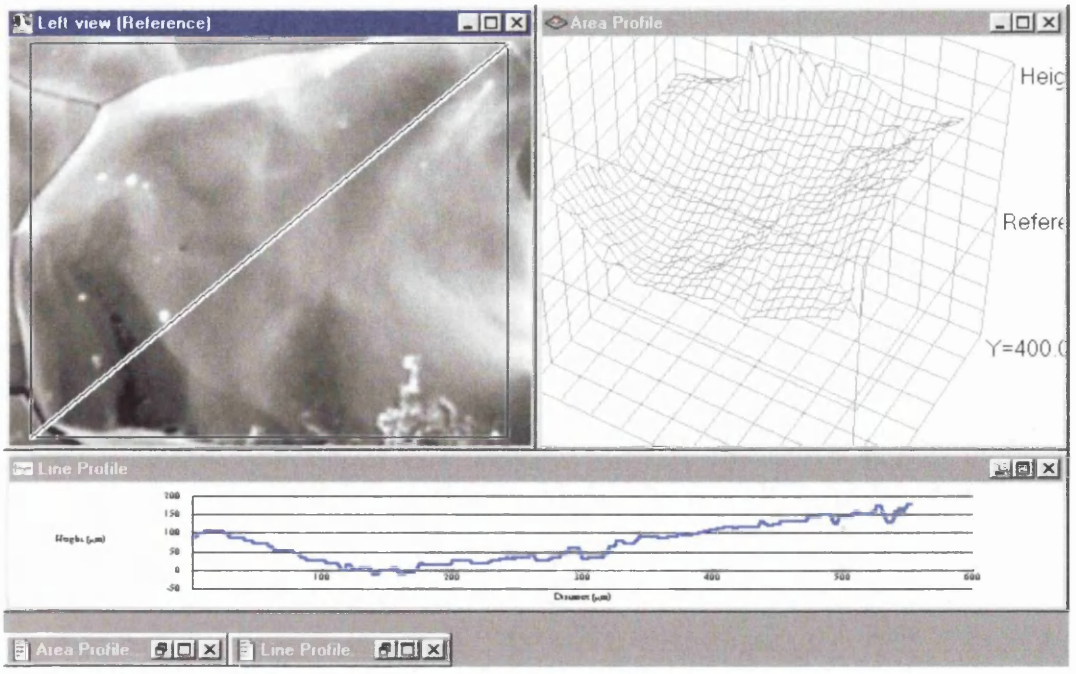

Figure 3.5 An image showing the application of the 'Stereo Facet' software, used in order to produce a 3D elevation map of a fracture facet.

spectrometer with an in-situ fracture stage can be instrumental in the study of such phenomena (Cowan, 1997). In-situ fracture of the specimen in a UHV chamber is the only way in which the chemistry of the grain boundaries can be retained for analysis, due to the highly reactive nature of fracture surfaces.

All Auger analysis was carried out at Berkeley Technology Centre, using a Fisons Instruments 310-F Field Effect Scanning Auger Microprobe. The microprobe utilises a concentric hemispherical analyser (CHA) and a Field Effect Gun (FEG) source and is used in order to determine the atomic percentage segregation at grain boundaries in the material. A sample of the 0.06P wt% material was subjected to a heat treatment of 600°C for 1 hour and was then air-cooled. This sample was then machined into Auger 'matchsticks', in order for them to be mounted into the fracture stage. The microprobe was evacuated to a pressure of $<2x10^{-9}$ mbar and the sample cooled to below -120°C for around an hour before fracture. Both halves of the sample were retained after fracture, though Auger analysis was only performed on one half. The fracture surface was tilted so that the fracture surface normal was at 30° to the incident electron beam (5KeV). The fracture surface was first imaged using secondary electrons, and a suitable area chosen. Approximately 11 intergranular and 2 transgranular facets were then electronically marked for spectra collection. Each facet was then analysed 5 times and an average determined. This data and the corresponding images were then saved for subsequent analysis. Analysis of this data was performed at Berkeley Technology Centre, using software called PAuger. This software outputs the composition of the facet surface for the various points and for each element required. This data was then compiled into a spreadsheet for easy reference.

3.7 Grain Size Analysis.

The effects of different heat treatments on the grain growth of the first alloy was studied previously by Cowen (1997) and revealed much about the effects of different heat treatments. A investigation was performed on both alloys as a part of the investigation.

This information was then used to both confirm and advance the work done previously. Grain growth analysis was carried out both by linear intercept methods using optical microscopy and image analysis, and by software analysis as a part of the EBSD procedure, whereby the grain size information was exported to a spreadsheet for analysis.

3.8 Grain Boundary Analysis

From work done previously, (Williams, 1999) it was possible to deduce the optimum test matrix for determining the effects of heat treatment on the proportions of grain boundaries in the material. It was determined that the optimum temperature range for the heat treatments involving fracture surface analysis would be between 500°C and 900°C. A higher upper limit of 1000°C would be practical for samples involved in grain boundary analysis, where the large grain size is not as detrimental to the experimental technique being used. This test matrix would then be used for both materials in order to determine directly the effects of different quantities of phosphorus on the grain boundary proportions and grain growth in the material for a range of heat treatment temperatures and aging times. The chosen heat treatment matrix for this investigation is outlined in the table below:

Test Sample	Temperature	Aging time
Test 1, 2 and 3	600°C	1, 2 and 5 hrs
Test 4, 5 and 6	700°C	1, 2 and 5 hrs
Test 7, 8 and 9	800°C	1, 2 and 5 hrs
Test 10, 11 and 12	900°C	1, 2 and 5 hrs
Test 13, 14 and 15	1000°C	1, 2 and 5 hrs

This test matrix yields a total of 15 samples for both the 0.06wt%P and 0.12wt%P alloys, thus giving 30 separate test samples. These heat treatments were chosen in order to make it possible to determine the individual effects of temperature, the aging time, a parameter

not fully explored in the literature, and the effects these parameters have on both the phosphorous content on the proportions of grain boundaries and the degree of grain growth in the material. These samples were prepared for EBSD analysis as follows.

Samples were cut from the material to dimensions of 15mmx20mmx25mm using an Icotom diamond-cutting machine before heat treatment and then cut down to 5mmx10mmx25mm for preparation. This resulted in two samples per heat treatment one of which could then be used for other investigations. Each sample was mounted in conductive Bakelite and ground flat using silicon carbide paper of progressively finer grades whilst under flowing water (paper grades 150, 300, 600 and 1200). The samples were then polished using standard diamond polishing wheels, firstly with 6μm diamond paste, then finally with 1μm diamond paste. The samples were then etched using 2% nitric acid (HNO_3) for a period of approximately 30-45 seconds in order to reveal the microstructure. The samples were then mounted on an EBSD microscope stage, such that the polished surface of the sample was at 70° to the incident electron beam while facing the phosphor screen of the EBSD camera. Five COMs were then taken from five different areas of the sample at a magnification of approximately 100x-200x. These maps were then processed using the system software in order to get a map in which each grain is defined by using a threshold of >5° misorientation. The 'true grain ID map' enables the user to see one data point per grain and the crystallographic orientation data from this map was exported as a text file into Microsoft Excel where it was processed as required.

4. Modus Operandi

The methodologies described in this chapter were all developed within the duration of the project in order to acquire experimental data that was not possible to attain by any of the standard techniques reported within the literature. All of the following procedures lead to the development, during this project, of the innovative A-FSA analysis technique, which combines grain boundary segregation data attained through Auger electron microscopy with fracture facet crystallography acquired by EBSD.

4.1 Fracture Surface Analysis (FSA)

The development of the fracture surface analysis technique during the course of this project was required in order to accurately determine the orientation of the fracture plane of fractured samples. The completed technique was applied to a number of different analyses in order to determine such parameters as the transgranular cleavage plane, the preferred intergranular fracture plane and was also used in the development of the technique combining Auger analysis and fracture surface EBSD.

4.1.1 Error Determination

The first method used in order to determine the error in the fracture surface analysis technique was performed in two parts, these are described below: for both of these techniques, it was advisable to use a sample with a large grain size, in order to be sure that the electron beam was kept within one grain.

Sample Rotation

A sample was mounted at 70°C in the microscope (Standard EBSD set-up) and a Kikuchi pattern was acquired from its surface. The sample was then rotated about the microscope

z-axis, while patterns were still being acquired, until the pattern became unsolvable. The microscope chamber was then brought back atmospheric pressure and the angle by which the sample had been rotated about the z-axis was measured. This was done manually, as the microscope does not automatically provide this information. Diffraction patterns were systematically recorded while the sample was being rotated such that the degree of rotation was seen on the corresponding pole-figure.

From this experiment, it was determined that the sample could be rotated up to 28° about the z-axis while still resulting in a solvable EBSD diffraction pattern.

Sample Tilt

The same sample was again mounted on the holder, but tilted incrementally away from the standard 70° about the x-axis until the pattern became unsolvable. This was achieved by mounting metal 'wedges' of known angle behind the sample. The microscope was then brought back up to atmospheric pressure and the angle by which the sample had been tilted about the x-axis is recorded. Diffraction patterns were systematically recorded while the sample was being tilted such that the degree of sample tilt was seen on the pole-figure.

The results of this work showed that the sample could be tilted to 25° from its initial position. From this it was deduced that the fracture surface analysis technique could only be accurate to ±28° (the larger of the two measured errors). It was possible for any facet from which a pattern was indexed to be up to 28° away from the direction normal to the fracture face, so all results that would be acquired by this method would include this error, unless methods were developed to reduce it.

4.2 Three Dimensional Analysis of Fracture Surface.

To confirm that the errors in the fracture surface analysis technique were correctly determined, it was decided to prove the results by three-dimensional analysis. This was achieved by the application of calibrated serial sectioning:

Samples were carefully cut to lx2x30mm to aid specimen realignment after fracture and fractured under liquid nitrogen. After fracture the two specimens were mounted such that both fracture surfaces were normal to the camera. Careful attention was paid to the geometry of the two halves of the specimen so that all maps from the fracture surface and the Crystal Orientation Maps (COM) were taken from the both surfaces and the positions from which the maps were taken noted for subsequent use. Once a suitable number of COMs were acquired, the two halves of the sample were realigned as they were prior to fracture and mounted in conductive Bakelite and prepared using standard metallographic techniques. The sample was then treated as a normal FSA specimen.

Due to the size and geometry of the sample it was possible to analyse the whole fracture area on one COM. Once this COM was acquired, the specimen was removed from the microscope and prepared for serial sectioning. A hardness indent was placed on the material. The hardness indent was used to determine the amount of material removed after polishing using the equation:

$$X = \frac{d}{2.\tan(74.507)} \qquad \textbf{Equation 4.1}$$

Where x is the amount of material removed and d is the length of the indent diagonal. COMs were made at approximately 50 μm increments through the specimen in order to get a suitable number of COMs to compare with those taken from the fracture surface

From this work (Figure 4.0a,b,c) it was clear to see that it is possible to match the results from the two methods. The colours shown on the COM's from the fracture surface (figure 4.0a,b) were easily matched with the colours shown on the same sample when the polished fracture surface was analysed from the side (figure 4.0c). From this fact, it was possible to conclude that the correlation of the colours and hence the crystallographic data prove that the three-dimensional fracture surface analysis technique can provide usable results. Although there are significant errors in the method, the fracture surface analysis technique proves an effective method for the fast and large quantity acquisition of crystallographic information from fracture surfaces. The application of image processing to the two COMs allows the differences in the colours of the facets on the COM to be represented by an angle corresponding to the error in the fracture surface analysis technique.

Shown in figure 4.1 is the inverse pole figure colour key that corresponds to all of the crystal orientation maps that are shown throughout this thesis. It can be seen that the colours shown on the COMs correspond to a certain crystallographic orientation as described by the colour key. For example, it can be seen that a strong red colour corresponds to an crystal orientation close to [001].

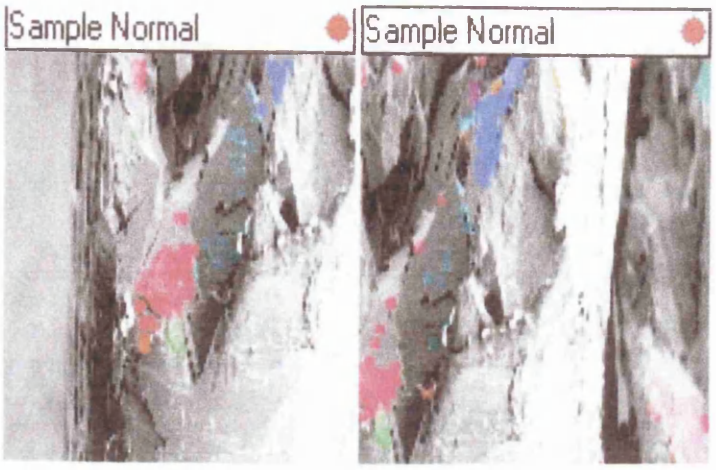

Figure 4.0a,b Above are two COMs taken from slightly different places in order to be able to see the whole of the side of the sample

Figure 4.0c The top images correspond to the bottom half of the matched fracture specimen Shown in the image above, which has been sectioned to a depth of 80 microns. It can be seen that there is a correlation in the colours shown by the orientation maps

Line 1 corresponds to the "red" facet at the bottom left of the top images.
Line 3 corresponds to the "blue/green" facet at the bottom middle of the top images.
Line 5 and 6 correspond to the "blue" facet at the bottom right of the top images.

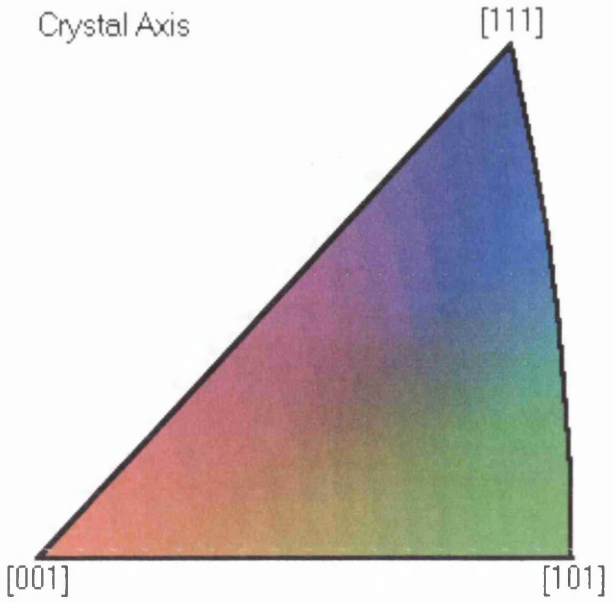

Figure 4.1 Shown above is the colour key that corresponds to all the crystal orientation maps that are shown throughout this thesis. It can be seen that a red colour corresponds to an orientation close to [001].

4.3 Fracture Surface Reconstruction

One method for the error reduction in the fracture surface analysis technique is to use computer aided stereo-photogrammetry in order to determine the macroscopic orientation of the fracture plane being analysed. It is then possible to determine the extent to which the facet normal is oriented away from being parallel to the sample normal direction (ND). This can be accomplished by the use of the "stereo facet" by Oxford Instruments. Stereo images are separately acquired at tilt angles of +2° and -2° with respect to the incident e^- beam; these images are then processed using a digital-image correlation analysis routine as a part of the software and the software produces a 3D-elevation model of the surface. Testing of the software and the technique involved was conducted on a Vickers hardness indent placed on a polished sample at 70° in the microscope.

A Vickers indent was introduced into the polished surface of a ferritic steel sample, and the depth of the indent was calculated from the digonal trace of the indent verticies and compared with the depth determined from the 3D elevation model.

The software was able to reconstruct the geometry of the indent, reading a depth of 32.81μm, a deviation of 0.19μm from the calculated depth of 32μm (Figure 4.2). Considering the fact that the software returned a 98% successful pixel match, and the fact that it was able to determine the depth of the indent to within 0.19μm of the calculated depth, it was concluded that the software can accurately produce 3D-elevation models of fracture surfaces. This technique has been used with a certain amount of success in the analysis of transgranular cleavage planes (Davies and Randle, 2001).

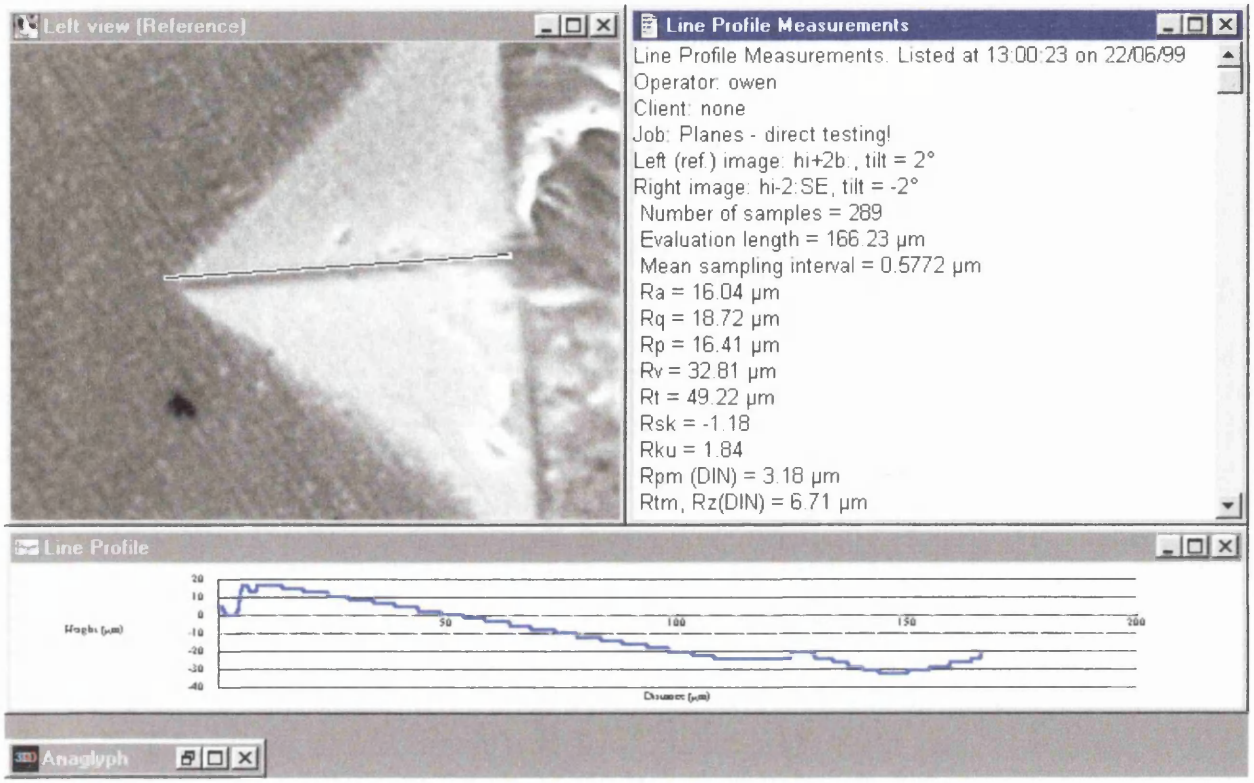

Figure 4.2 "Stereo Facet" software showing the measured depth of a 'Vickers' hardness indent The depth was shown to be 32.81 microns, a deviation of only 0.19 microns for the known value

4.4 Method for Fracture Surface Electron Back-Scatter Diffraction with Fracture Surface Topography.

First, a normal COM was acquired from the fracture surface of the sample, as for the case of the normal FSA technique. The COM was then studied in order to determine from which facets EBSD was successful. These facets were then magnified to the extent where they filled most of the screen (figures 4.3a,b). These specific facets on the specimen were then analysed by the stereo facet software, which reconstructs the two tilted images to form a 3 dimensional representation of the topography of the fractured facets. From this 3D representation, it was possible to determine which facet normals were parallel to the sample normal. Results from facets for which this was not the case were disregarded, as the EBSD data from them deviates from its actual value by an amount equal to the angle that the facet normal makes to the sample normal. This technique was best used to get crystallographic data directly from the fracture surface, though data acquisition was usually only possible from a maximum of 50% of the facets on the fracture surface (Field, 1997).

4.5 Fracture Surface Serial-Sectioning (FSS)

The Fracture Surface Serial-Sectioning (FSS) technique was developed in order to analyse the populations of fractured grain boundaries present in mounted fracture samples. This technique allowed the fractured grain boundary populations to be compared with the grain boundary populations for un-fractured boundaries. Thus, it was possible to determine the types of boundaries that were resilient to fracture and those that tended fracture preferentially.

This technique involved mounting both halves of a fractured sample in such a way that they were positioned as they were before they were fractured. It was then possible to section through the sample, taking COMs from the polished side of the fracture surface (Figure 4.4)

Figure 4.3a,b Crystal Orientation Maps taken from fracture surface facets

These COMs were then used to extract data about the nature of the fractured boundaries, by inputting into the software information about the grains that were adjoining before fracture. Grain boundary population results were acquired for all the 1hr, air-cooled heat-treated samples (600, 700, 800, 900 and 1000°C) and these results were then analysed. It was possible to acquire data sets of approx 100-150 misorientations per sample by this technique, despite the problems and limitations outlined below.

For the FSS technique to be successful, the mounting process has to be done in an extremely accurate manner; such that the two halves of the fracture surface line up in exactly the same position as they were prior to fracture. Misalignment by an amount as small as 20-30 microns can render the sample and subsequent analysis useless. Other problems arise because non-conductive material and other contaminants regularly become trapped between the two mounted fracture surfaces and subsequently, cause flaring on the electron image (Figure 4.5), in some cases making the analysis impossible. This effect was limited by the application of silver dag to both fracture surfaces before realignment. This limits the amount of contaminants that were able to find their way between the mounted fracture surfaces. However, sample preparation has the effect of removing some of this protective silver medium, especially during the etching process, and sample flaring again becomes a problem. This preventative method also has the undesirable effect of allowing etchant and other liquid mediums to penetrate into the fracture surface only to be released when the specimen is placed under vacuum. This can then cause damage to the polished surface under investigation and could lead to the damage of microscope and camera components, such as the phosphor screen.

Other difficulties encountered by this method include the inability to distinguish between transgranular fracture and low angle intergranular fracture due to the errors in realignment, which can be as much as 5°. These errors were found to arise during the realignment process or during the mounting process, where the sample is subject to adverse temperature and pressure conditions.

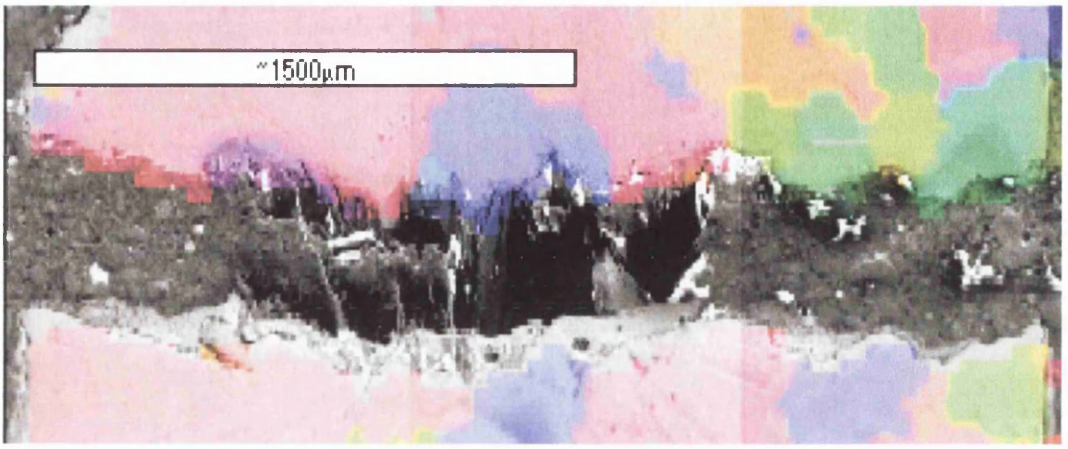

Figure 4.4 An example of a' matched fracture sample' used in the 'Fracture Surface Serial-sectioning' (FSS) analysis technique, showing the method of data acquisition From fractured grain boundaries

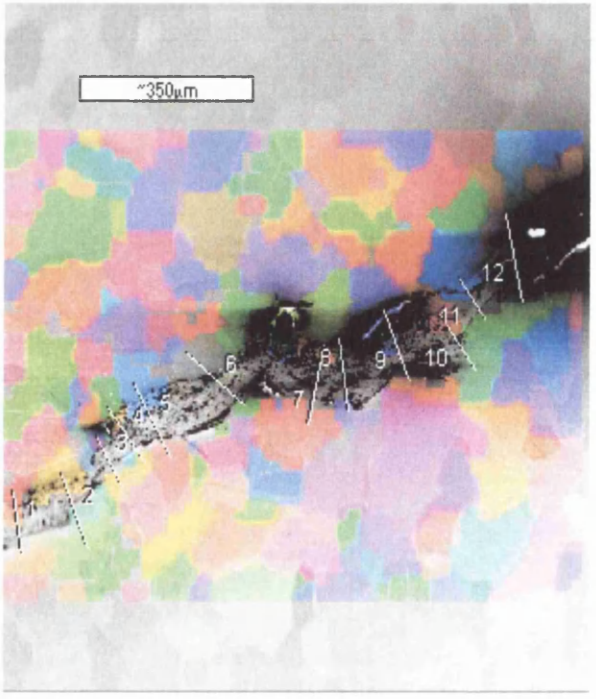

Figure 4.5 An example of a 'matched fracture sample' showing a high degree Of 'flaring' caused by an interaction between contaminants and the electron beam

Despite the limitations described above, the technique was able to reveal a great deal of valuable information about the fractured grain boundaries, information that would be extremely difficult to acquire by other means. A number of the difficulties outlined here would not be such an issue with specimens having a larger grain size, and as with all techniques, there is significant scope for refinements which will allow much more accurate information to be acquired from the samples.

The accuracy of the results from samples that have been successfully mounted and aligned can on occasion be questionable however, because it is not possible to be sure that none of the material has broken off the fracture surface. In some cases, quite substantial pieces of material have become detached from the fracture surface. These losses were quite easy to detect. It is however, the loss of individual grains from the fracture surface that causes the most concern, because it is very difficult to notice the loss of such small quantities of material (especially in the smaller grained material). These losses, however small, can lead to false results from the samples. Other problems arose due to the residual strain produced by the propagating crack. The residual strain is at its greatest intensity near the fracture surface and thus can have detrimental effects on the quality and accuracy of EBSP's acquired at these locations.

In conclusion, this technique was used as a very valuable tool in the analysis of both grain boundary fracture and transgranular cleavage. However, great care must be taken in its application, as there are many factors that can introduce errors into the analysis.

4.6 Polished Fracture Surface Analysis (PFSA)

During this technique, the samples to be analysed were left un-mounted, making it possible to remedy the majority of problems encountered by the FSS technique. However, unmounted sectioning could only be done to one half of the sample at a time, meaning that was not possible to section and analyse the grain boundaries across the fracture surface for both halves of the sample.

The major benefit of this method is that it is possible to simultaneously analyse the fracture surface itself and the polished surface at the side of the fracture surface, thus allowing a greater amount of valuable data to be extracted from the sample.

As can be seen from figure 4.6, it was possible to determine if a particular grain has fractured in a transgranular or intergranular manner whilst performing EBSD analysis of the sample (assuming all trangranular cleavage facets can be identified by the presence of river lines on the facet surface). It was possible to montage this image with the corresponding image from the other half of the sample, though care had to be taken to ensure that the geometry of the two images was retained. This type of analysis also allowed a thorough analysis to be made of the fracture surface of the material, as it is not buried in the mounting process. This made it possible to compare features found by EBSD on the polished surface with those present on the fracture surface itself, such as deformation twinning along the fracture path created during the fracture process, (Figure 4.7). These deformation twins are represented by light green lines extending away from the fracture surface. Other features that could be seen on the fracture surfaces include the effects of residual strain created in the wake of the fracture path which can be seen as a varying colour gradient across the surface of the grains near the fracture surface, such as displayed on the grain towards the right of figure 4.6.

4.7 Fracture Surface Analysis of Auger Samples (A-FSA)

The course of action that must be taken in order to be able to perform an EBSD analysis on fracture facets that have been previously analysed by Auger analysis is a non-trivial and intricate procedure. The exact same facets needed to be located on the surface of the sample in order for this analysis to be possible, a task that was complicated by the fact that Auger and EBSD use very different sample geometries and the fact that Auger is performed at 5KeV and EBSD at 20KeV. This lead to the fracture surfaces appearing very different in the two microscopes, not only in the angles and orientation of the fracture facets but also in the contrast and detail of the secondary electron image.

Figure 4.6 Showing the application of the 'Polished Fracture Surface Analysis technique

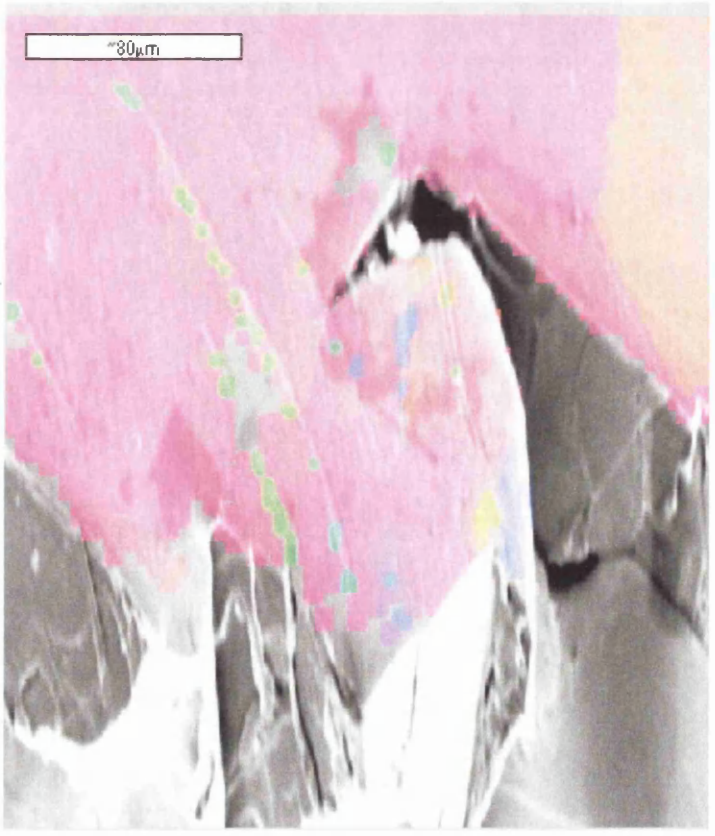

Figure 4.7 Showing the application of the PFSA analysis technique to the simultaneous analysis of deformation twins and fracture surface features.

After the area that was subject to Auger analysis was located, a 3-dimensional reconstruction of the area was made, by the application of the 'Stereo Facet' software by Oxford Instruments' (Figure 4.8). This reconstruction was done with the fracture surface normal to the incident electron beam and provided a visual representation of the facets that were under analysis. This was necessary in order to determine if the facets were orientated parallel to the fracture surface, in order to determine if the application of an 'error factor' was required for correction.

The 3-dimensional reconstruction of the fracture facets was done in the usual manner, with two images being taken at a tilt of ±2° about the incident electron beam. The software then used these images in the generation of a 3D-elevation model of the surface. Line profiles were taken at this time, at various points on the fracture surface (Figure 4.9), in order to assist in facet matching further on in the analysis process, when the two halves of the sample would be realigned, mounted and polished through from the side in order to acquire grain boundary information from the Auger analysed facets.

After the 3-dimensional reconstruction was performed, the samples were mounted in Bakelite in order to acquire Kikuchi patterns from the fracture facets. The samples were orientated such that the normal to the fracture surface was at 70° to the incident electron beam. The facets on which the Auger analysis was performed then had to be relocate. This proved especially difficult, as the 70° inclination of the surface resulted in the surface appearing vastly different from its appearance at either 30° or 0°. Some facets were also obscured or 'shadowed' by surrounding facets, making the identification of certain areas very difficult, while also preventing the acquisition of Kikuchi patterns from the shadowed facet.

It was found that a higher percentage of indexable patterns could be acquired if a number of separate analyses were performed at different sample orientations. The samples were rotated incrementally by 360° about the normal to the fracture surface in order to find a position where facet shadowing was reduced to a minimum. The sample was also rotated about the microscope 'z axis' (normal to the incident beam), as certain facets were

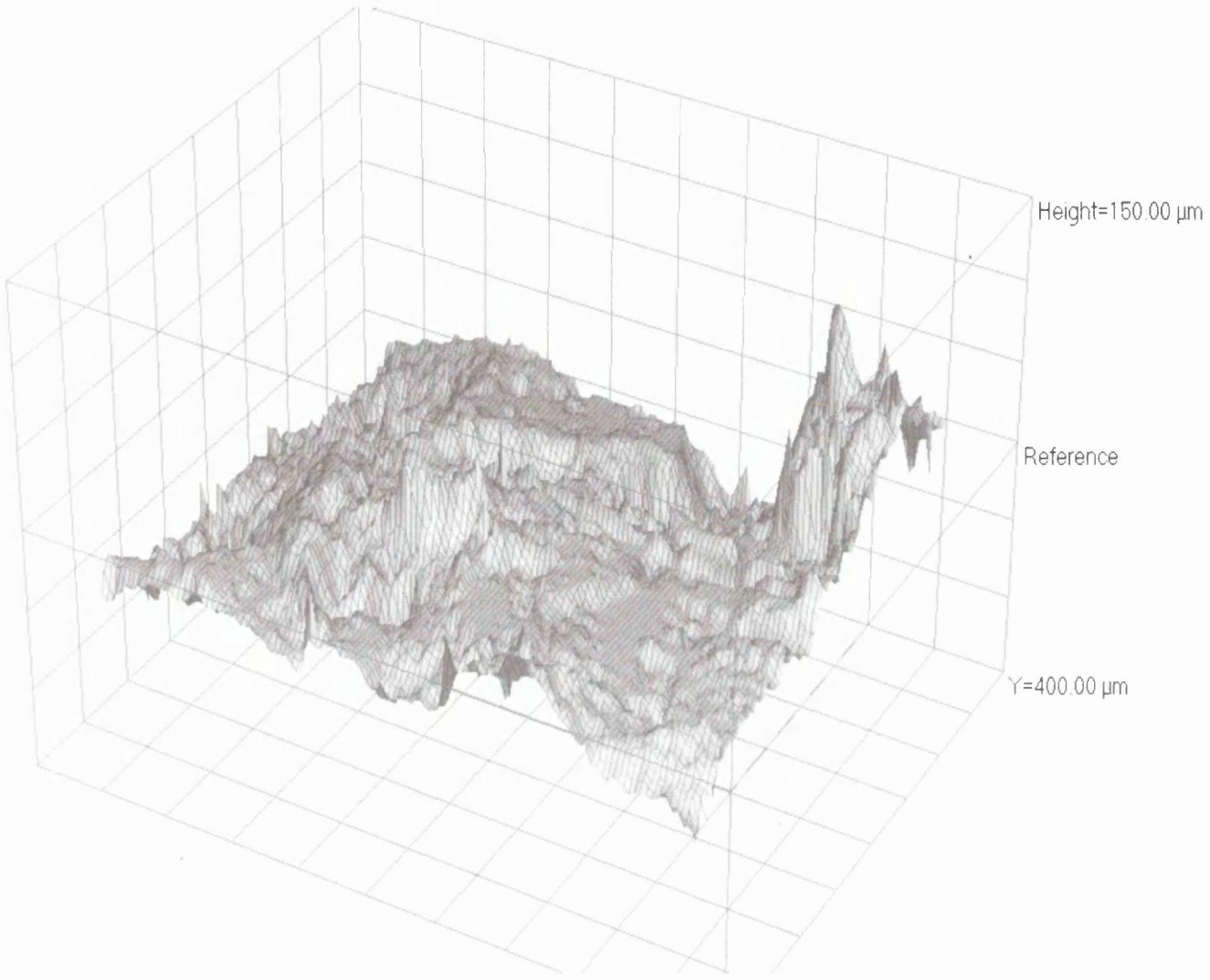

Figure 4.8 Three dimensional reconstruction of fracture surface using the 'Stereo Facet' software

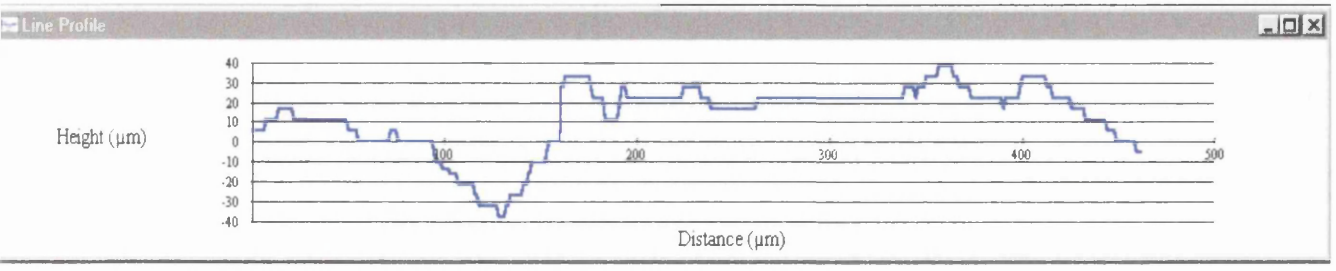

Figure 4.9 Line profile taken across a fracture surface in order to aid in the sectioning process.

orientated away from the direction normal to the fracture surface, as determined by reference to the 3D elevation map acquired by 'Stereo Facet'. These rotations resulted in a relatively high proportion of the 'Auger facets' being successfully analysed by EBSD.

4.8 Matched Fracture Analysis of Auger Sample

After all the direct surface analysis was performed on the Auger samples, they were realigned as they were before fracture and mounted in conductive Bakelite. The 'matchstick' was first removed from the Auger 'collet' in order for it to be mounted successfully. This was best achieved by carefully grinding away the remains of the screw that locked the matchstick into place within the collet. The matchstick was then easily removed from the Auger collet. Care was needed during this procedure, firstly due to the very small size of the matchsticks, which can easily become lost, and secondly for the protection of the integrity of the fracture surface.

Once the two halves of the Auger sample were removed from the collets, they were aligned and mounted in exactly the same manner as for 'Fracture Surface Serial Sectioning' (FSS). The sample was then polished through to the area where the Auger and EBSD analysis was performed. Great care was taken during this procedure, as it is very easy to polish too far and destroy the required area.

Areas that were located close to the edge of the sample were easily located, as only a small amount of material needed to be removed. Areas close to the centre of the sample provided more of a challenge, and experience proved very beneficial in determining how much material should be removed to get to the required area.

Once the required area was reached, it was confirmed by reference to the 'line profile' data acquired during the 3D surface reconstruction by 'Stereo Facet'. The sample was then analysed in exactly the same manner as described for the FSS technique.

5. Results

5.1 Grain Growth.

The initial microstructure of both of the as-rolled alloys consisted of equiaxed grains, approximately 80μm in diameter. A thorough grain growth analysis was performed on all the heat-treated samples, using data from both the COMs and also from linear intercept methods using optical microscopy.

From the results of this analysis (Figures 5.1, 5.2), it was clear that grain growth is prolific in the 0.06wt%P alloy as the aging temperature is increased to 1000°C. The microstructure changed from being made entirely of equiaxed grains of approximately 80μm diameter, to a structure with a high degree of abnormal grain growth and an average grain size of over 300μm. The abnormal grain growth exhibited by the 0.06wt%P alloy at 1000°C gives rise to a number of large, irregularly shaped grains, often with a number of small island grains within the large irregular grains. These island grains can range from 30μm to less than 5μm and can themselves be irregular in shape (Figure 5.3).

The 0.12P alloy does not exhibit the same degree of grain growth as that of the 0.06wt%P alloy, only having a small amount of abnormal grain growth at 1000°C. It also has a much lower average grain size than the 0.06wt%P alloy, reaching a maximum of 140μm as opposed to the 330μm maximum of the 0.06wt%P alloy

It was also seen that the aging time has little influence on the extent of grain growth, though it does seem that there is a smaller average grain size for the 1000°C samples that were aged for 5 hrs. This was clearly seen for the 0.12wt%P alloy, where there was a consistent decrease in grain size as the aging time was increased from 1hr to 50hrs. The annealing time has no noticeable effect on the grain growth of the heat-treated samples

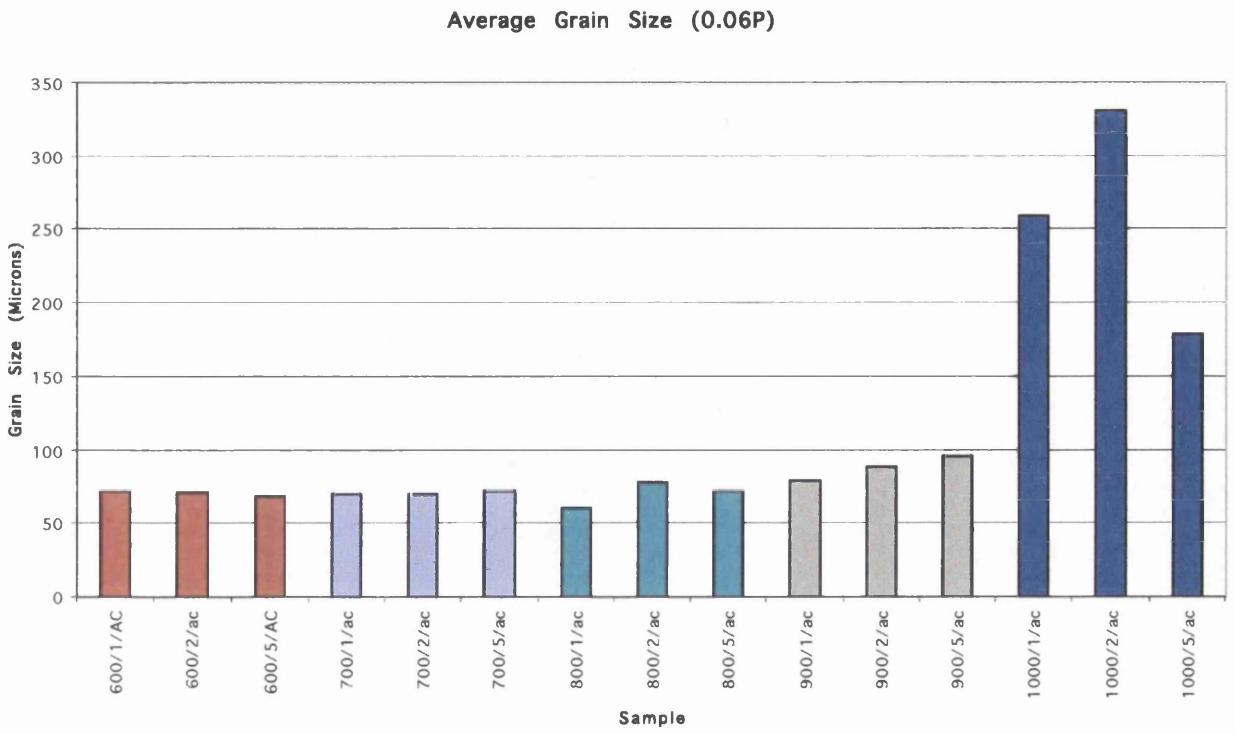

Figure 5.1 Showing the effect of annealing time and temperature on the grain size of the 0.06P alloy

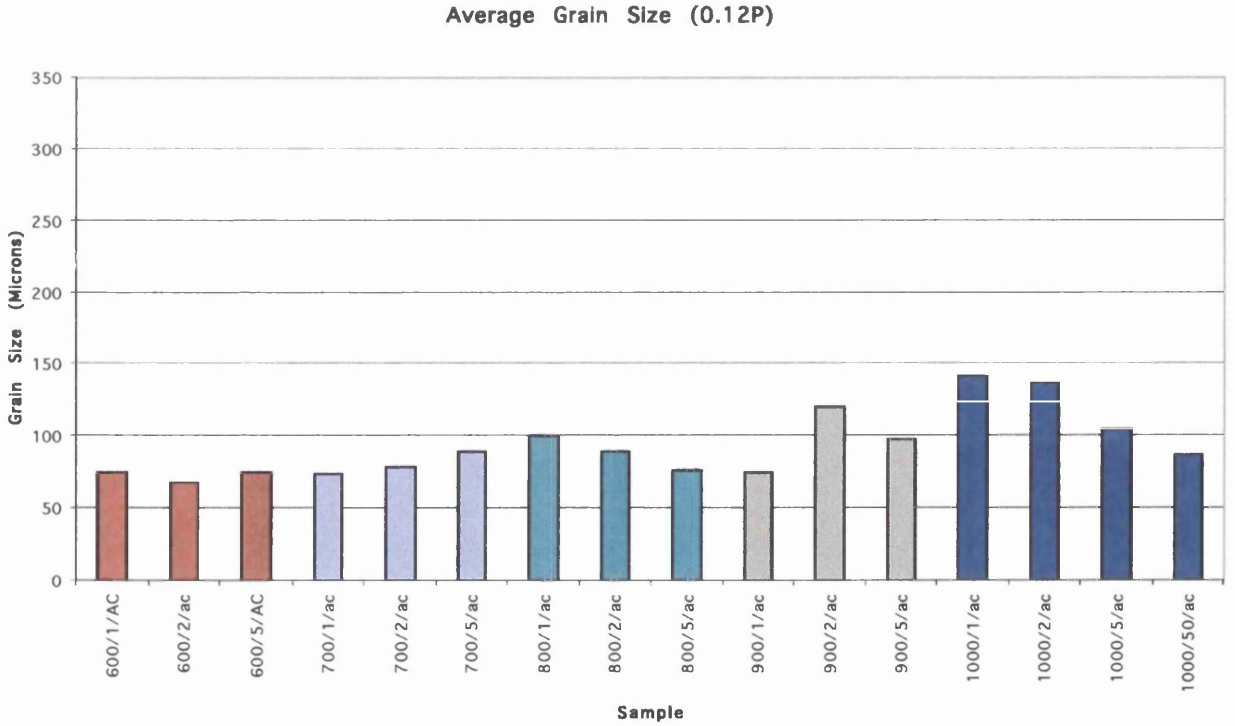

Figure 5.2 Showing the effect of annealing time and temperature on the grain size of the 0.12P alloy

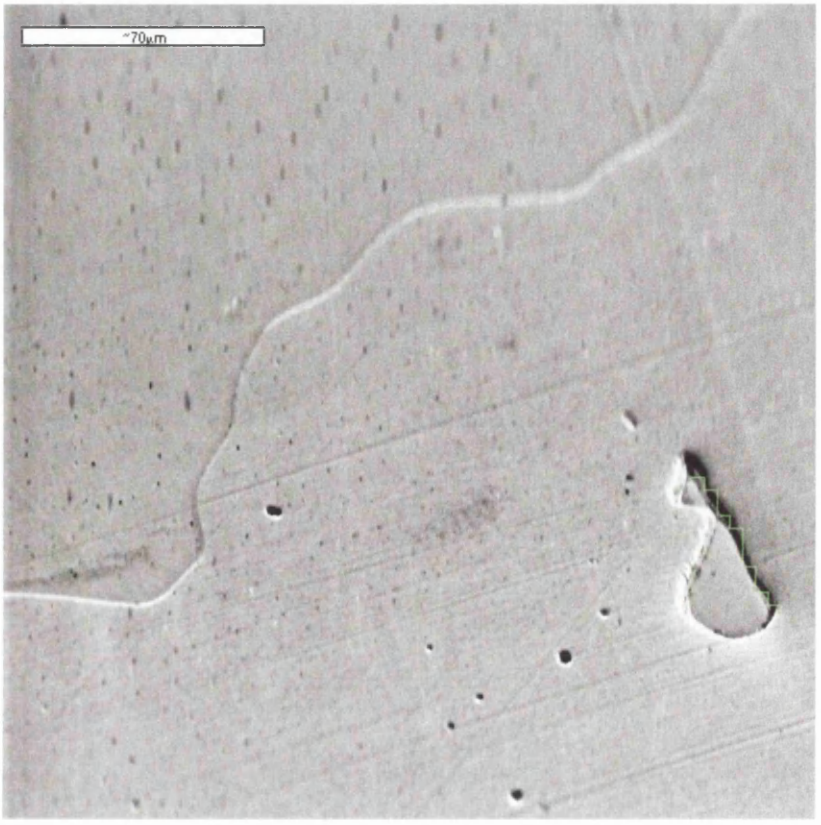

Figure 5.3 Showing an irregularly shaped ∑3-bounded grain within a large abnormally grown grain

except for those that are aged at a temperature of 1000°C. The errors in this analysis can be assumed negligible, due to the high resolution of the data acquisition process, which was set to a resolution of between 1 and 3 microns. So for an average grain in this material the error in data acquisition is less than 3.75%

5.2 Material Microtexture

The EBSD analysis of the as rolled material showed almost no texture present in the material, and this can be seen in the random distribution of points shown on the pole figure for the as rolled sample (Figure 5.4). Pole figures were recorded for each heat-treatment of the both alloys, and it was found that the texture remained very weak for all heat treatments and for the both alloys under investigation. An example pole figure for a heat-treated sample can be seen in Figure 5.5. All pole figures display one data point per grain.

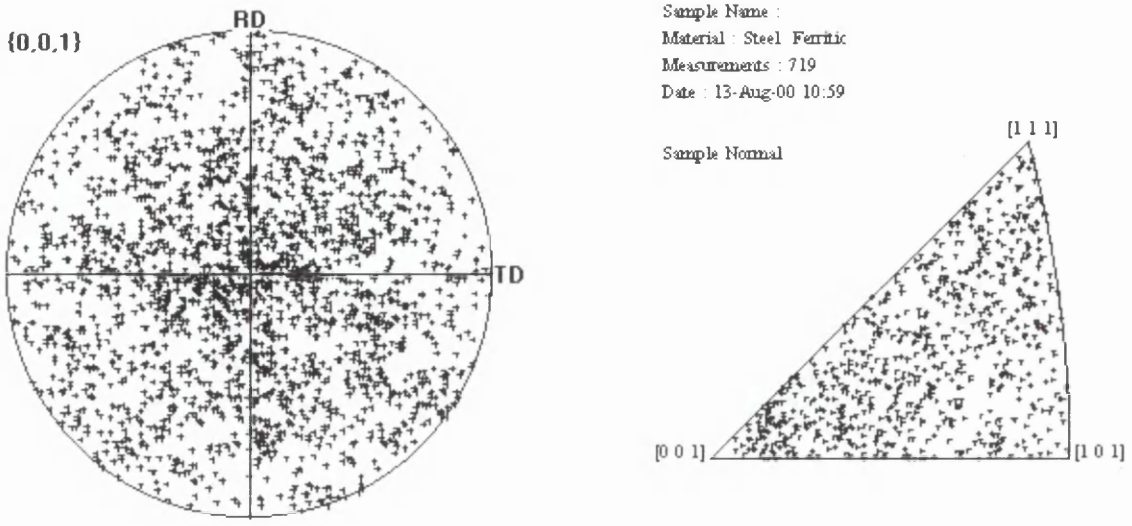

Figure 5.4 Pole figures showing the almost random texture of the 'as rolled' material

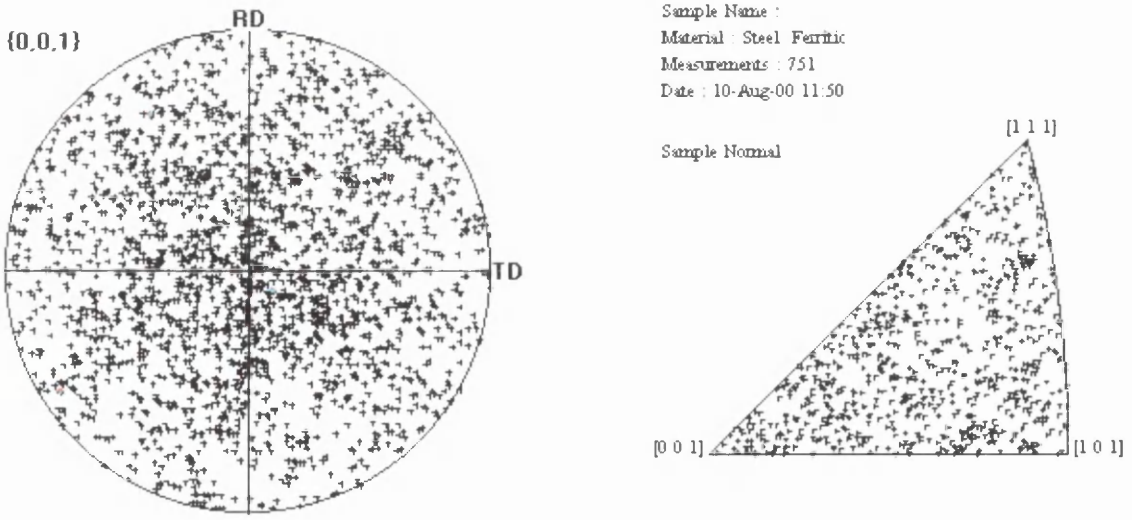

Figure 5.5 Pole figures showing the very weak texture of the 800/1/AC material

5.3 Grain Boundary Proportions

Analysis of both the as-rolled alloys by EBSD showed that the grain boundary proportions, which were measured by grain boundary number, deviated from what would be expected from a random distribution, with 5% $\sum 1$ and 3% $\sum 3$ for the as rolled material. Computer simulations by Warrington and Boon (1975) determined there to be no more than 2% of $\sum 1$ boundaries and 1% of $\sum 3$ boundaries present for a sample of random texture. Other CSL boundaries showed little deviation from what would be expected for a random distribution. The mean grain boundary misorientation angle for this sample was found to be 40° with a uni-modal angular distribution and a peak at 51°.

It is clear to see from the results for the 0.06wt%P alloy (Figures 5.6-5.8) that both the heat treatment temperature *and* the heat treatment time have an effect on the proportions of CSL boundaries present in the material. From these results, it can be seen that an increase in the aging temperature leads to an increased proportion of $\sum 3$ boundaries in the material. This is best seen in the results for the 0.06wt%P 1hr/AC samples (Figures 5.9-5.11), where the proportions of $\sum 3$ boundaries can be seen to increase linearly from 2.7% at 600°C to 6.9% at 900°C with a much greater increase as the temperature reaches 1000°C with the proportions of $\sum 3$'s rising to 10.7%. This increase at 1000°C is supplemented by the onset of abnormal grain growth, which leads to the conclusion that the two effects must be in some way linked.

The proportions of $\sum 1$ boundaries in the 1hr/AC material were unaffected by increasing temperature showing a percentage of 3.6% at 600°C rising to 3.7% at 900°C with no deviation greater than 0.4% as the temperature rises. As the aging temperature reaches 1000°C there is a decrease in the proportions of $\sum 1$ boundaries, falling from 3.7% at 900°C to 2.8% at 1000°C.

Figure5.6 Grain boundary Proportions for the 0.06wt%P alloy Annealed for a period of 1 hour

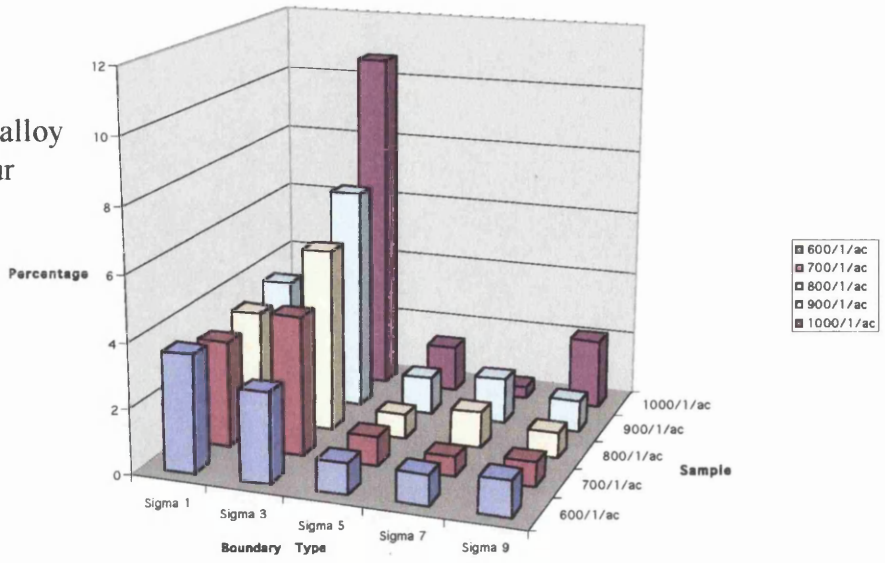

Figure5.7 Grain boundary Proportions for the 0.06wt%P alloy Annealed for a period of 2 hours

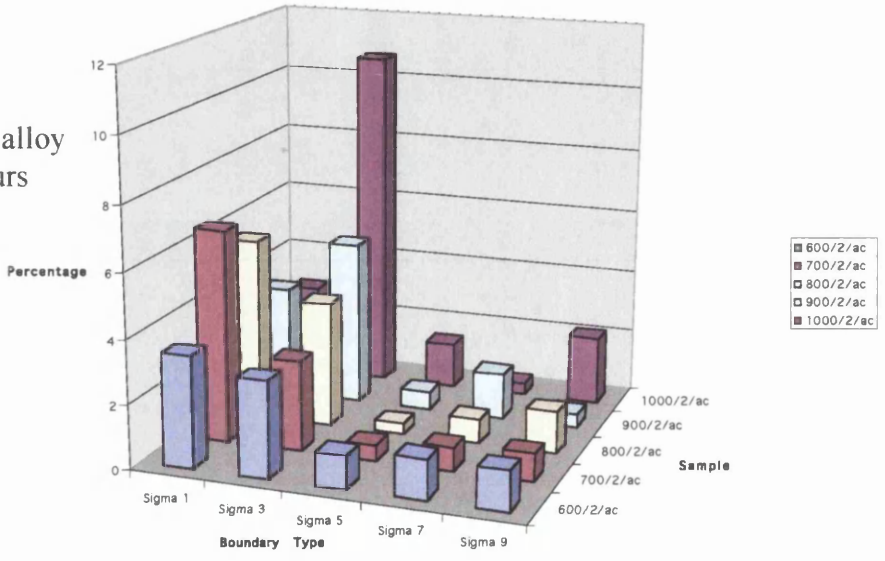

Figure5.8 Grain boundary Proportions for the 0.06wt%P alloy Annealed for a period of 5 hours

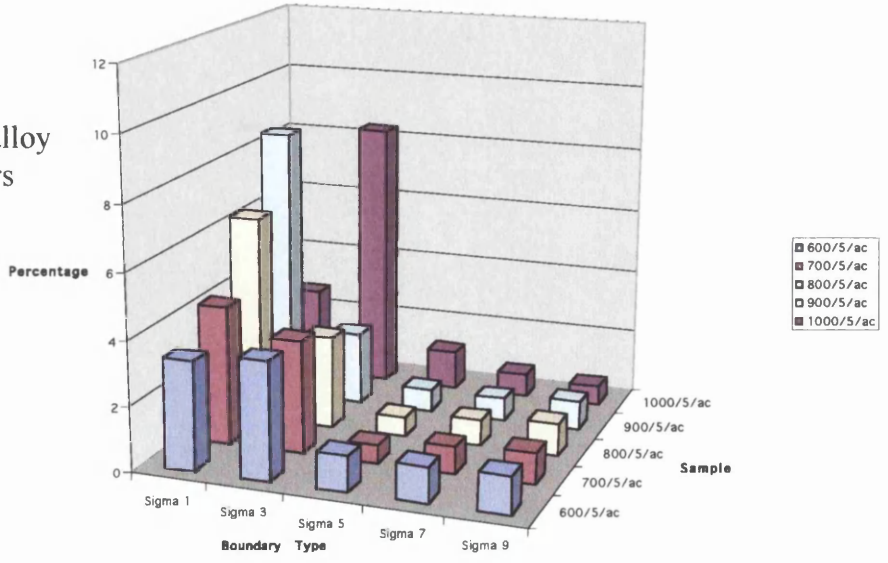

Figure5.9 Grain boundary Proportions for the 0.12wt%P alloy Annealed for a period of 1 hours

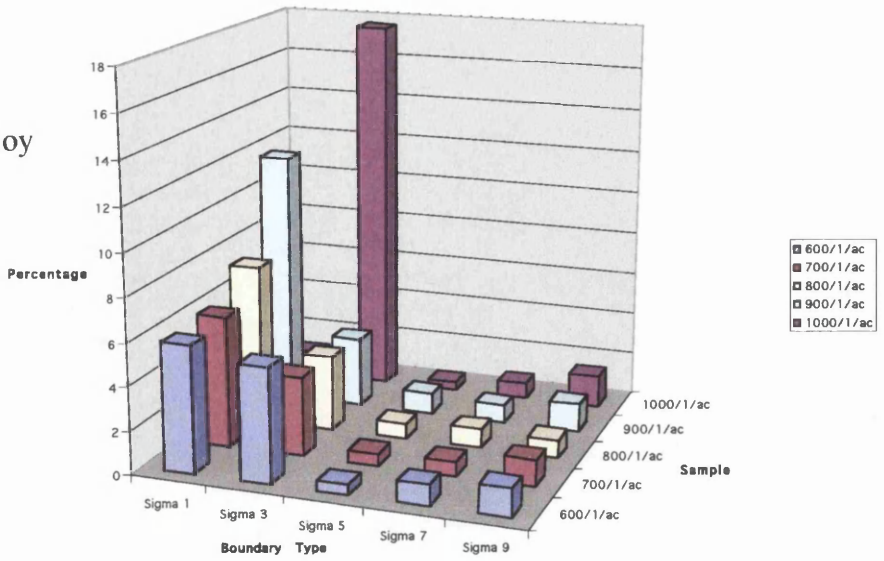

Figure5.10 Grain boundary Proportions for the 0.12wt%P alloy Annealed for a period of 2 hours

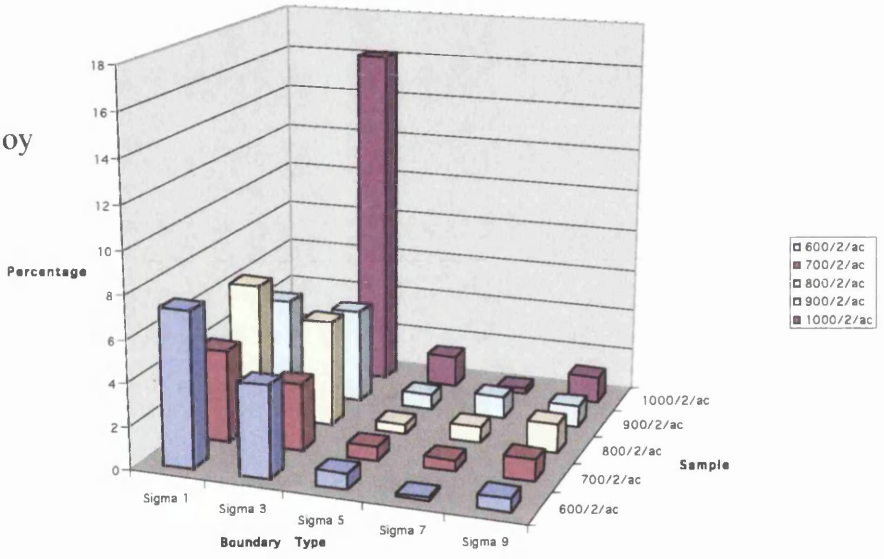

Figure5.11 Grain boundary Proportions for the 0.12wt%P alloy Annealed for a period of 5 hours

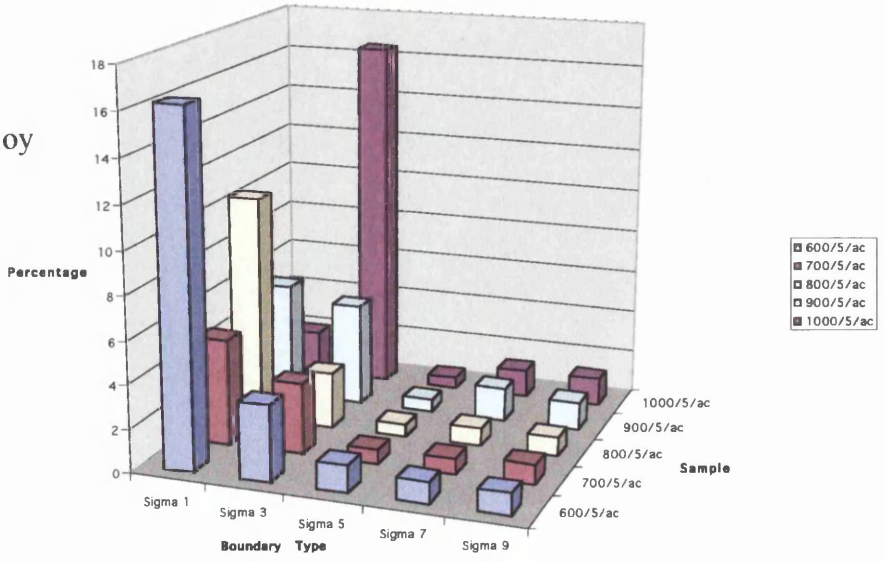

The aging time for which the samples are treated is also an important factor affecting the proportions of boundaries that are present in the material. From the results of the test matrix it can be seen that there is an increase in the proportions of $\sum 1$ boundaries for the 900°C samples as the aging time is increased from 1 to 5 hours, the proportion of $\sum 1$ boundaries being 3.7% at 900/1hr/AC rising to 8.5% at 900/5hr/AC. The opposite can be seen for the $\sum 3$ proportions in the 900°C samples, falling from 6.9% at 900/1hr/AC to 2.2% at 900/5hr/AC.

Similar changes are not evident for the samples aged at 600°C, where neither the $\sum 1$ or $\sum 3$ boundary proportions are seen to alter by as much as 1%. This can be attributed to the fact that very little structural changes occur in this material at temperatures ~600°C, and any changes that are occurring are doing so at a very gradual rate, hence little is to be seen unless the heat treatment times are made sufficiently large such that these gradual changes become discernable.

This idea was tested on two samples that had been heat-treated previously (Cowan, 1997), one for 475°C/5600hrs/WQ and the other for 500°/1800hrs/WQ. The first sample 475°C/5600hrs/WQ showed only a small deviation from what would be expected for a random distribution (Warrington and Boon, 1975), with 3.9% $\sum 1$ and 3.0% $\sum 3$ boundaries present in the material. This result is probably greater attributed to the fact that the temperature at which the sample has been aged is too low for grain boundary migration to occur in the material. An increase in temperature to 500°C/1800hrs/WQ however, gives results that deviate greatly from those expected for a random distribution, with 9.1% $\sum 1$ and 6.3% $\sum 3$ boundaries. This 25°C increase in annealing temperature seems to be enough for changes in the microstructure to take place, though it would be doubtful if the results would have been seen should the sample have been aged for a time ~5hrs, as it takes a long time for microstructure changes to become apparent at this low a temperature. This result is consistent with the results from the test matrix where there is an increase in the proportions of $\sum 1$ boundaries present in the material as the aging time is increased

Results for the 0.12wt%P alloy show a much greater proportion of Σ3 boundaries for the samples aged at 1000°C with as much as 17.6% Σ3 present for the 1000°C/1hr/AC sample. This only dropped slightly to 16.2% Σ3 at 1000°C/2hr/AC and 16.5% Σ3 at 1000°C/1hr/AC. The proportion of Σ3 boundaries remained between 2.5% and 5.3% for all other 0.12P heat-treated samples.

The proportions of Σ1 boundaries for the 0.12wt%P material showed a general trend dependent on the aging time. At annealing times of 1hr, the higher temperature heat treatments produced the higher proportions of Σ1 boundaries, with 11.8% at 900°C and only 5.9% at 600°C. The proportions at 1000°C fell abruptly to 1.1% Σ1, coinciding with the large increase in the proportions of Σ3 boundaries. At annealing times of 5 hrs, the opposite trend seems to take place, with there being 16.3% Σ1 boundaries for the 600°C sample and only 5.4% for the 900°C sample. Again, the proportions of Σ1 boundaries remained low for the 1000°C sample at 2.0%. At an annealing time of 2 hrs, the Σ1 proportions remain between 7.2% and 2.2%, indicating there to be a transition between the trends seen at the 1hr and 5 hr annealing times where neither case is prominent, the proportions appearing consistent for all temperatures.

5.3.1 Misorientation Angles

Other results uncovered during the analysis (Figure 5.12) showed that the mean misorientation angle was approximately 40° for all the samples analysed, regardless of heat treatment temperature or aging time, varying by a maximum of 6° to reach 36.0° for the 900/5/AC sample and rising to 42.0° for the 1000/1/AC sample for the 0.06wt%P alloy. Mean misorientation angles for the 0.12wt%P alloy varied to a slightly greater extent reaching a minimum value of 34.9° for the 900/1/AC sample and rising to 43.4° for the 1000/1/AC sample, giving a misorientation range of 8.5°, a significant deviation from the results that would be expected for a random distribution (Mackenzie 1958). The value of the misorientation angle that is the mid-point value of the set of misorientation values, the misorientation median, showed a very good correlation to the mean value for all heat treatments and alloys (Hutchinson et al, 1996). Values for the most frequently occurring misorientation value, the misorientation mode, displayed a significant deviation from the values of the mean and median misorientation values. The values for the misorientation mode tended to fluctuate greatly between the different heat treatments, especially for the longer annealing times for the 0.06wt%P alloy, reaching a maximum value of 58.7° for the 700/5/AC sample, and a minimum of 34.9° for the 600/2/AC sample. The average value of the misorientation mode for the 0.06wt%P material was 44.1° even though it displayed a high degree of fluctuation.

The results of the misorientation mode data for the 0.12wt%P alloy also showed a high degree of fluctuation, however the average value tended to be a lot higher that for that of the 0.06wt%P alloy; the maximum being 59.7° for both the 1000/1/AC and 1000/2/AC samples, with a minimum of 40.9° for the 800/1/AC sample. The average value for the misorientation mode for the 0.12wt%P alloy was a value of 51.9° (Figure 5.13)

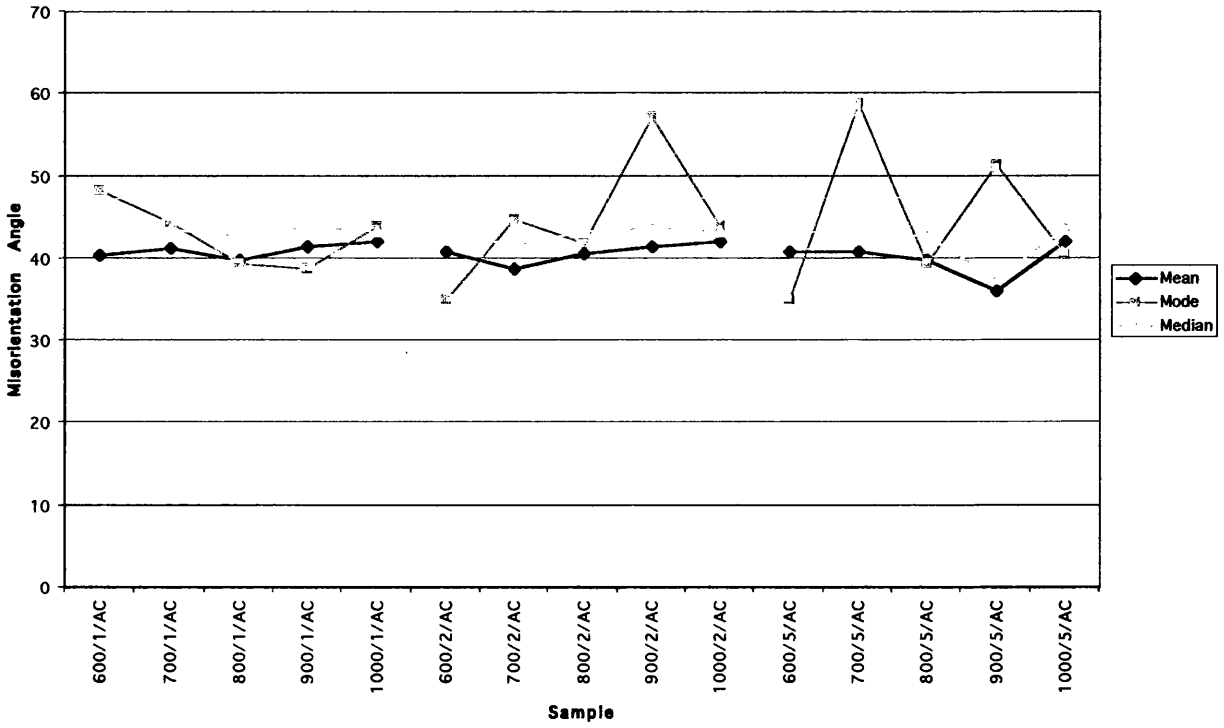

Figure 5.12 Average misorientation values for the 0.06wt%P alloy

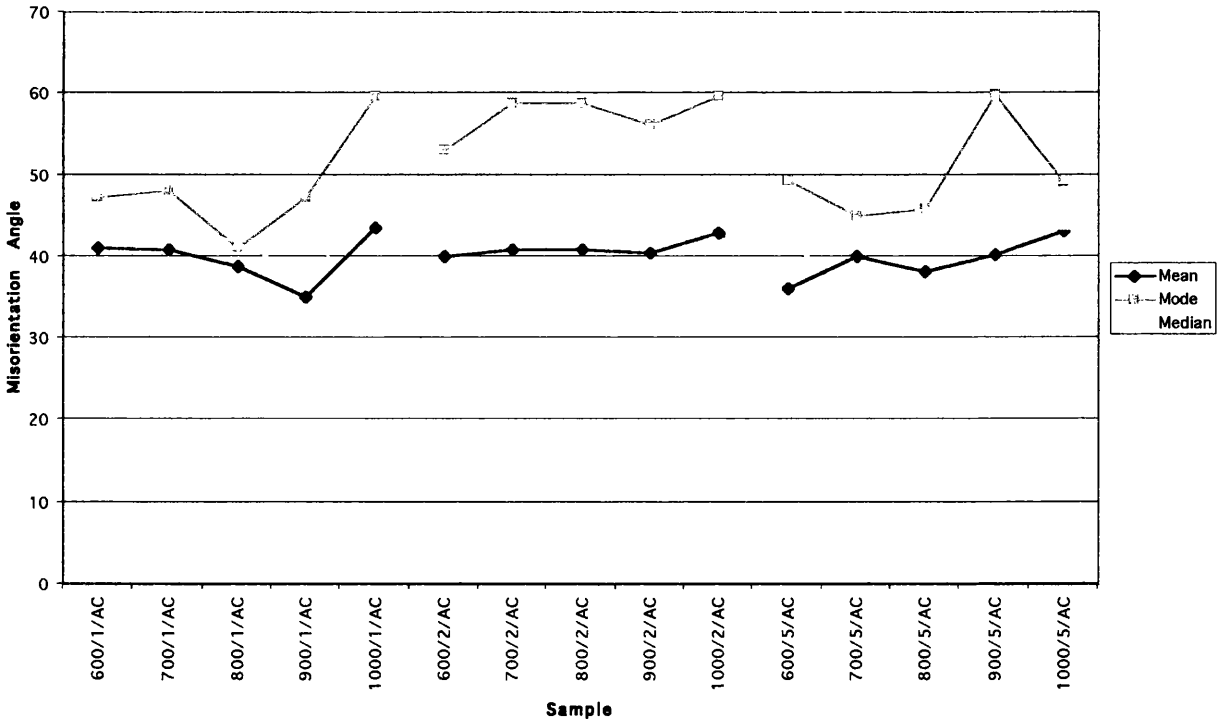

Figure 5.13 Average misorientation values for the 0.06wt%P alloy

5.3.2 Misorientation Angle Frequency Distributions

The misorientation angle distribution normalised data for the 0.06wt%P alloy (Figures 5.14-5.16) showed a tendency for the peak misorientation value to increase with increasing annealing temperature in a manner similar to that of a Mackenzie distribution for samples aged at lower annealing temperatures. It was seen (Figure5.14) that for the 600/1/AC and 700/1/AC heat treatments, there is a definite peak at 50°. As the heat treatment temperature is increased, there is a reduction in this 50° peak, until 1000/1/AC where the peak has disappeared, becoming instead, an almost linear increase toward the value of 60°. Almost exactly the same trend is seen in the data for all the 0.06wt%P samples that were annealed for two hours, there being a definite change in the shape for the distribution curve with increasing annealing temperature. For the 0.06wt%P samples that were aged for 5 hours, this trend is no longer exhibited; instead, all of the heat treatments have very similar shape misorientation distribution curves.

The Misorientation distribution curves for the 0.12wt%P alloy (Figures 5.17-5.19) showed a similar trend to that of the 0.06wt%P alloy, though with a much higher degree of scatter in the data. The 1000°C samples could be seen have a linear increase toward 60°, as oppose to the peak at 50° exhibited by the samples that had been subject to lower annealing temperatures as in the case of the 0.06wt%P alloy. The trends exhibited by the 0.12wt%P alloy were not as clearly defined as those for the 0.06wt%P alloy though they tended to be very similar for the two alloys, the only differences being attributed to the high degree of scatter in the curves for the 0.12wt%P alloy.

Figure 5.14 Misorientation angle distribution for the 0.06wt%P alloy annealed for 1 hour

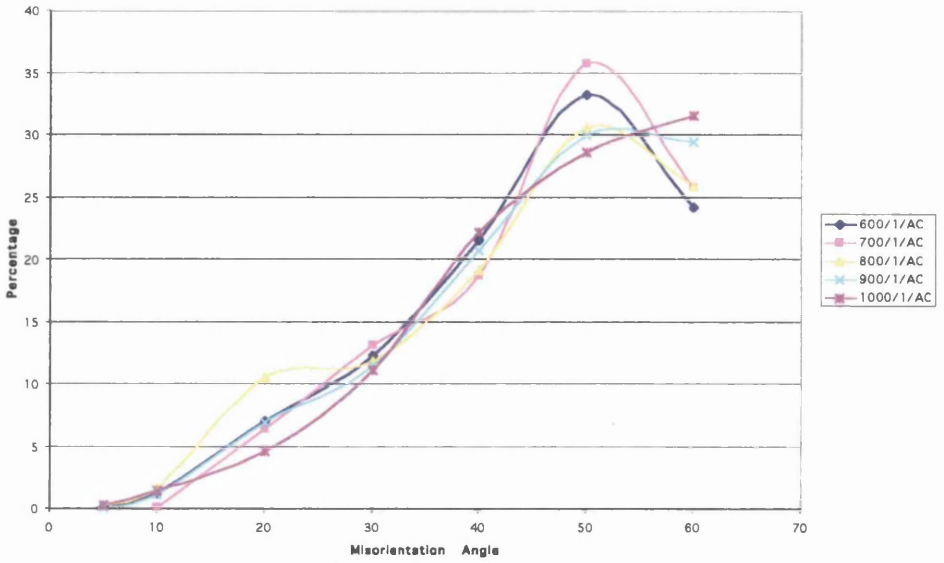

Figure 5.15 Misorientation angle distribution for the 0.06wt%P alloy annealed for 2 hours

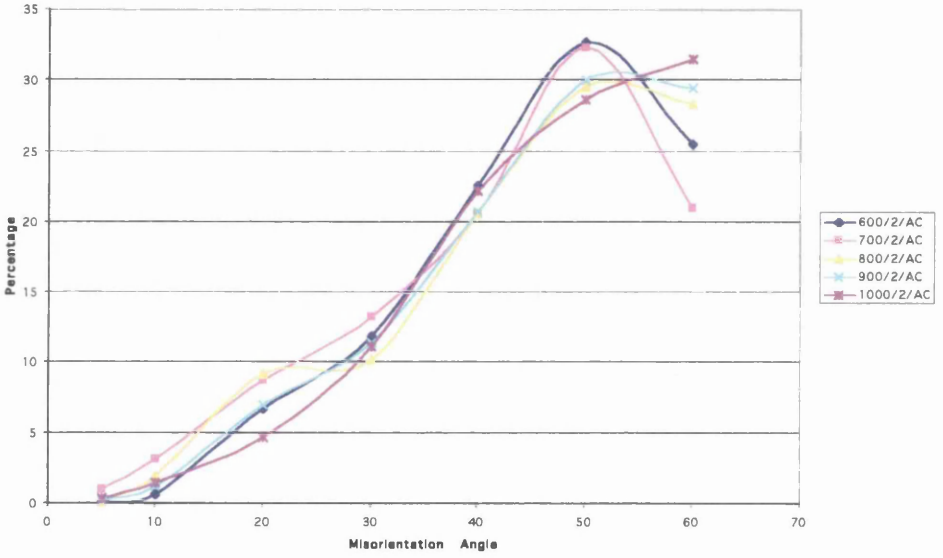

Figure 5.16 Misorientation angle distribution for the 0.06wt%P alloy annealed for 5 hours

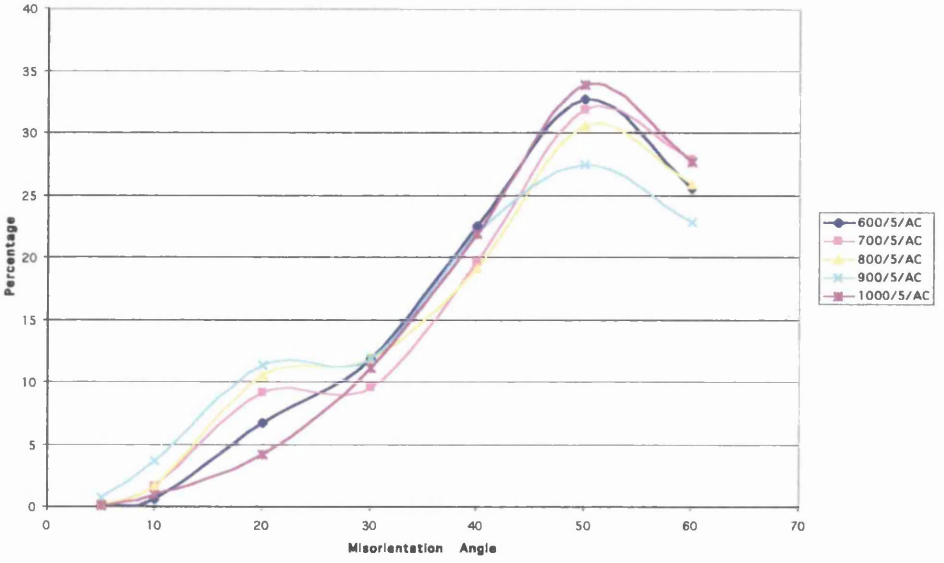

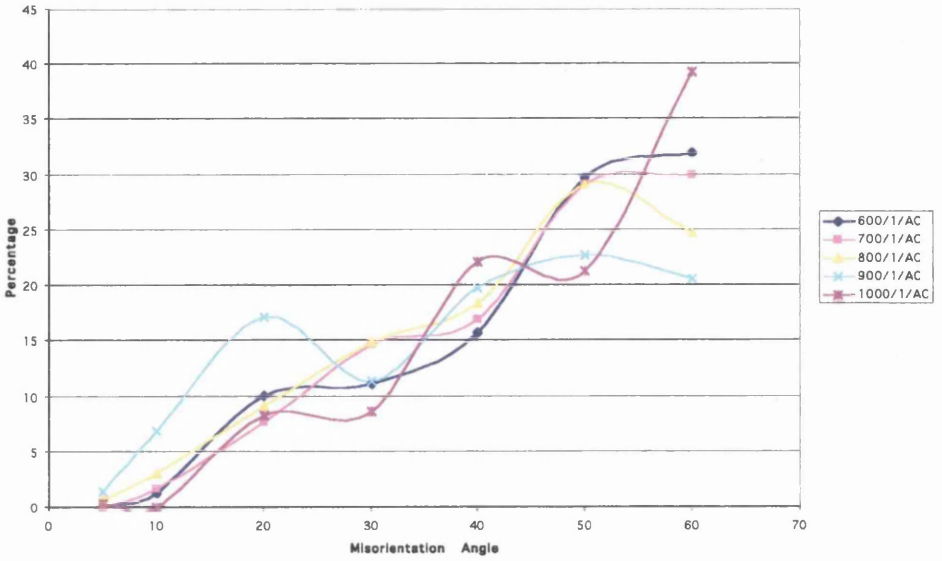

Figure 5.17 Misorientation angle distribution for the 0.12wt%P alloy annealed for 1 hour

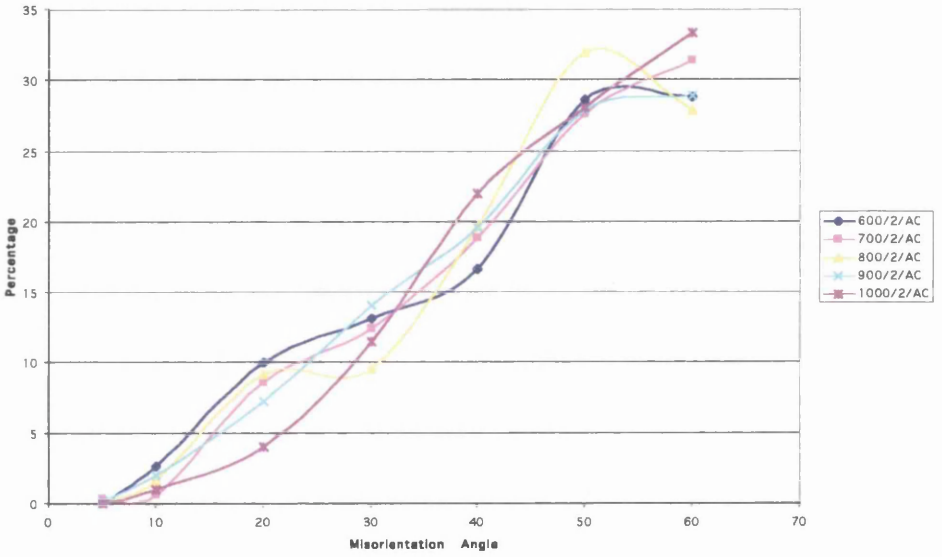

Figure 5.18 Misorientation angle distribution for the 0.12wt%P alloy annealed for 2 hours

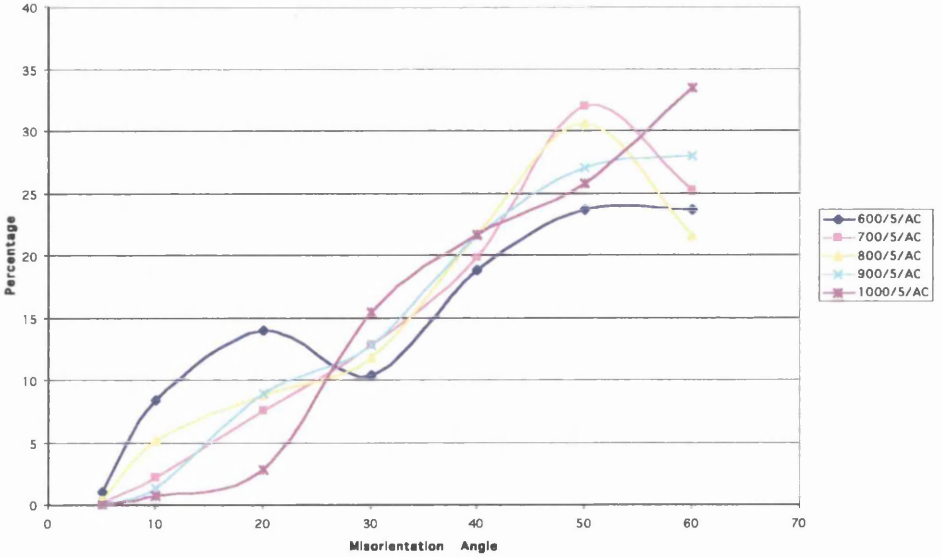

Figure 5.19 Misorientation angle distribution for the 0.12wt%P alloy annealed for 5 hours

5.4 Fracture Surface Serial-Sectioning (FSS)

The results from the FSS analysis (Figure 5.20) are accumulations of a number of sections (up to 20) taken at various depths through the material. An equal number of results from un-fractured and fractured sample regions were acquired at each section in order to eliminate the possibility of structural changes at different depths through the material. Results were complied and analysed in Excel, and plots made of the proportions of boundary types for the different heat treatments. The results for the un-fractured samples are consistent with the results that would be expected from work done previously (Williams, 1999), showing a definite increase in the proportion of $\sum 3$ boundaries as the aging temperature of the sample is increased; rising from 2.6% $\sum 3$ for a sample aged at 600°C to 10.7% $\sum 3$ for a sample aged at 1000°C. The proportions of $\sum 1$ boundaries (defined as low angle boundaries between 5 and 15 degrees) were seen to stay between 2.9% and 4.7% for all the heat treatments, and other $\sum$ boundaries showed no deviation from those that would be expected from a random distribution.

Results acquired across the fracture surface showed little resemblance to the results from the un-fractured sample region (Figure 5.21). The proportions of $\sum 1$ boundaries stayed at a value between 6.5% and 4.5% for all the heat treatments, though due to the complexities involved in this technique, it is not possible to determine if these results are a true representation of the $\Sigma 1$ boundary proportions. This is largely due to the ambiguity between low angle boundaries and transgranular cleavage across the fracture surface, as the realignment process introduces an angular error, which can be as much as 5°. This would easily be enough to cause a transgranular boundary to be misidentified as a low angle intergranular boundary, introducing an error in the proportions of $\sum 1$ boundaries.

The proportions of $\sum 3$ boundaries across the fracture surface are not plagued by the same problems as $\sum 1$ boundaries, hence the results can be considered a great deal more accurate.

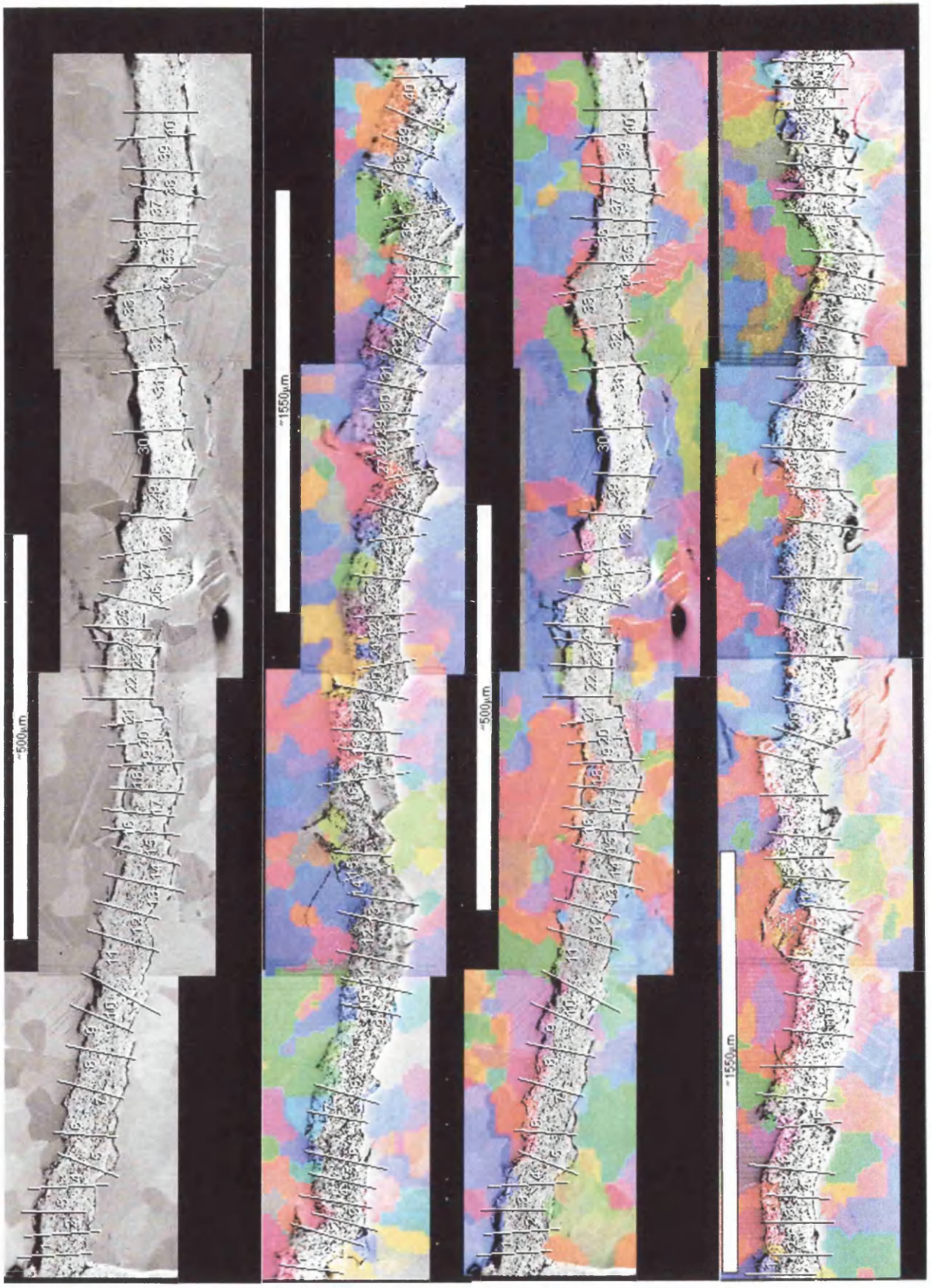

Figure 5.20 Montaged Crystal Orientation Maps Acquired by FFS Analysis

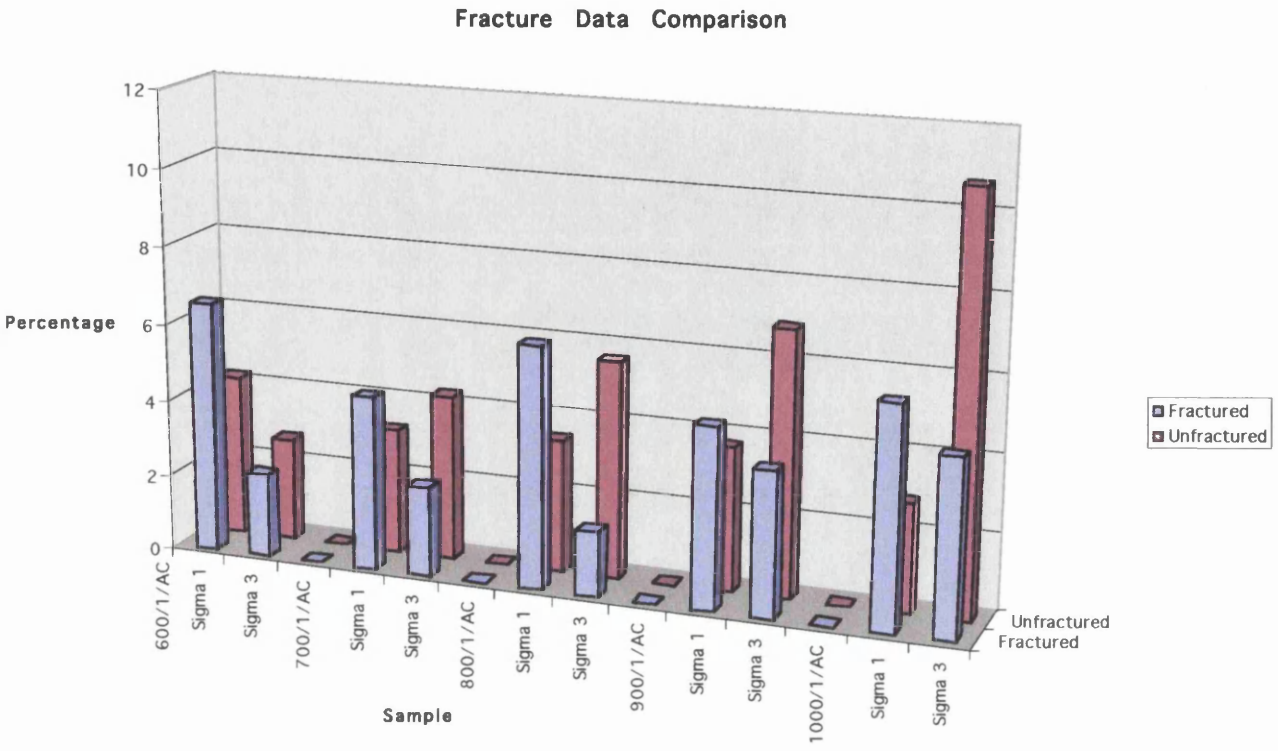

Figure 5.21 Chart showing the proportions of Sigma 1 and Sigma 3 boundaries in a fractured sample (Red) compared to unfractured control data from the same samples (Blue)

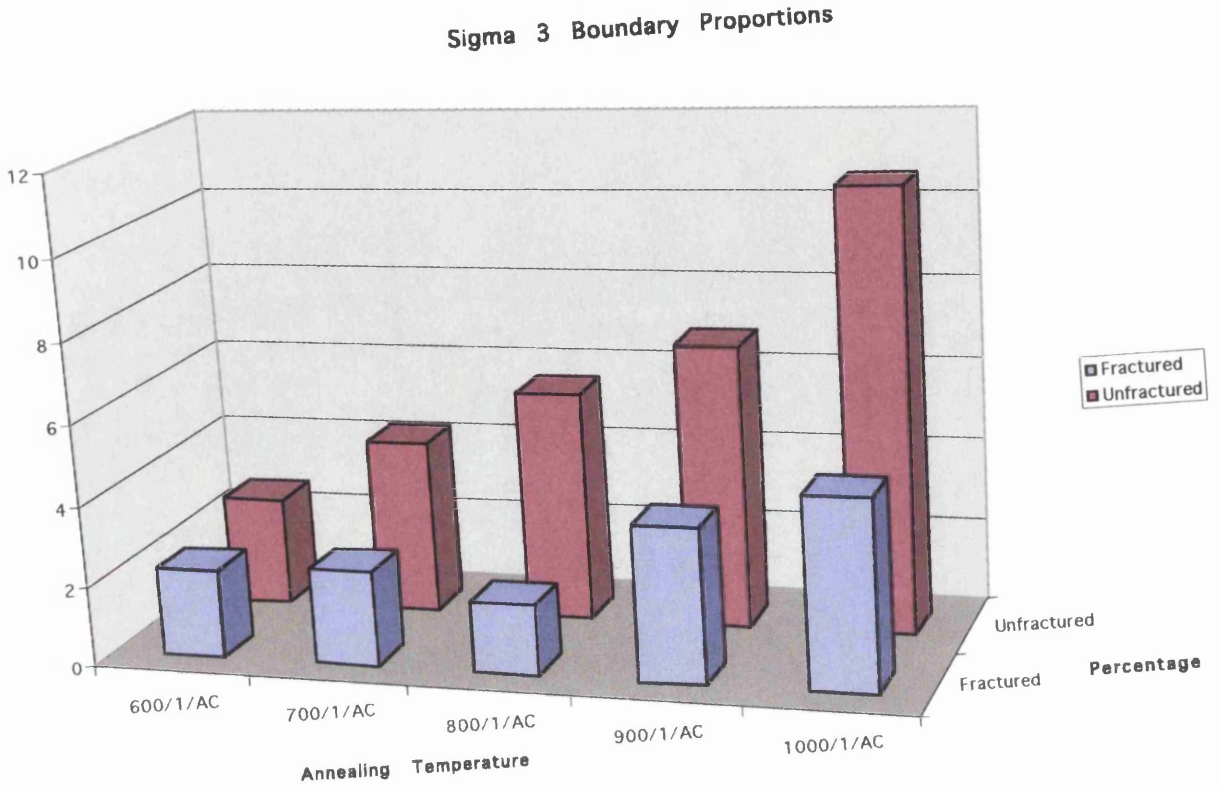

Figure 5.22 Chart highlighting the proportions of sigma 3 boundaries in fractured and unfractured samples

The proportions of Σ3 boundaries were found to be between 1.7% and 2.1% for the 600°C to 800°C samples, rising to 3.8% at 900°C and 4.6% at 1000°C. This trend is consistent with the increase in Σ3 boundary proportions seen for the un-fractured samples, though the degree to which the increase occurs is markedly less; There being 10.7% Σ3 boundaries in an unfractured sample at 1000°C and only 4.6% Σ3 boundaries across the fracture surface of the same sample.

5.5 Deformation Twinning.

A high degree of deformation twinning occurs near the fracture surface and may be a contributing factor to the chosen fracture path through the sample. This effect should be taken into consideration, in addition to the determination of the effects of grain boundary types and segregation levels on the brittle fracture path, as it may have an equally important effect (Smida and Bosansky, 2000). Results show that deformation twins are generally formed ahead of the crack tip with the crack then propagating through them. This can be seen in the way that they align exactly, on both sides of the crack, equidistant from the crack tip. From this it can be inferred that they were at one time connected, prior to the crack propagation. The effect of deformation twins on the fracture path can easily be seen on secondary cracks propagating away from the fracture surface (Figure 5.23). From this it can be seen that the crack front is deflected by the deformation twin, following perpendicular to the twin for a short distance, before breaking through it, returning to its original path. This shows that the deformation twins are able to act as crack arresters in this material. They seem to have less of an influence on the fracture path when they form perpendicular to the propagating crack, where it seems easier for the crack to go straight through them. They have their greater influence on the fracture path when the angle between them and the propagating crack is lower, where they can be seen to be the initiators for the propagation of secondary cracks which tend to follow parallel to the deformation twin (Figure 5.24).

Figure 5.23 Crack deflection by deformation twins

Line	Angle	Axis	Sigma	V/Vm
1	59.36	-0.57,-0.62,0.54	3	0.39
2	59.25	-0.59,-0.57,-0.58	3	0.14
3	1.23	-0.11,0.98,0.17	None	None
4	2.26	-0.21,-0.70,-0.68	None	None
5	4.37	0.34,0.32,-0.88	None	None

Figure 5.24 Crack propagation/initiation parallel to a deformation twin

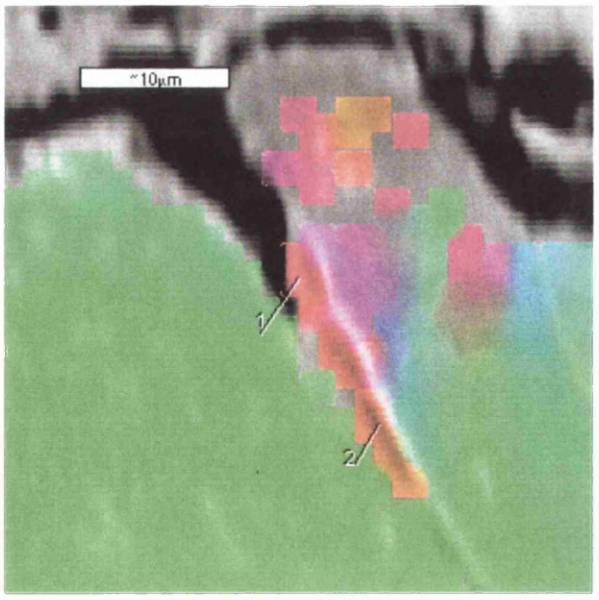

Line	Angle	Axis	Sigma	V/Vm
1	57.39	-0.65,-0.52,-0.55	3	0.69
2	62.62	-0.68,-0.47,-0.57	3	0.72

5.6 Determination of the Grain Boundary Plane.

Work done previously (Davies et al., 2002) has shown that there is a strong correlation between facets exhibiting river-lines and an {001} surface orientation, corresponding to a {001} cleavage plane. This result proved consistent with the fact that {001} is the most usual cleavage plane in bcc material. Other work had successfully confirmed this for almost all facets, with the occasional occurrence of a {110} cleavage plane. This can be explained by considering the fact that the Young's modulus of iron has a minimum value for <001> directions, hence iron is most likely to cleave on {001} planes. {110} planes do not cleave as easily due to the fact that {110} planes are more closely packed than {001} planes.

The analysis of intergranular fracture planes is far more complicated in this material, due to the geometry of the fractured facets. The analysis of intergranular facets in the SEM showed that almost all intergranular facets on the fracture surface exhibited a curved surface, a fact that was confirmed by the application of the 'Stereo Facet' program to the fractured facets. It can be seen (Figure 5.25a,b) that the majority of IG facets consist of an irregular curved structure. This is confirmed by the 3D reconstruction (Figure 5.26) where the degree of curvature for a typical grain can be seen. This result leads to the conclusion that the intergranular boundary plane is not a significant factor in the structure of the material, as the grains do not form planar surfaces.

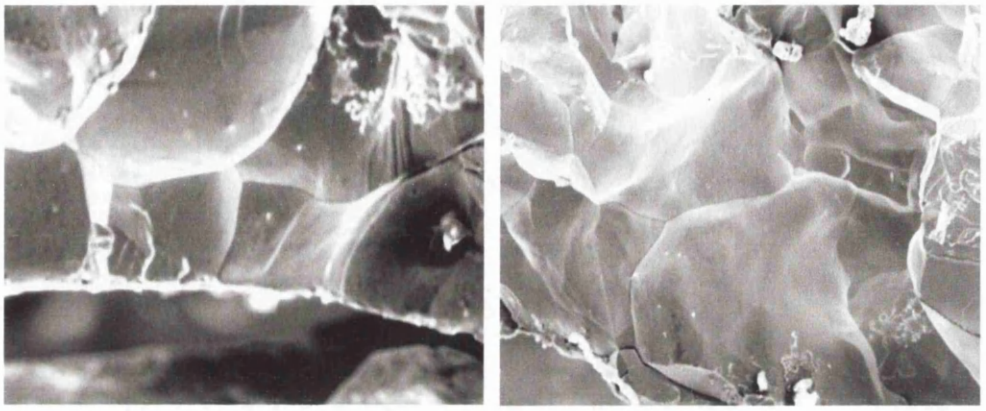

Figure 5.25a,b Intergranular facets displaying irregular curved surfaces

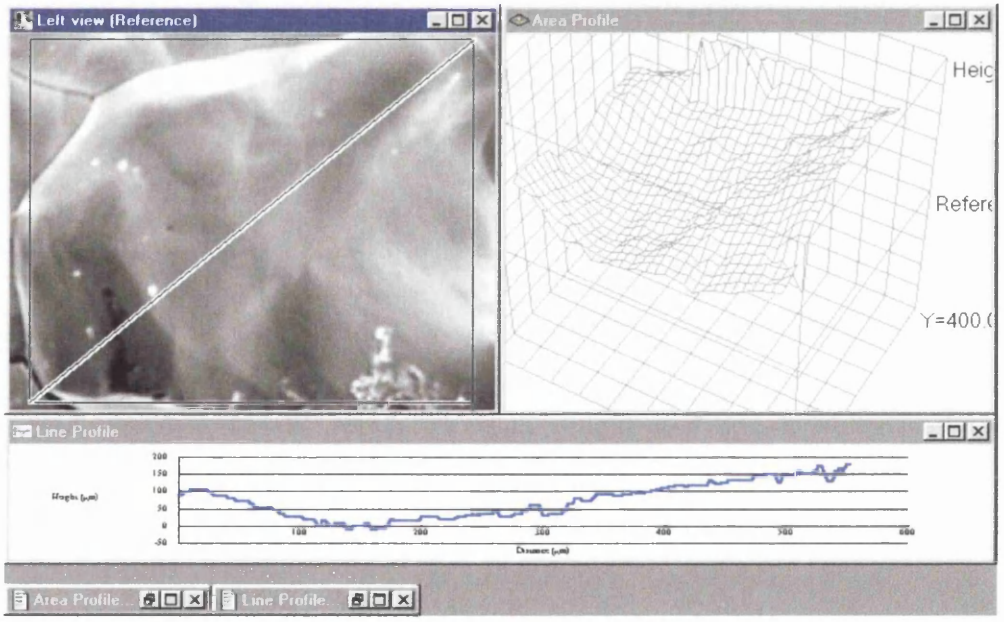

Figure 5.26 Three dimensional elevation model of a curved fracture facet using the 'Stereo Facet' software

5.7 Auger Analysis

The fracture surfaces to be analysed were first imaged using a secondary electron detector, the images were digitally marked and each facet to be analysed numbered accordingly. It can be seen from figure 5.27 that the identification of transgranular and intergranular facets can be easily determined by the presence of 'river lines' on the surface of the transgranular facets, an Auger map was still taken of the area in order to ensure that the transgranular facets were labelled correctly. Approximately 13 intergranular and 2 transgranular facets were electronically marked by number, and analysed for each of the samples. All analysis of Auger data was done at Berkeley Labs, using in-house software (Cowan, 1997).

It can be seen from table 5.1, that for the 4 samples, there is an average of 6.7 at% phosphorus and 10.7 at% carbon present at the surface of the intergranular facets analysed. This results in an average of 82.6 at% Fe present at the intergranular boundaries. Data for the transgranular boundaries shows and average of 99.1 at% Fe, 0.8 at% C and 0.1 at% P.

5.8 Auger / Fracture Surface Analysis (A-FSA)

The first part of the A-FSA procedure was the identification of corresponding facets from the two different microscope images. This was best achieved with the sample mounted flat in the microscope, with the fracture surface normal to the incident electron beam. An image of the fracture surfaces was then printed, and compared with the image from the Auger microscope which had the facets numbered on it. The facets were then carefully matched and the numbers marked on the new printout.

The sample was then mounted at 70° in the microscope and the procedure repeated. The facets were a lot more difficult to identify at this inclination angle, and the two previous images were used as reference, in order to accurately determine the correct facets. An

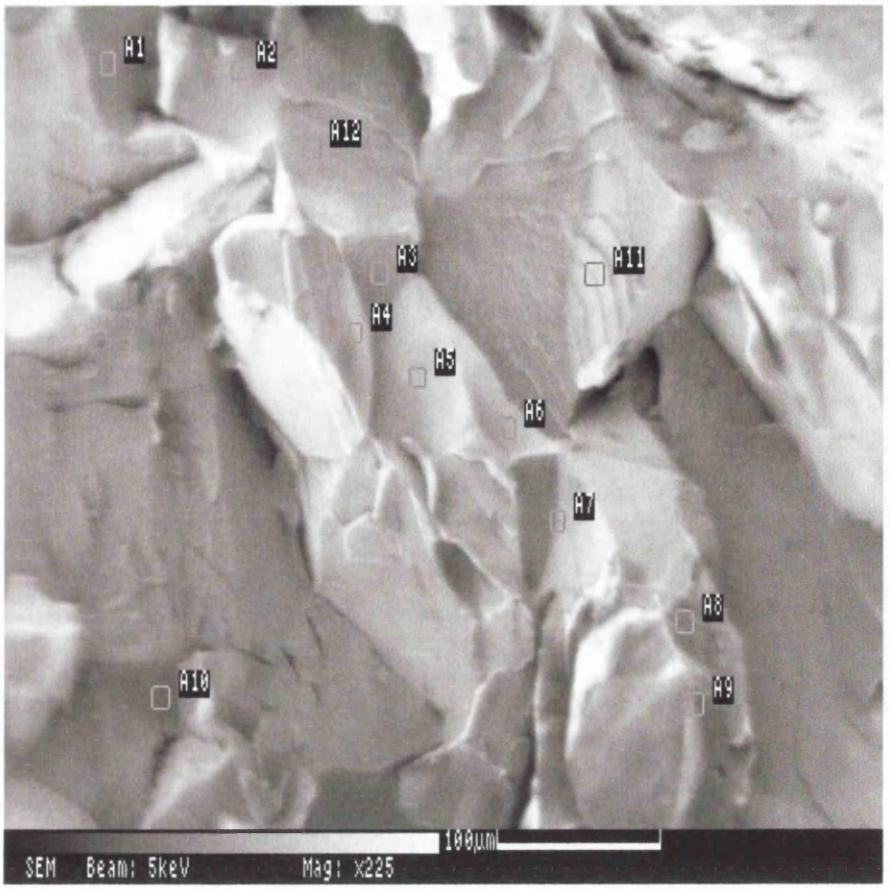

Figure 5.27 Typical Auger 'matchstick' fracture surface taken on the 310-F Auger Microprobe showing a brittle fracture surface consisting of smooth intergranular facet sand cleavage facets. The cleavage facets being easily identified by the presence of river lines, such as the facet labelled A11.

	Mean % Fe	Mean % P	Mean % C
Sample 1	82.972	6.967	10.06
Sample 2	83.136	6.885	9.978
Sample 3	82.3107692	6.54076923	11.1492308
Sample 4	81.96	6.44642857	11.5914286
Total	82.5946923	6.70979945	10.6946648

Table 5.1 Shown above is the segregation data for the four samples analysed by Auger electron microscopy.

example of the difficulties in determining the correct facets can be seen in figures 5.28a-5.28f. Once the facets were accurately determined at 70°, another image was recorded, and the facets on it numbered accordingly. Topographical and crystallographic information was then acquired from the facets by the consecutive application of 'Stereo Facet' and EBSD, using the procedure described previously.

Once as many facets as possible were indexed, it was necessary to extract the crystallographic data from the COM. This was best achieved by utilising some of the features provided by the 'Texture Rendering' option within the Oxford software, a method for which the software was never designed. The software was utilised in such a way that a high number of results could be accurately extracted in a relatively short time, compared to the laborious manual methods used previously (Randle and Davies, 1999). Pole figures were also be saved at this stage and the data point corresponding to each facet was identified. Extraction of the facets orientation matrix is also possible, but is not a straight forward procedure. If the orientation matrices are exported without preparation then a matrix for every data point is recorded, resulting in huge amounts of superfluous data. It was necessary to filter the maps a number of times, until the facets were represented by an un-fragmented colour, it was then possible to obtain a 'true grain ID map', making it is possible to export only the required orientation matrices, the result of which were one, or occasionally two matrices per facet as oppose to the 20-50 recorded previously.

These matrices are however, not related to the image, so it was necessary to identify which matrix corresponded to which facet. This was best achieved by magnifying the COM and drawing a small line on the facet required in the centre of the coloured region. An X-Y coordinate was then be displayed for this central point, and this was compared with the X-Y coordinates shown by the orientation matrices in order to identify the correct one. This process was repeated until all facets and corresponding matrices were identified.

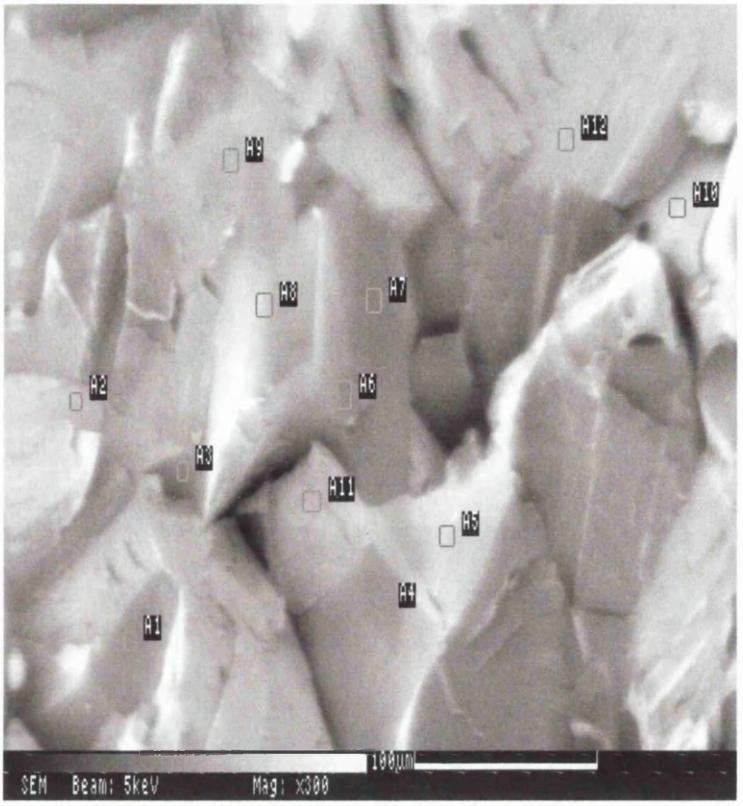

Figure 5.28a,b Secondary electron images from the 310-F Auger microprobe (above) and from the JEOL 6100 scanning electron microscope (below). The corresponding facets are marked on each image and the imaging difference between the two instruments can be clearly seen

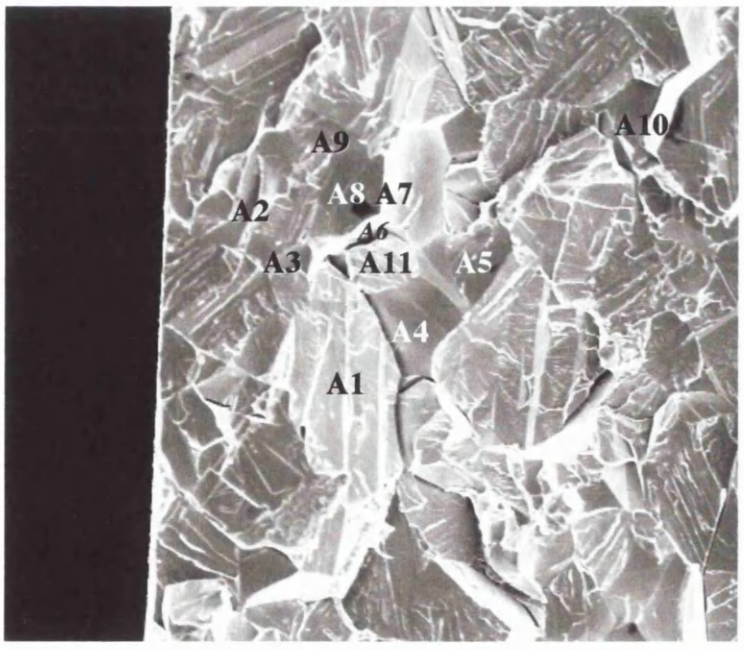

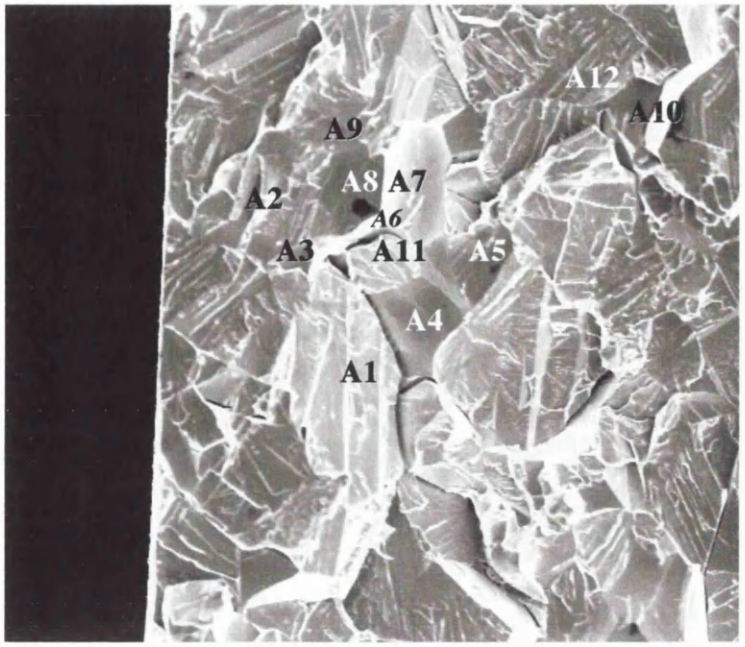

Figure 5.28c,d These images illustrate the difficulties in matching the facets imaged at 0 degrees (Above) and at 70 degrees (below). The problems encountered by 'shadowing' and the surface topography can be clearly seen when the sample is mounted at 70 degrees.

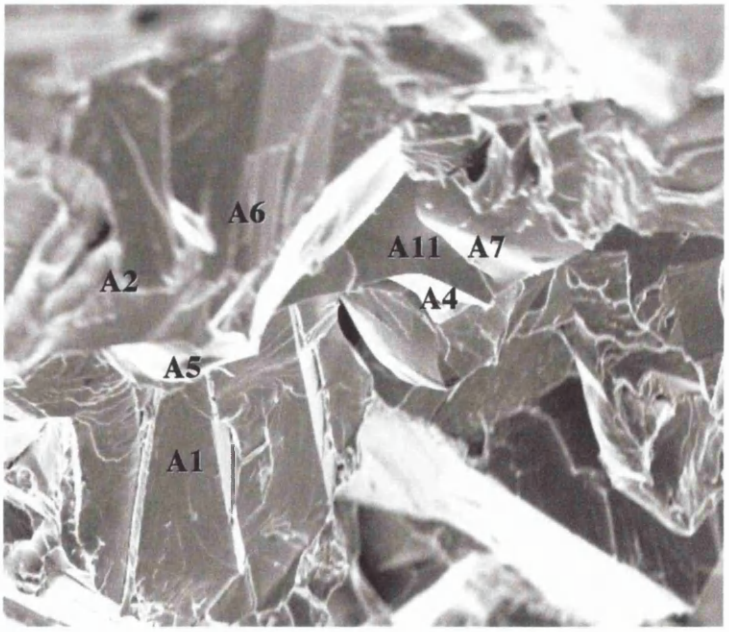

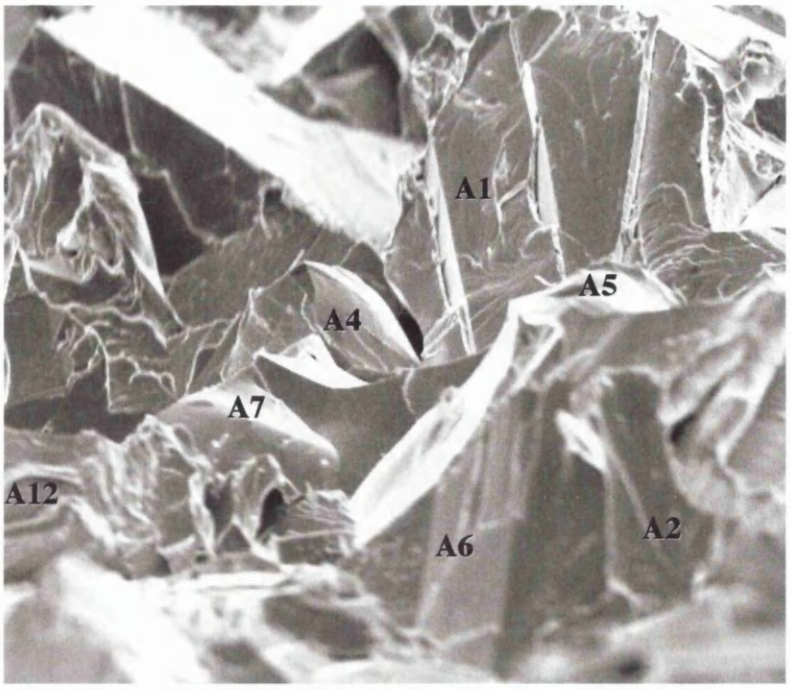

Figure 5.28e,f Area matching at 70 degrees (above) and on a tilt corrected Crystal Orientation Map at 70 degrees (below)

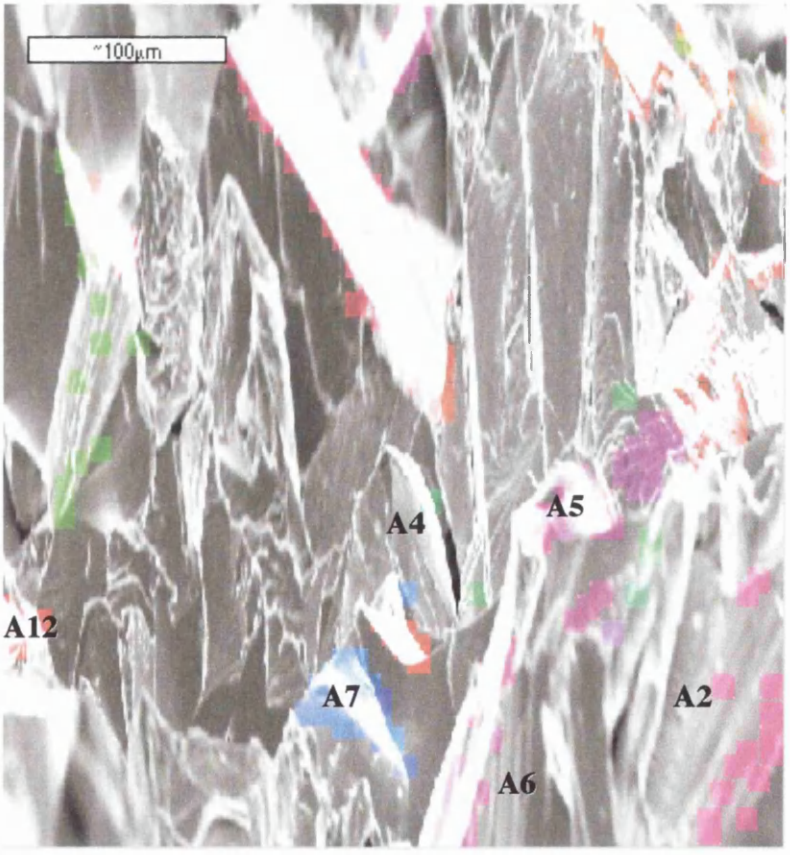

Figure 5.29 Screenshot of the 'Texture Rendering' software, showing how the software can be adapted and utilised in order to determine the orientation of the grain boundary plane for grains on the surface of a fractured sample.

The results of the A-FSA analysis in table 5.2 show that a total of 16 Auger facets were successfully analysed from the 4 samples, of which 2 were transgranular fracture facets. It can be seen from this data that both of these transgranular facets have fractured along the {001} plane, this is also shown in the inverse pole figure corresponding to one of the sample COMs (Figure 5.30a,b). This result proves consistent with work done previously on the same materials (Williams et al, 2000).

The remaining 14 intergranular fracture facets were found to have a wide selection of crystallographic fracture planes, though the majority proved to be {110} and {112}. Other crystallographic planes showed no statistical anomalies, having a maximum of one occurrence out of the combined data set

In all cases, it was possible to measure exactly the plane indices shown in table 5.2, due to the fact that the facets were curved in nature and hence, the electron beam could be moved around the facet until the average value for the facet plane was determined from the spread of measured values. The errors present in this technique are very difficult to calculate accurately due to the large number of process involved. The largest error is in the mounting and realignment for EBSD which may be as high as 10°. It was shown however (Table 5.2), that all transgranular fracture planes were measured to be exactly {001} in all cases, showing there to be a high degree of accuracy for planer fracture facets.

Area	Atomic %Fe	Atomic %P	Atomic %C	Fracture	Facet Plane
1	99.27	0	0.73	Transgranular	{001}
2	99.9	0	0.1	Transgranular	{001}
3	82.07	8.18	9.75	Intergranular	{012}
4	83.18	4.88	11.94	Intergranular	{110}
5	83.08	7.87	9.05	Intergranular	{110}
6	83.43	4.47	12.1	Intergranular	{110}
7	82.45	5.16	12.39	Intergranular	{110}
8	79.82	11.83	8.34	Intergranular	{112}
9	79.28	5.48	15.24	Intergranular	{112}
10	83.08	7.39	9.53	Intergranular	{113}
11	80.58	7.62	11.8	Intergranular	{114}
12	82.89	7.98	9.13	Intergranular	{122}
13	82.97	7.44	9.58	Intergranular	{123}
14	84.47	5.5	10.03	Intergranular	{133}
15	83.22	6.25	10.53	Intergranular	{233}
16	90.42	4.1	5.47	Intergranular	{234}

Table 5.2 The table above shows the data from the 16 facets acquired by the innovative A-FSA analysis technique

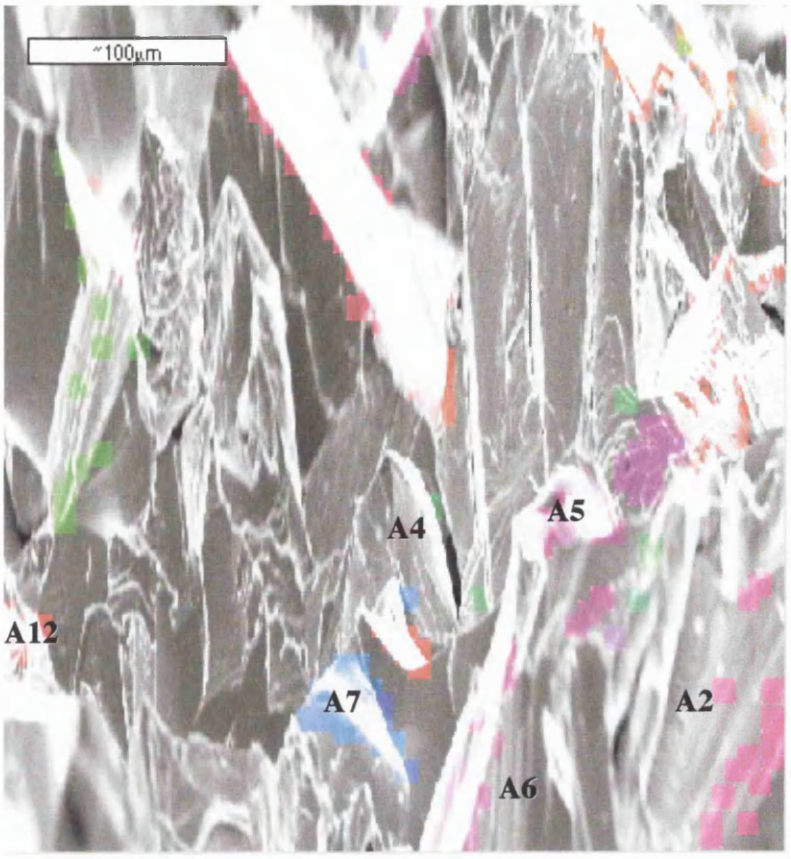

Figure 5.30a,b Crystal orientation map with Facets marked (above) and corresponding Inverse pole figure showing orientation of the crystallographic fracture plane (below).

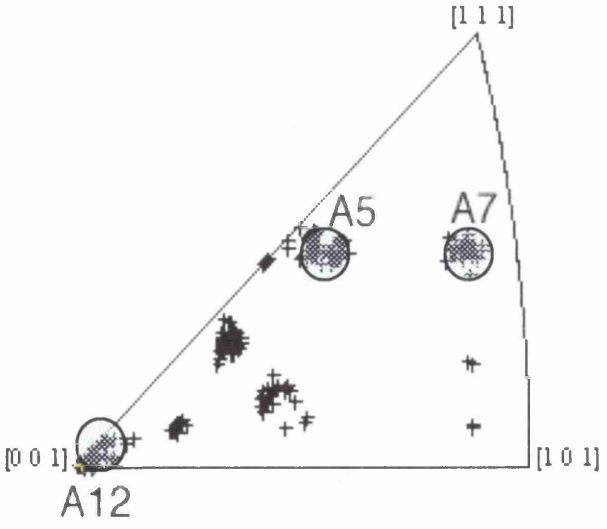

6. Discussion

6.1 Grain Growth.

It can be seen from the results (Chapter 5.1) that there are two distinct mechanisms having an influence on the degree of grain growth in the material. The first occurs at lower temperatures, where the effects of annealing temperature and time have little effect on the grain size of the material. Above a certain 'transition temperature' of approximately $0.7T_m$, another growth mechanism becomes dominant. This mechanism is responsible for the abnormal grain growth that is seen at higher annealing temperatures in both materials.

The transition between these two mechanisms is very similar to that described by Simpson et al (1971) in his description of the four stages of grain growth. It seems to have some dependency on the composition of the alloys with a lower transition temperature of between 800°C and 900°C for the alloy with the higher phosphorus content and a temperature of between 900°C and 1000°C for the alloy with the lower phosphorus content.

Grain growth occurring at annealing temperatures above the transition temperatures described above was usually found to be abnormal in nature. The highest degree of grain growth was found for samples that were aged at 1000°C, though samples of the 0.12P alloy aged at 900°C also showed some degree of abnormal grain growth. In most cases, there would be a few abnormally large grains, a few very small grains and the rest of the grains would be seen to be growing normally. The very small grains tended to be irregular in shape and usually manifested themselves within the larger abnormally grown grains. Work by Rajmohan and Szpunar (2001) attributed the formation of island grains to the fact that they possessed a low mobility boundary with a low (<20°) or high (>45°) misorientation, suggesting a low mobility for boundaries such as Σ3, Σ5 and Σ11. This is inconsistent with CSL theory and the work of Lin et al (1996), a point which Rajmohan

and Szpunar themselves describe. It is possible that these small grains are remnants of grains that are being consumed by the larger growing grains, or they may be newly created grains that are themselves growing, formed due to imperfections in the crystal structure of the large grain causing nucleation, though this is unlikely thermodynamically. If however this is the case, it would be expected that the grains be irregular in shape due to the fact that they have had insufficient time in which to reach an equilibrium energy and to form a uniform shape. It would be reasonable to assume that they would choose to form a high mobility CSL boundary structure, due to the lower energy required in the formation of such a CSL bounded grain, as oppose to a more random boundary.

The extent to which grain growth occurs in the material also seems to be dependent on the composition of the alloy, since the degree of grain growth in the 0.06P alloy proved to be much greater than for that of the 0.12P alloy. This can partly be attributed to a greater propensity of solutes at the grain boundaries of the alloy with the higher phosphorus content causing a greater level of grain growth inhibition and grain boundary pinning in the alloy with the higher phosphorus content (Juul Jensen, 1995). The alloy with 0.06wt%P was found to have a constant grain size distribution of approximately 70μm in size for all annealing temperatures between 600°C and 900°C and was independent of the annealing time. At 1000°C the average grain size of the material increased to 260μm, 340μm and 180μm for the 1, 2 and 5 hour annealing times respectively. The maximum grain size reached was found to be after an annealing time of 2 hours at 1000°C, after that the grain size decreased to almost half its value in a further 3 hours. This could be attributed to the fact that the small irregular shaped grains located within the larger abnormally grown grains that became apparent after the 1 and 2 hour heat treatments are beginning to grow and are hence reducing the average grain size in the material. This is very unlikely thermodynamically, though would account for the more uniform microstructure in the samples that are annealed for 5 hours, as the small grains grow within the larger grains. It could then be assumed that as the larger grains grow further, the higher number of smaller grains growing within the larger grains, break up the larger grains as the smaller grains grow and coalesce. This process could then lead to a reduction in average grain size as the annealing time is increased.

The alloy with 0.12wt%P had a grain size that was consistently between 70μm and 100μm for all annealing temperatures between 600°C and 800°C, again independent of the annealing time. At temperature between 900°C and 1000°C, the grain size increased to a maximum value of 145μm at an annealing time of 1 hour, falling to 140μm for a 2 hour anneal and 110μm for a 5 hour anneal. In order to confirm the fact that there is a reduction in average grain size as the annealing time is increased, a 50 hour anneal at 1000°C was performed and this gave an average grain size of 75μm. This confirmed the fact that the average grain size of the material is reduced with increasing annealing times for annealing temperatures above the transition temperature at which abnormal grain growth occurs, a fact little reported in any of the literature.

The formation of small irregular grains within the larger abnormally grown grains may be affected by the phase-change in the material. At 928°C, the crystal structure changes from bcc to fcc as the material changes from a ferrite to an austenite. As it is heated, the restructure of the crystal lattice may allow the nucleation of these small irregularly shaped grains. For short annealing times, these small grains can be seen to be growing within the larger abnormally grown grains. As the annealing times are increased there is sufficient time for these grains to grow and hence for the microstructure of the material to arrange itself into a more energetically favourable state with a uniform equiaxed grain structure with grains of approximately 70μm. This phase change cannot responsible for the initiation of abnormal grain growth in the material due to the fact that abnormal grain growth in the 0.12wt%P material can be seen to be occurring at temperature of 900°C, 28°C below the transition temperature. Hence the onset of abnormal grain growth in the material must be attributed to some other factor.

The data presented here is consistent with work done by Simpson et al (1971), who postulated that there are a four stages of grain growth, stage one and three being comparable; suggesting that they have the same rate controlling mechanism of the form

$$D^{1/n} - D_0^{1/n} = K(t-t_0) \qquad \textbf{Equation 6.1}$$

where D_0 is the starting grain size of each stage and n is the growth law index. The interrupting second stage is a period of rapid irregular growth to which the kinetic rate equation does not apply. It is this second stage that is responsible for the rapid abnormal grain growth in the material before the process of grain shape equilibration after the irregular growth stage. For work done by Simpson et al (1971) and Horton et al (1995), and the results of this investigation, the irregular growth stage seems to manifest itself between 0.65 and 0.75 of the melting temperature of the material, for all the materials investigated. This implies that the onset of abnormal grain growth is a physical factor related to the melting temperature (T_m) of the material, occurring at a temperature of $0.65T_m$ to $0.75T_m$.

The fact that there is little normal grain growth occurring at the lower temperature ranges of 600 to 900°C may be attributed to the fact that it is being impeded by precipitates in the material which are causing grain boundary dragging or grain boundary pinning effects. Such inhibition of grain growth has been assumed a necessary condition for the onset of secondary recrystallisation (Padilha et al, 1998). It seems that for most non-pure materials, grain boundary pinning and dragging effects are a controlling factor on the degree of normal grain growth exhibited by the material up until a temperature equivalent to $0.65\text{-}0.75T_m$ is reached, at which point abnormal grain growth becomes dominant. This implies a physical alteration in the structure of the grain boundaries or the quantity or distribution of the precipitates and alloying elements on the grain boundaries of the material. After the relatively short period of abnormal grain growth, there is a return to the normal grain growth mechanism that does not appear to be pinned of suffer any of the effects associated with precipitates or grain boundary dragging (Aust and Rutter, 1959). This may be due to the fact that at these elevated temperatures, there is either a sufficient

energy supplied to the material in order to overcome the effects that are associated with grain boundary pinning by precipitates, or it may be that the precipitates de-segregate back to the matrix at elevated temperature and hence cannot have any effect on the process of grain growth.

6.2 Grain Boundary Structure

An analysis of the grain boundary structure of both alloys was conducted, considering the effects of annealing temperatures and annealing times on the grain boundary misorientations angles present in the samples microstructure and the proportions of 'special' boundaries in the material, as defined by coincidence site lattice notation.

6.3 Grain Boundary Misorientation Angles

The grain boundary misorientation angles that were revealed during the analysis show a number of trends related to both the annealing temperature and the annealing time to which the material was subjected. It can be seen from the results presented in section 5.3.1, that there is significant deviation from what would be expected for a random misorientation distribution, shown originally by Mackenzie (1958) (Figure 6.1), there being a general increase in the mean misorientation with increasing annealing temperature. In all cases, the highest mean misorientation angle corresponds to the samples that were annealed at 1000°C. This trend exists for all the different annealing times and for both the alloy compositions, implying that it is related directly to the annealing temperature to which the sample was subject.

The misorientation mode showed a great deal of scatter in it value for the 0.06wt%P alloy, principally in the values for the samples that were aged for two and five hours. The 1hour annealing time did not produce a large amount of deviation in the mode misorientation; instead, it produced values that were comparable to the values for the

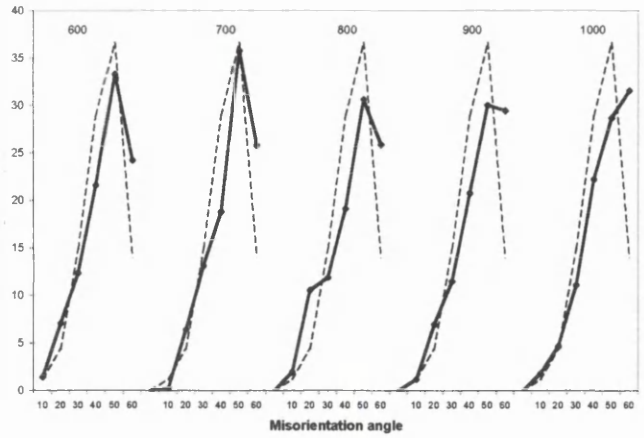

0.06wt%P 1hr anneal

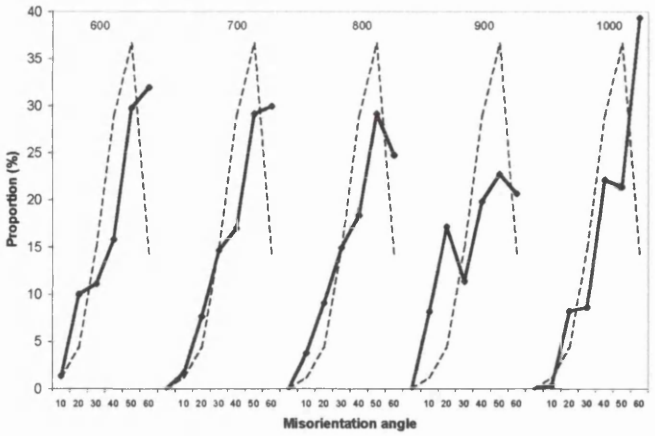

0.12wt%P 1hr anneal

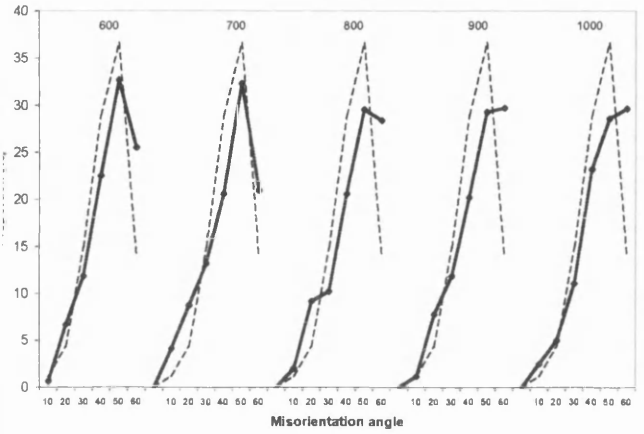

0.06wt%P 2hr anneal

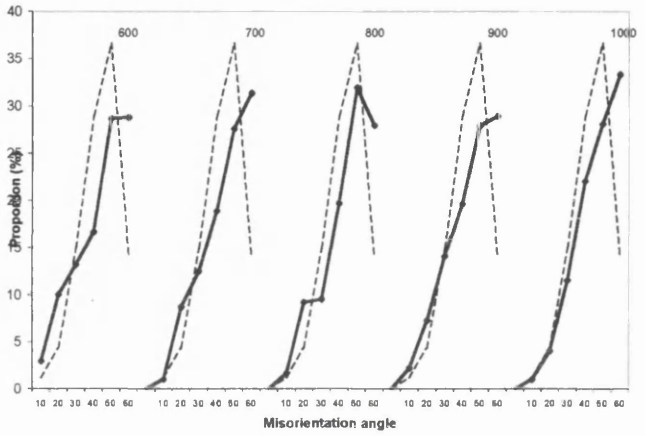

0.12wt%P 2hr anneal

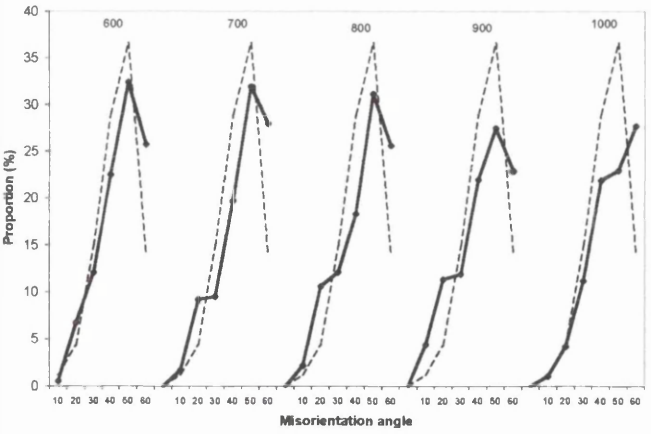

0.06wt%P 5hr anneal

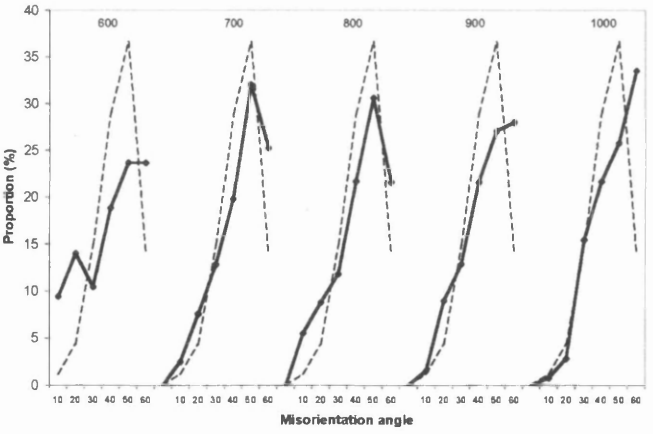

0.12wt%P 5hr anneal

Figure 6.1 Comparison between misorientation angle distributions for all samples (Solid Lines) and isorientation angle distributions for a random set of misorientations, known as the Mackenzie distribution Dashed line), allowing assessment of the degree of randomness in the misorientation angle distributions.

mean/median misorientation. The misorientation mode value for the 0.12wt%P alloy did not exhibit the same large fluctuation as was seen in the 0.06wt%P alloy, instead it produced values that were consistently higher than those for the mean/median misorientation data. This could be seen most prominently in the sample that was aged for 2 hours, where the misorientation modes could be seen to be consistently 10° to 15° higher than those for the mean misorientation.

6.3.1 Misorientation Angle Distribution Curves

It is clear to see from the misorientation distribution curves, that there is a definite trend in misorientation angle distribution, and it is directly related to both annealing time and temperature. With reference to the 1hr/AC data for the 0.06wt%P alloy (Figure 5.14), it can be seen that there is a definite shift in the shape of the curve with increasing annealing temperature. As the temperature is increased, there is a reduction in the peak that is present at 50° in the case of the lower temperature heat treatments. This reduction continues to the point where the peak in the curve has dissipated totally, leaving a uniform, and almost linear increase in the data from 5° to 60° by the time the annealing temperature has been increased to 1000°C. A similar scenario is seen for the 2hr/AC heat treatments for the 0.06wt%P alloy, but at an annealing time of 5 hours the same trend is not seen. Instead there is a similar distribution curve for the high temperature heat treatments as for the low temperature heat treatments with a definite peak in the misorientation angle distribution at 50°. This coincides very well with the fact that there is a reduction in the extent of abnormal grain growth in the samples that were annealed for 5 hours, implying a relation between the misorientation angle distributions and the extent to which abnormal grain growth occurs in the material (Lee and Szpunar, 1995). For after an annealing time of 5 hours, there is a change in the trends exhibited by both the extent of abnormal grain growth in the material, and the shape of the misorientation distribution curve for the range of heat treatments.

The data for the 0.12wt%P alloy shows a similar, general trend in the misorientation distribution curves, though there is a lot of scatter in the data. The data for this alloy seems to suffer from a high degree of scatter, causing the curves to look a lot more chaotic and random, hence the trends that are exhibited by this alloy are much more difficult to positively determine. This high degree of randomness in the data must be in some way related to the high phosphorus content of the alloy and the effect that is has on both the crystallography of the material and its ability to impede the extent of abnormal grain growth in the material, as it is the only real difference between the two alloys.

It seems that there is a relation between the grain boundary misorientation angles in the materials and the extent of abnormal grain growth in the material, due to the fact that after annealing times of 5 hours, both factors are seem to undergo a change in their general trends, there being a reduced degree of abnormal grain growth after a 5 hour anneal and a breakdown in the relationship between the misorientation distribution curve peak and the heat treatment temperature after the 5 hour annealing period. This fact has not been reported in the literature to date.

For annealing times of 1 and 2 hours there is a relation between the peak in the misorientation distribution curve and the heat treatment temperature, there being a peak at 50° for lower heat treatments which dissipates to become a more linear relationship for higher heat treatment temperatures. This relationship between the more linear misorientation distribution curves and higher degrees of abnormal grain growth in the material, implies that there exists a physical relationship between the two parameters and that grain growth is affected by the misorientation angles in the material (Randle et al, 1986). It should also be noted that results for the 0.06wt%P alloy show more consistent, definitive and easily recognisable data trends than are shown be the 0.12wt%P alloy where there is a much higher degree of scatter in the experimental data.

The results for the misorientation angles show no correlation to the temperature range of $0.65T_m$ to $0.75T_m$, which seems to be a contributing factor in the onset of abnormal grain growth in the material.

6.4 Grain Boundary Proportions

One of the first relationships to become immediately apparent on the examination of the grain boundary data is that of the high proportions of Σ3 boundaries present at higher annealing times. This is especially so for the higher heat treatment temperatures of 900°C and 1000°C. It can be seen that there is a steady linear increase in Σ3 proportions for the 0.06wt%P samples that were aged for 1 hour that is proportional to the annealing temperature.

From the results, it can be clearly seen that there is a transition between two states occurring at about 900°C at which point there is a considerable increase in the proportion of Σ3 boundaries present in the material, rising from 6.9% at 900°C to 10.7% at 1000°C. This change in state is consistent with the results for the grain growth of the material where there is also seen to be a dramatic change in the degree of abnormal grain growth occurring at 900°C. Both the proportions of Σ3 boundaries in the material and the degree of abnormal grain growth in the material both seem to be occurring at a temperature of approximately $0.7T_m$. This implies that there is a distinct relationship between the mechanisms responsible for the onset of abnormal grain growth and the Σ3 boundary. Both are dependent on the annealing temperature and both are affected by a transition that occurs at $0.65\text{-}0.75T_m$. This dependency may be explained by the fact that the Σ3 boundary is a low energy, highly mobile boundary, and the fact that the majority of the abnormally grown grains were Σ3 bounded. These factors imply the rapid formation of the Σ3 boundaries during annealing, occurring due to their low energy compared to other boundaries, is responsible for the high proportions of Σ3 boundaries in the material. These Σ3 bounded grains then grow rapidly due to the high mobility exhibited by the Σ3 boundary leading to a high proportion of Σ3 bounded abnormally grown grains. This is consistent with the results of the analysis presented in section 5.3.

The $0.7T_m$ transition can be seen more clearly for the 0.06wt%P samples where there is an increase from 5.2% Σ3 boundaries at 900°C to 10.7% Σ3 for samples aged at 1000°C, reinforcing the relationship between the proportions of Σ3 boundaries and the transition at $0.7T_m$. The samples that were annealed for 5 hours display a slightly different trend to those for the 1 and 2 hour annealing times. For the 5 hour samples there is a steady decrease in the proportions of Σ3 grain boundaries in the material as the annealing temperature is increased. The decrease is not large, falling only 1.3% from 600°C to 900°C but it can be clearly seen as a trend in the data. At 900°C, the transition temperature is reached and the proportion of Σ3 boundaries in the material rises dramatically from 2.3% to 8.3% at 1000°C.

The results for the 0.12wt%P material show a much higher proportion of Σ3 boundaries for all the 1000°C samples, regardless of the annealing time. The proportion of Σ3 boundaries for samples annealed at 900°C and below, gave results that were very similar to those of the 0.06wt%P material. Above 900°C, the proportions of Σ3 boundaries rose from an average of 10% for the 1000°C annealing times for the 0.06wt%P, to an average of 16.8% for the 1000°C annealing times for the 0.12wt%P material.

From this information, it is possible to determine that the phosphorus content of the material has little influence on the proportions of Σ3 boundaries present in the material until the $0.7T_m$ transition temperature is reached.

From the grain growth data, it can be seen that the average grain size at 1000°C for the 0.06wt%P alloy was approximately 250μm. For the 0.12wt%P alloy, the average grain size was found to be 125μm at 1000°C, a value of nearly half. By considering this fact, it is possible to deduce that the grains in the 0.06wt%P alloy are on average twice the size as the grains in the 0.12wt%P alloy, thus the boundaries in the 0.06wt%P alloy must be on average, twice the length than those in the 0.12P alloy. Since the proportion of Σ3 boundaries are 11% and 16% for the 0.06wt%P and 0.12wt%P alloy respectively when measured by boundary number, it can be concluded that there are probably more, or at

least equal proportions of Σ3 boundaries, when measured by length, in the 0.06wt%P alloy at 1000°C than are found in the 0.12wt%P alloy at the same temperature.

Other special boundaries (>Σ3) were not present in any of the heat treatments in quantities greater than what would be expected for a random distribution (Warrington and Boon, 1975), though in some cases, the Σ1 low angle boundaries seem to have a slight dependency on the proportions of Σ3 boundaries in the material, implying that there is a competing mechanism for the formation of Σ1 and Σ3 boundaries; in some cases there will be a high proportion of Σ1 boundaries present only when there are low proportions of Σ3 boundaries. It may be the case that the formation of Σ1 boundaries is slightly less energetically favourable than the formation of Σ3 boundaries, so they only become abundant in the material when the formation of Σ3 boundaries is impaired in some way. This trend can be seen most clearly for the 0.06wt%P, 5-hour samples where there is clearly an increase in the proportions of Σ1 boundaries and a decrease in the proportion of Σ3 boundaries from 600°C to 900°C. The difference in mobility between the ∑1 and the highly mobile ∑3 boundary may also be a contributing factor in the boundary proportions, as the presence of a high proportion of mobile ∑3 boundaries may cause a reduction in the proportions of ∑1 boundaries in the material.

6.5 Effect of Grain Boundary Proportions on Grain Growth

It would seem reasonable to assume that the processes controlling the grain boundary proportions and the constraints on the grain growth of the material were two distinct mechanisms. However, due to the fact that both have similar, temperature dependent trend patterns, it can be deduced that the two processes are intimately linked (Lin et al, 1996), with the grain boundary proportions being a contributing factor to the grain growth of the material (Lee and Szpunar, 1995). Though there is reason to believe that it is the grain growth that affects the grain boundary proportions, indeed both phenomena may be mutually dependent in the material.

The annealing temperatures to which the material is subject is a major constraint on both these processes as it is the means by which sufficient energy is supplied to the material in order for boundaries to re-arrange themselves and change to boundary types that are more energetically favourable. These boundary transformations are a contributing factor to the grain growth of the material as the boundaries re-organise. One such example of this is the dependency of abnormal grain growth on the Σ3 boundary. The Σ3 boundary is a low energy, highly mobile boundary, and it prolific at higher annealing temperatures in the material. These Σ3 bounded grains then grow rapidly, enveloping other grains as they grow, due to the high mobility exhibited by the Σ3 boundary leading to the high proportion of Σ3 bounded abnormally grown grains seen in the results of this study.

6.6 Grain Boundary Fracture

The results of the fracture analysis show there to be a marked decrease in the proportions of Σ3 boundaries that are present across a fracture surface in comparison to what is found in a non fractured sample, a result that confirms work done by Lopes et al (1997) on the possible fracture resistance of low Σ boundaries.

As the annealing temperatures are increased, the greater the difference in the data from the fractured and unfractured specimens becomes; there being 0.6% difference in fractured and unfractured proportions at 600°C rising linearly to a difference of 6.1% between the fractured and unfractured Σ3 data at 1000°C. This linearly increasing difference in proportions shows that the Σ3 boundaries play an important role in the fracture of the material. At 1000°C in the unfractured material, 10.7% of the grain boundaries are Σ3 boundaries. At the same temperature, the results from the fracture surface show there to be only 4.6% of Σ3 boundaries in the material. This difference can be attributed to the fact that the Σ3 boundary is less susceptible to intergranular fracture than other grain boundaries in the material. This may be due to the fact that it is a low energy 'special' boundary, known for the improvement of the physical properties of materials (Lehockey and Palumbo (1997). This implies that a greater amount of energy is required in order to cause fracture. Thus an increase in the proportions of Σ3 boundaries, proportional to the annealing temperature would be expected though it would still be significantly less of an increase than for the data from the unfractured samples, as the Σ3 boundaries still need more energy than other boundaries in the material for them to be able to fracture. This is consistent with the results, which show an increase from 2.1% to 4.6% Σ3 for the data from the fractured specimens, and an increase from 2.7% to 10.7% Σ3 for the data from the unfractured samples.

From this it can be determined that the Σ3 boundary has a resistance to fracture due to its low energy, and hence, a high proportion of Σ3 boundaries in the material will assist in fracture prevention. This leads to the conclusion that Σ3 boundaries are instrumental in

the fracture of the material and may assist in preventing crack propagation, for if there are fewer Σ3 boundaries than expected, present across a fracture surface, then it is reasonable to assume that Σ3 boundaries are better at resisting intergranular fracture than other boundaries in the material.

It is possible to conclude from this, that 'Grain Boundary Engineering' (Watanabe and Tsurekawa, 1999) is possible in this material, for as the results show, it was possible to produce samples that had high proportions of Σ3 boundaries by annealing at ~1000°C for an hour. These samples were then less likely to undergo intergranular brittle fracture, due to the fact that the intergranular crack propagation is hindered by the presence of a high proportion of fracture resistant Σ3 boundaries.

A contributing factor to the fracture resistance of the Σ3 boundary may be the fact that as a low energy (Wolf, 1991), good fit, boundary, there is less 'space' available for segregated phosphorus to reside within the boundary (Muller and Mills, 1999). This may provide an added degree of fracture resistance as the imbrittling phosphorus atoms are expelled from the boundary to reside in other boundaries that have more 'space' for them.

6.7 Effects of Grain Boundary Segregation.

From what is known about the segregation processes in this material (Cowan et al, 1998) it is possible to determine that the segregation of phosphorus plays an important role in the formation of Σ3 boundaries in the material, at temperatures below the 'T_m' transition region. When this material is annealed at lower temperatures there is a high degree of segregated phosphorus present on the boundaries. As the annealing temperature is increased, the phosphorus desegregates from the grain boundaries back in to the matrix of the material. This process makes the formation of Σ3 boundaries at elevated temperatures more favourable, as there are less phosphorus atoms restricting to formation of 'good fit' Σ3 boundaries. At lower temperatures, the excess segregated phosphorus inhibits the formation of Σ3 boundaries, so other, higher energy boundaries are formed instead.

The effects of higher concentrations of phosphorus can be seen in more detail by referring to the data for the 0.12wt%P alloy. From this data it can be seen that for temperatures between 600°C and 900°C there is a lower proportion of Σ3 boundaries present in the material when compared to the data for the 0.06wt%P alloy. This can be attributed to the fact that the higher concentrations of phosphorus in the 0.12wt%P alloy are inhibiting the formation of Σ3 boundaries. Due to the fact that the phosphorus atom is relatively large, the presence of such atoms will make the formation of a 'good fit' boundary considerably more difficult than its formation in the absence of such species would be. For this reason, there are low proportions of Σ3 boundaries in the 0.12wt%P alloy for temperatures up to 900°C. At annealing temperatures of 1000°C, the above description does not apply, as there are high proportions of Σ3 boundaries present in the 0.12wt%P alloy. The population of Σ3 grain boundaries at 1000°C in this alloy is over 16%, regardless of the annealing times. This is a significantly higher proportion than is observed for the 0.06wt%P alloy, which has a maximum Σ3 population of less than 11% at 1000°C.

The fact that there are higher proportions of Σ3 boundaries present for the 0.12wt%P alloy at 1000°C than for the 0.06wt%P alloy may be attributed to the fact that there is significantly less grain growth in the 0.12wt%P alloy at high temperatures. Thus, there will be a higher number of Σ3 boundaries recorded for this material as there will be a significantly higher number of Σ3 bounded grains per sample area, hence a greater number of Σ3 boundaries will be recorded, though the total proportion of Σ3 boundaries by length will be a lot lower than for the 0.06wt%P alloy where there are a number of very large Σ3 bounded grains which are not given a true representation in the data. This leads to the conclusion that the phosphorus content is not the deciding factor on the proportion of Σ3 boundaries for samples aged at 1000°C, though it my be the case for samples aged between 600°C and 900°C.

6.8 Modus Operandi

A number of different experimental techniques were developed in order to be able to acquire the data required from the two alloys. Most of the procedures involved the analysis of fracture surfaces and a number of error reduction and quality refinements were developed in order to better acquire accurate and reliable results.

6.8.1 Fracture Surface Analysis

The technique of fracture surface analysis is very much a compromise between large experimental errors and high-speed acquisition of data that would be very difficult to obtain be other means. The large experimental errors associated with this technique can be reduced by a number of methods, but all these methods lend to make the data acquisition a more laborious process. Its application is best suited in situations where a practical compromise between the experimental errors and the acquisition of a suitably large data set can be achieved (Wright and Field, 1998). The fast acquisition of data from a fracture surface is also very valuable as a preliminary test, before more accurate and laborious tests are attempted.

The methods of error reduction in this technique range from simple methods involving the careful set-up of experimental conditions and intuitive error compensation, to the computer assisted reconstruction of the fracture surface, a method that may one day be automated, allowing the high speed acquisition of highly accurate data directly from fracture surfaces.

The PFSA technique also has a number of benefits and experimental drawbacks. Its main advantages are due to the fact that the technique is non-destructive, compared to the normal mounted fracture surface sectioning, leaving the fracture surface intact for any other subsequent analysis that may be required. It also allows the effects of deformation twinning and residual strain in the sample to be analysed simultaneously from both the

fracture surface and the polished side normal to the plane of the fracture surface. This technique does however make it extremely difficult to simultaneously polish through both halves of the sample to the same depth, due to the fact that the two halves remain as two independent samples.

The fracture surface analysis of this material reinforced what was already known about the transgranular fracture plane in bcc steels, with nearly all cleavage planes being {001} (Davies and Randle, 2001) A few cleavage planes were found to be the {110} type, which is not too much of a surprise considering that the {110} planes are the next most closely packed plane after the {001}. The analysis of the intergranular fracture plane in this material proved to be unfeasible, due to the fact that all the intergranular boundaries in this material were curved, implying that the intergranular plane is of little consequence in this material. There seems to be no preferred intergranular boundary plane, so the intergranular facets can be curved in nature, possibly being planer on a very small, sub micron scale.

6.9 Auger Microscopy / EBSD Combination (A-FSA).

The method by which segregation data and crystallographic data from the same fracture facet is acquired is by no means trivial. Much preparation and experimental planning must be employed before such an attempt is undertaken and a great deal of care must be taken throughout the experimental procedures in order that the results are not corrupted. The experiment needs to be sympathetic to the requirements of both the Auger technique and those of EBSD, such as the angle that the sample is to make with the incident electron beam. For if the two angles are made as close as is possible, then the matching of the facets after Auger analysis will be made a lot more straight forward. Other factors which influence the ease of facet matching is the accelerating voltage used, as large differences in accelerating voltages lead to images with very different contrast gradients, which can render some features very difficult to recognise when the other voltage is used.

Great care must be taken of the samples after the Auger analysis is complete, as the fracture surfaces of the samples can easily become damaged during transit or during storage prior to the application of EBSD. Corrosion must also be minimised as it will make recognition of specific facets extremely difficult and will also impair the chances of getting good Kikuchi diffraction patterns from the fracture surfaces of the samples. When the A-FSA technique is utilised correctly, a substantial amount of data can be acquired, the accuracy of which is dependant on the time available for the experiment, as refinements can easily be made in order to reduce the experimental errors as much as possible, exactly as with the normal 'fracture surface analysis' technique described in section 4.1.

It can be seen from the results of this technique that the data for the transgranular facets accurately shows all the fracture planes are {001}, which confirms results acquired by other means and proves that the data acquired by this technique can be considered to be very accurate, due to the fact that it accurately confirms known results. From this data it

can be assumed that the results for the intergranular facets are equally accurate and that the technique is a successful means of acquiring crystallographic data from Auger facets.

The results acquired by this technique do not provide a significant representation of the physical properties of the intergranular fracture plane of this material, due to the fact that the intergranular facets in this material are constantly of a curved nature, implying that the intergranular fracture plane is not a factor of physical significance in this material as all planes are produced equally, thus allowing the curvature of the facets to be possible. The data acquired from each facet can only be considered accurate for the small area of the facet surface whereby the electron beam was incident during the acquisition of the data. The intergranular facet plane data that is outlined for each facet in the results section is an average of a number of data acquisitions from that facet, created using the facilities provided by the software. This was performed in order to give a better representation of the orientation of the fracture plane, even though its true value varies to correspond with the curvature of the facet surface.

A total of 16 results were successfully acquired from the 4 samples, 2 of these results corresponding to transgranular fracture facets. Thus, 14 results corresponded to intergranular fracture facets from where Auger measurements had been made. It was found that 28.6% of these planes were {110}, 14.3% were {112) planes and all others planes each featured less than 7.1% of the total. However, due to the same amount of data acquired and the consequences of the high degree of facet curvature, it is difficult to draw any real definite conclusions about the role that the intergranular plane has on the segregation of phosphorus or carbon. Once noticeable occurrence is the fact that there is 3at% more phosphorus present on the {112} planes than there is on the {110} planes, illustrating the importance of considering the grain boundary plane in the characterisation of a grain boundary (Lejcek et al, 1997). The carbon content changes only by 0.41at% between the two plane types (Perhacova et al, 2000 and Suzuki et al, 1983). This implies that the {112} planes provide a more favourable site for phosphorus segregation, possibly due to the fact that the {112} planes allow more free space, thus permitting the segregation of larger atoms such as phosphorus. The {110} planes may be more resistant

to the segregation of elements such as phosphorus due to the amount of free space (Thompson and Knott, 1993) that exists along the plane, as it is known to be a low energy plane corresponding to a Σ1 'good fit', low angle boundary (Randle, 1996).

The fact that these {110} planes occur in higher proportions than other planes during fracture can be confirmed by reference to figure 5.21, where it can be clearly seen that the proportions of Σ1 boundaries present in the fractured samples are significantly higher than those in populations from unfractured specimens. This helps to confirm that the population of {110} planes measured by the fracture surface analysis method is an accurate representation of the population of intergranular boundary planes present on the fracture surface of the material. From this it can be deduced that the procedure for combining Auger electron microscopy with the application of EBSD on the same facets is capable of yielding scientifically accurate results, despite all of the potential difficulties presented by the technique. With more time and development, this technique could be used to accurately correlate the effects of the grain boundary crystallography and the grain boundary plane on the segregation of species to the grain boundaries of the material.

7. Conclusions

1. The fracture surface analysis technique (FSA) developed here, proved a very useful tool for the acquisition of crystallographic data that would be unfeasible by other means. The errors in the FSA technique can be minimised, though this will increase the data acquisition time for the analysis. The choice of optimisation for speed or accuracy is a factor that must be decided by the user in view of the data that is required.

2. The method for the combination of Auger microscopy and EBSD (A-FSA), which has been designed here, is an excellent method for conclusive determination of the effects of crystallography on the segregation of species in the material, a process that is not yet possible by any other means. The A-FSA methodology is currently in very early development stages, and the acquisition of data is laborious, but the results clearly show the considerable potential possessed by this technique. Further refinements should ensure that this technique becomes a valuable experimental technique for the analysis of the properties of materials.

3. There are two separate grain growth mechanisms operating in this material at different temperature ranges. Abnormal grain growth is prolific in this material at annealing temperatures above 900°C, whereas normal grain growth is the dominant grain growth mechanism for annealing temperatures of below 900°C. For both alloys, this transition corresponds to a temperature of 0.65 T_m to 0.75 T_m of the melting temperature in Kelvin of the material, a temperature where other researchers have reported similar effects (Simpson et al, 1971). This implies that the onset of abnormal grain growth is a physical factor related to the melting temperature (T_m) of the material, occurring at a temperature of $0.65T_m$ to $0.75T_m$.

4. The formation of small irregular grains within the larger abnormally grown grains may be attributed to the phase change in the material at 928°C, where the crystal structure changes from ferrite to austenite. The re-structuring of the crystal lattice as the material cools, may allow the nucleation of these small irregularly shaped grains. For short annealing times, these small grains are seen to be growing within the larger abnormally grown grains. As the annealing times are increased there is sufficient time for these grains to grow and hence for the microstructure of the material to arrange itself into a uniform grain structure with equiaxed grains of approximately 70μm in size.

5. The population of Σ3 boundaries in the material is a temperature dependent factor that is also influenced by the degree of segregated phosphorus in the material for temperatures below the $0.7T_m$ 'transition' temperature. Above the $0.7T_m$ 'transition' temperature, a much greater proportion of Σ3 boundaries are produced, regardless of the phosphorus content of the material. This implies that at temperatures above the $0.7T_m$ transition, almost all the phosphorus has desegregated to the matrix so that the proportions of Σ3's produced is comparable for the two alloys, a fact consistent with work done previously (Cowan, 1997). The abnormal grain growth exhibits a very similar trend to the proportion of Σ3 boundaries, implying that the onset of abnormal grain growth is caused by the production of the lower energy, mobile Σ3 boundaries. Both abnormal grain growth and Σ3 proportions are dependent on the annealing temperature and both are affected by a transition that occurs at $0.65\text{-}0.75T_m$. However, the abnormal grain growth of this material is affected by the phosphorus content of the alloy at temperatures above the $0.7T_m$ transition, whereas the proportion of Σ3 boundaries is not. From this information, it is possible to determine that the phosphorus content of the material has little influence on the proportions of Σ3 boundaries present in the material as the $0.7T_m$ 'transition' temperature is reached.

6. Though the total amount of data acquired was relatively small, the A-FSA analysis technique was able to determine that a significantly higher proportion of {110} intergranular boundary planes exist on fracture surfaces than other intergranular boundary planes. It was also found that 3at% more segregated phosphorus was present on {112} boundary planes than on {110} boundary planes on the fracture surfaces of the material. This result confirms what would be expected, as Σ1 boundaries are considered to be 'good fit' boundaries, hence will have little free space for segregated species. The fact that {001} planes are found to have less segregated phosphorus than other planes analysed confirms this assumption.

7. It has been shown by statistically significant results, that Σ3 boundaries exhibit a resistance to intergranular fracture in this material and also that the proportions of Σ3 boundaries can be increased by annealing for 1 hour at 1000°C. Thus it can be concluded that the fracture properties of this material can be improved by 'Grain Boundary Engineering'

8. Further Work

The results of this study show that there are a number of areas where further work should prove to be productive. These include the further analysis of current samples using the techniques described here and also by applying refinements and improvements to the techniques that have been developed during the course of this study.

1. The populations of Σ3 boundaries and the onset of abnormal grain growth at the temperatures of $0.65\text{-}0.75T_m$ should be investigated in greater detail in order to determine the causes and physical implications of this $0.7T_m$ transition region. A thorough study of the physical changes exhibited by the samples between the temperatures of 900°C and 1000°C should divulge a substantial amount of information on the effects of the $0.7T_m$ transition region and the 928°C phase change that occurs in this material. This should in turn provide further information on the process of abnormal grain growth that occurs in this material at higher annealing temperatures.

2. The effect that the population of Σ3 boundaries has on the fracture of the alloys should be further investigated in order to more quantitatively determine the influence that Σ3 boundaries have on a sample's propensity to fracture. This should be done for alloys of different compositions in order to better determine the effects of phosphorus segregation on both the proportions of Σ3 boundaries in a fractured sample and also the fracture process itself.

3. The FSA technique, whereby crystallographic data is acquired directly from the fracture surface of the material can be further developed in order to further reduce the experimental errors that and naturally inherent in this technique with the aim

to develop to the extent where automation of the error reduction process is possible.

4. The combined application of Auger electron microscopy for the determination of grain boundary segregation and the EBSD technique for the determination of fracture facet crystallography (A-FSA) has the potential to become a very powerful analysis technique. Further refinements that allow better integration of the two techniques should facilitate rapid development, as would the production of a microscope with both Auger and EBSD facilities insolence.

5. Other work to be undertaken, involves the application of the above techniques to a real life industrial material, as all work to date has been performed on an experimental Fe-P-C alloy. Results for this alloy have proved to be very encouraging and pave the way for the successful analysis of industrial materials by the many different techniques developed and refined in this study.

There is still a great deal of information to be learned about processes of grain growth segregation and grain boundary crystallography, and the effects that each process have on each other. Only then will the combined effects of these three distinct processes be fully understood.

9. References

Anderson, M. P., Srolovitz, D. J., Grest, G. S., and Sahni, P. S., *Acta. Metall.*, **32**, p.783, 1984.

Aust, K. T., and Rutter, J.W., *Trans. Metall. Soc.*, A.I.M.E., **215**, p.119, 1959.

Biggs, W. D., and Pratt, P. L., *Acta. Metall.*, **6**, p.694,1958.

Briant, C. L., *Impurities in Engineering Materials*,1999

Briant, C. L., *Acta. Metall.*, **33**, 7, p.1241, 1985.

Bollman,W., *Crystal Defects and Crystalline Interfaces.*, Springer Verlag., 1970.

Chen, J. H., Zhu, L., Wang, G. Z., and Wang, Z., *Metall. Trans.*, **24A**, p.659, 1993.

Christian, J. W., and Mahajan, S., *Progress in Mat. Sci.*, **39**, p.1995.

Cocks, A. C. F., and Gill S. P. A. *Acta mater.*, **44**, p.4765, 1996..

Cowan, J., *PhD Thesis*, University of Birmingham., 1997

Cowan, J. R. Evans, H. E. Jones, R. B. and Bowen, P. *Acta. mater.*, **46**,18, p.6565, 1998

Crocker, A., Smith, G., Flewitt, P., and Moskovic, R., *Grain Boundary Fracture in the Cleavage Regime of Polycrystalline Metals.*, 1996.

Davies, P. A., Novovic, M., Randle, V., and Bowen, P., *J. Mic.***205**.Pt.3 p.278, 2002.

Davies, P. A., and Randle, V., *J. Mic.*, **204**, Pt.1 p.29, 2001

Dingley, D. J., and Randle, V., *J. Mat. Sci.* **27**. p.4545, 1992

Erhart, H., and Grabke, H., *J. Met. Sci.* **15**, p.401, 1981

Escher, C., Neves, S., and Gottstein, G., *Acta mater.*, **46**, p.441, 1998.

Field, D. P., *Ultramicroscopy.*, **67**, p.1, 1997.

Gardner, J., *Welding Science and Metallurgy.*, **2**, 1966.

Gomez, A., Beltran, L., Aragon, J.L., and Romeu, D., *Scripta Mater.*, **38**, 5, 1998

Goodhew, P. J., and Humphreys, F. J., *Electron Microscopy and Analysis.*, 1992

Grabke, H. J., *Martinus Nijhus Dordrecht.*, p.23, 1987

Grabke, H. J., Hennesen, K., Moller, R., and Wei, W., *Scripta. Metall.*, **21**, p.1329, 1987.

Griffith, A. A., *Phil. Trans, Roy. Soc. London.*, 1920

Gumbsch, P., and Cannon, R. M., MRS Bulletin., 2000

Harase, J., Shimizu, R., and Dingley, D. J., *Acta. Metall. Mater.* **39**, 5, p.763, 1991

Hartweck, W. G., and Grabke, H. J., *Acta. Metall.* **29**, p.1237, 1981

Hauch, J. A., Holland, D., Marder, M. P., and Swinney, H. L., *Phys Rev Lett.*, **82**, 1999

Hayakawa, Y., Muraki, M., and Szpunar, J. A., *Acta mater.*, **46**, 3, p.1063, 1998

Hayakawa, Y., and Szpunar, J. A., *Acta mater.*, **45**, 3, p.1285, 1997

Hayakawa, Y., Szpunar, J. A., Palumbo, G., and Lin, P., *Magn. Magn. Mater.*, **160**, p.143, 1996

Hillert, M., *Acta. Metall.*, **13**, p.227, 1965

Horton, D., Thomson, C. B., and Randle, V., *Mat. Sci. Eng.*, **A203**, p.408, 1995.

Humphreys, F. J., and Hatherly, M., *Recrystallisation and related annealing phenomena.* 1995

Hunt, C. P., and Seah, M. P., *Mat. Sci. Tech.*, **8**, p.1023, 1992

Hutchinson, W. B., and Ryde, L., *Proc. 16th Riso Int Symp.*, p.105, 1995

Hutchinson, W. B., Ryde, L., Bate, P. S., and Bacroix, B., *Scripta. Mater.* **35**, 5, p.579, 1996

Ibe, G., and Lucke, K., *fur das Eisenhuttenwesen.*, **29**, p.693, 1968

Irwin, G. R., *In Fracturing of Metals.*, 1948

Kawasaki, K., Nagai, T., and Nakashima, K., *Phil. Mag.*, **B60**, p.399, 1989

Kim, B., *Mat. Sci. Eng.*, **A283**, p.164, 2000

Kim, S., and Marrow,T. J., *Scripta. Mater.*, **40**, 12, p.1395, 1999

Kobayashi, R., Warren, J. A., and Carter, W. C., *Physica D.*, **140**, p.141, 2000

Kobayashi, T., and Shockey, D. A., *Advanced Materials and Processes.*,**11**, p.28, 1991

Kumar, M., King, W. E., and Schwartz, A. J., *Acta mater.*, **48**, p.2081, 2000

Lee, H. J., and Morris, J. W. Jr., *Metall. Trans.*, **14A**, p.913, 1983

Lee, K. T., and Szpunar, J. A., *Canadian Metall. Quarterly.*, **34**, 3, p.257, 1995

Lehockey, E. M., Palumbo, G., Mat. Sci. Eng., **A237**, p.168, 1997

Lejcek, P., Paidar, V., Adamek, J., and Hofmann, S., *Acta mater.*, **45**, 9, 3915, 1997

Lin, P., Palumbo, G., and Aust, K. T., *Scripta. Mater.*, **36**, 10, p.1145, 1997

Lin, P., Palumbo, G., Harase, J., and Aust, K. T., *Acta mater.*, **44**, 12, p.4677, 1996

Liu, S. C., Hashida, T., Takahashi, H., Kuwano, H., and Hamaguchi. Y., *Matall. Metar. Trans.* A., **29A**, p.791, 1998

Lopes, L. R. C., Thomson, C. B., and Randle, V., *Scripta. Mater.*, **37**, 12, 1997

Loretto, H.M., Electron Beam Analysis of Materials., 1994

Mackenzie, J. K., *Biometrika*, **45**, 1958

Matsuzaki, T., Sasaki, T., Tsurekawa, S., and Watanabe, T., *Mat. Sci. forum.*, **304-306**, p.585, 1999.

Menyhard, M., Rothman, B., and McMahon, C. J. Jr. *Acta. Metall. Mater.*, **39**, 6, p.1289, 1991

Messmer, R. P., and Briant, C. L., *Mat Sci Tech.*, **30**, p.457, 1982

Muller, D. A., and Mills, M. J., *Mat. Sci. Eng.*A260. 1999.12-28.

Ogawa, K., *Phil. Mag.*, **11**, p.217, 1965

Ogura, T., McMahon, C. J. Jr., Feng, H. C., and Vitek, V., *Acta. Metall.*, **26**, p.1317, 1978

Ono, N., Kimura, K., and Watanabe, T., *Acta mater.*, **47**, p.1007, 1999

Padilha, A. F., Dutra, J. C., and Randle, V., *Mat. Sci. Tech.*, **15**, p.1009, 1998

Perhacova, J., Vyrostkova, A., Sevc, P., Janovec, J., and Grabke, H. J., *Surface Science.*, **454-456**, p.642, 2000

Rajmohan, N., Szpunar, J. A., and Hayakawa, Y., *Acta Mater*, **47**, 10, p.2999, 1999

Rajmohan, N., and Szpunar, J. A., *Scripta. Mater.*, **44**, p.2387, 2001

Randle, V., *Acta mater.*, **47**, 15, p.4187, 1999

Randle, V., *Acta. Metall. Mater.*, 39, 4, p.481, 1991

Randle, V., *Phil. Mag.*, **67**, 6, p.1301, 1993

Randle, V., *Acta mater.*, **46**, 5, p.1459, 1997

Randle, V., *Ironmaking and Steelmaking.*, **21**, 3, p.209, 1994

Randle, V., *Materials Characterization.*, **34**, p.29, 1995

Randle. V., *The role of the Coincidence Site Lattice in Grain Boundary Engineering.*, 1996

Randle, V., *Mat. Sci. forum.*, **94-96**, p.233, 1992

Randle, V., *Materials Characterization.*, **47**, p.411, 2001

Randle, V., *J. Mic.*,**195**, Pt.3, p.226, 1999

Randle, V., and Brown, A., *Phil. Mag.*, **58**, 5, p.717, 1988

Randle, V., and Caul, M., *Mat. Sci. Tech.*, **12**, p.844, 1996

Randle, V., and Davies, H., *Ultramicroscopy.*, **90**, p.153, 2002

Randle, V., and Davies, P., *Interface Sci.*, **7**, p.59, 1999

Randle, V., and Engler, O., *Introduction to Texture Analysis.*, 2000

Randle, V., and Hoile, C., *Mat. Sci. Forum.*, **273**, 1998

Randle, V., and Ralph, B., *J. Mat. Sci.*, **23**, p.934, 1988

Randle, V., Ralph, B., and Hansen, N., *Proc. 7th Riso int Synop.*, p.123, 1986

Ray, R. K., and Jonas, J. J., *Int. Materials Reviews.*, **35**, 1, p.1, 1990

Reid, C. N., *Metall. Trans.*, **12A**, p.371, 1981

Schwarzer, R. A., *Microscopy and Analysis.*, p.35, 1997

Selinger, R. B., and Farkas, D., MRS Bulletin, 2000

Semprimosching, G. O. A., Stampfl, J., Pippan, R.., and Kolednik, O., *Fat. Fract. Eng. Mater. Struct.*, **20**, 1997

Simpson, C. J., Aust, K. T., and Winegard, W. C., *Metall. Trans.*, **2**, p.987, 1971

Slavik, D. C., Wert, J. A., and Gangloff, R. P., *J. Mater. Res.*, **8**, 1996

Slavik, D. C., and Gangloff, R. P., *Acta mater.*, **44**, 9, p.3515, 1996

Smida, T., and Bosansky., *J. Mat. Sci. Eng.*, **A287**, p.107, 2000

Suzuki, S., Obata, M., Abiko, K., and Kimura, H., *Scripta. Metall.*, **17**, p.1325, 1983

Themelis, G., Chikwembani, S. and Weertman, J. Mat. Char. **24**., p.27. 1990

Thomson, A. W., and Knott, J. F., *Metall. Trans.*, **24A**., p.523, 1993

Thomson, R., Hsieh, C., and Rana, V., *J. Appl. Phys.*, **42**, 8, 1971

Thuvander, M., Miller, M. K., and Stiller, K., *Mat. Sci. Eng.*, **A270**, p.38, 1999

Warrington, D. H., and Boon, M., *Acta. Metall.*, **23**, p.599, 1975

Watanabe, T., and Tsurekawa, S., *Acta mater.*, **47**, 15, p.4171, 1999

Weiland, H., Schwarzer, R., *Informationsgesellschaft.*, p.301, 1986

West, J. K., Mecholsky, J. J. Jr., and Hench, L. L., *J. Non. Crys. Solids.*, **260**, p.99, 1999

Williams, D. F., and Reid, C. N., *Acta. Metall.* **19**, p.931, 1971

Williams, O., *MRes Thesis.*, UWSwansea, 1999

Williams, O., Randle, V., Spellward, P., and Cowan, J., *Mat. Sci. Tech.***16**, p.1372, 2000

Wolf, D., *Phil. Mag.*, **63**, 6, p.1117, 1991

Wright, S. I., and Field, D. P., *Mat. Sci. Eng.*, **A257**, p.165, 1998

Yamaura, S., Nakashio, K., Igarashi, Y., and Watanabe, T., *Scripta. Mater.*, **37**, 2, p.141, 1997

Yu-Qing, W., McMahon, C. J. Jr., *Mat. Sci. Tech.*, **3**, 207, 1987